Sedimentary Basins

Evolution, Methods of Formation and Recent Advances

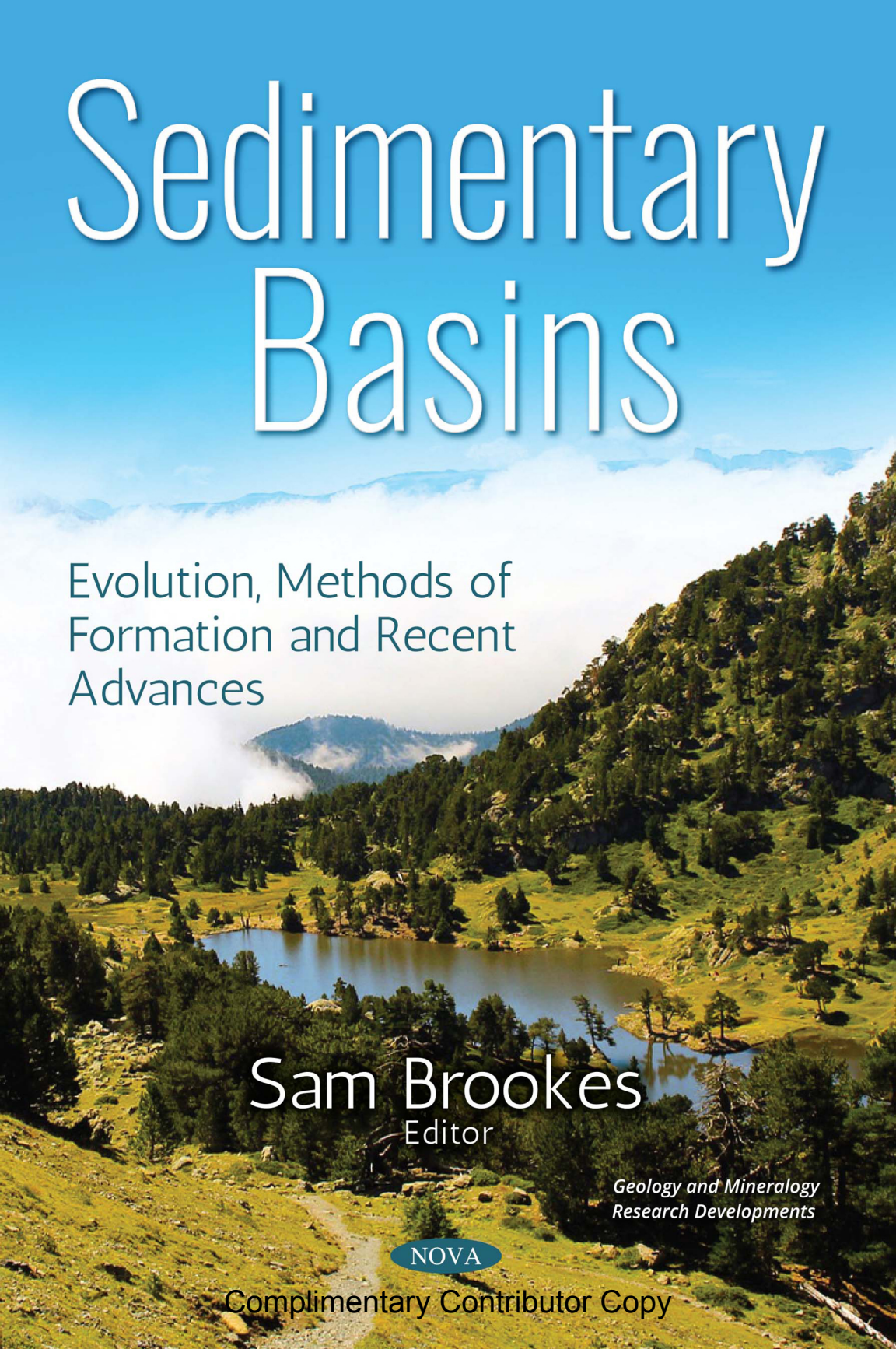

Sam Brookes
Editor

Geology and Mineralogy Research Developments

NOVA

GEOLOGY AND MINERALOGY RESEARCH DEVELOPMENTS

SEDIMENTARY BASINS

EVOLUTION, METHODS OF FORMATION AND RECENT ADVANCES

GEOLOGY AND MINERALOGY RESEARCH DEVELOPMENTS

Additional books in this series can be found on Nova's website under the Series tab.

Additional e-books in this series can be found on Nova's website under the e-Books tab.

GEOLOGY AND MINERALOGY RESEARCH DEVELOPMENTS

SEDIMENTARY BASINS

EVOLUTION, METHODS OF FORMATION AND RECENT ADVANCES

SAM BROOKES
EDITOR

nova
science publishers
New York

Library of Congress Cataloging-in-Publication Data

ISBN: 978-1-53613-923-5 (eBook)

Published by Nova Science Publishers, Inc. † New York

CONTENTS

Preface		**vii**
Chapter 1	The Sedimentary Basins of the Northern Campania Tyrrhenian Margin (Southern Italy): Geologic Evolution and Advances in Seismic Stratigraphy *Gemma Aiello*	**1**
Chapter 2	Formation of Pull-Apart Basins, Cretaceous Volcano-Sedimentary Sequence, Hydrocarbon Pools and Sub-Volcanic Exploration: Case Studies from Peninsular India and Adjoining Indian Ocean *K. S. Misra and Anshuman Misra*	**43**
Chapter 3	XRF Analysis Applied to the Batateira River Formation (Araripe Sedimentary Basin, Ceará State, Brazil) *Gabrielle Roveratti and Daniel Marcos Bonotto*	**75**
Index		**101**

PREFACE

In this collection, the sedimentary basins of the northern Campania Tyrrhenian margin have been investigated in detail aimed at studying and reconstructing their Quaternary geologic evolution through seismo-stratigraphic data. This analysis, carried out using multichannel seismic data of the Zone E, has allowed to infer the subsurface volcanism in the Gaeta Gulf through the identification of a wide buried volcanic edifice, fossilized by the prograding sequences supplied by the Volturno River. This volcanism seems to be related to the oldest phases of volcanism in the Campania Plain, evidenced by the Parete and Villa Literno volcanic complexes, detected in the subsurface of the Campania Plain onshore. Continuing, the presence of volcano-sedimentary sequence in pull-apart basins has intrigued the geologists for several decades. The authors explain that the extensional tectonic processes are not only responsible for formation of these basins but also eruption of volcanic units and emplacement of dykes swarms. High resolution seismic data processed by Pre-Stacking and Depth Migration (PSDM) and Pre-Stacking and Time Migration (PSTM) techniques and hundreds of drill-hole logs have made for an eloquent exposition of basin forming tectonics in different regions of India. Several case studies have also illustrated that the Pre-Cretaceous period is characterized by prolonged extensional tectonics, development of nearly vertical faults, subsidence and formation of basins and

sedimentation. In the final chapter, the results obtained from several essays held with aliquots of a sample of the lithostratigraphic formation known as "Batateira Layers" are reported, occurring in the Araripe Sedimentary Basin, Ceará State, Brazil. The tests were realized with powdered aliquots, considering the oxides often used in geochemical investigations: SiO_2, Al_2O_3, TiO_2, Fe_2O_3, MnO, CaO, MgO, Na_2O, K_2O and P_2O_5. The maximum voltage and current were 50 kV and 50 mA, respectively.

Chapter 1 - The sedimentary basins of the northern Campania Tyrrhenian margin have been investigated in detail aimed at studying and reconstructing their Quaternary geologic evolution through seismo-stratigraphic data. The seismo-stratigraphic analysis herein presented regards the sedimentary basins located in the northern Campania continental margin from Monte di Procida to Mondragone. This analysis, carried out using multichannel seismic data of the Zone E, has allowed to infer the subsurface volcanism in the Gaeta Gulf through the identification of a wide buried volcanic edifice, fossilized by the prograding sequences supplied by the Volturno River. This volcanism seems to be related with the oldest phases of volcanism in the Campania Plain, evidenced by the Parete and Villa Literno volcanic complexes, detected in the subsurface of the Campania Plain onshore. Moreover, the interpreted data have inferred the occurrence of the Meso-Cenozoic acoustic basement in the area between Monte di Procida and Mondragone, composed of the tectonic units pertaining to the Campania-Lucania platform *Auct.*, overlain by Miocene siliciclastic sequences. The Volturno delta has been recognized as distinguished by bottomset, foreset and topset sequences, similarly to the delta deposits of the Mediterranean continental margins.

The stratigraphic and tectonic setting of the Napoli basin has been studied based on the geologic interpretation of a multichannel seismic profile. It is a Pleistocene half-graben which can be compared, from a geodynamic point of view, to the other peri-tyrrhenian basins of the Campania Tyrrhenian margin. The Naples Bay, including the Napoli basin, is a significant part of a belt of coastal tectono-stratigraphic depressions, including the Campania Plain, the Volturno Plain and the Sele Plain. The Campania Plain is bounded by important normal faults, whose tectonic

activity is concentrated at the margins of the coastal plain. The onshore basin is filled by several thousand of meters of Quaternary sediments and volcanic rocks, emplaced during the eruptive activity of the Vesuvius, Phlegrean Fields and Ischia and Procida volcanic complexes. Different seismo-stratigraphic units have been distinguished, representing the Naples basin filling. The first unit is distinguished by progradational to parallel reflectors, overlying the Meso-Cenozoic carbonates and downthrown by normal faults, probably Early Pleistocene in age. The second unit is represented by a syntectonic wedge, deposited during the tectonic tilting of the carbonate strata pertaining to the acoustic basement and is probably Middle Pleistocene in age. The third unit is distinguished from progradational to parallel seismic reflectors and is probably Late Pleistocene in age. The NE-SW trending horst of the Sorrento Peninsula, which separates the Naples and the Salerno Bays is long (about 20 kilometers) and is characterized by the occurrence of listric faults that downthrow some of the main blocks composed of Meso-Cenozoic units of carbonate platform pertaining northward towards the Southern Apennines.

The Naples Bay, including the Napoli basin, is crossed by two main systems of normal faults, both NE-SW and NW-SE trending, along which the Nisida and Pentapalummo volcanic banks are located. A complex fault system with a NNE-SSW trend offshore the Vesuvius has been individuated in correspondence with the Torre del Greco volcanic structure, representing the offshore prolongation of the volcanic complex.

Chapter 2 - Presence of volcano-sedimentary sequence in pull-apart basins has intrigued the geologists for several decades. We explain that the extensional tectonic processes are not only responsible for formation of these basins but also eruption of volcanic units and emplacement of dykes swarms. High resolution seismic data, processed by Pre-Stacking and Depth Migration (PSDM) and Pre-Stacking and Time Migration (PSTM) techniques and hundreds of drill-hole logs have made on eloquent exposition of basin forming tectonics in different regions of India. Several case studies have also illustrated that the Pre-Cretaceous period is characterized by prolonged extensional tectonics, development of nearly vertical faults, subsidence and formation of basins and sedimentation. With

progressive downward continuation, the faults reached to critical limits to cause decompression melting and rampant outpouring of lava units. These units are inter-layered with fossil bearing sediments from the beginning to the end of Cretaceous. This volcano-sedimentary sequence is logged invariably from different basins in and around peninsular India. It is also logged in Andaman, Male and Lakshadweep basins of Indian Ocean. This sequence also covers entire Bay of Bengal and the Arabian Sea and also forms technical basement for the deposition of uninterrupted Tertiary succession. Processing by PSDM and PSTM techniques have also made it possible to get information about the thickness of volcanic units as well as the sediments below them. Improved resolution has helped to identify several basins with thick Pre-Cretaceous Mesozoic succession and differentiate various litho-units of Tertiary succession. These litho-units have various proportions of limestone, shale and sandstone and are some of the finest source rocks of hydrocarbons.

Mesozoic rocks are more severely deformed mainly by nearly vertical faults and the effects gradually diminish in successive overlying younger Tertiary succession. Most of these faults show upward or downward convergence, intersecting each other in the Oligocene stratigraphic horizon, thus forming an hour-glass structure. The basal portions of these structures are often occupied by oceanic ridges while prolific growth of corals reefs in upper portions. These reef complexes are most favorable for hydrocarbon accumulation and also suggest gradual subsidence of blocks. The study of thickness pattern and facie changes, have also suggested continued extensional tectonics. The tectonic grain of these ocean basins is defined by elongated basins and ridges which have originated at K-T boundary. These sheltered basins were most appropriate sites for deposition of sediments rich in good quality organic matter, as source rock for hydrocarbon generation.

Valuable seismic and drilling data obtained at very high cost, makes it clear that there was long duration extensional tectonic activity, during which sedimentation and spasmodic volcanism gave rise to unique volcano-sedimentary sequence. This study enumerates the mechanism of simultaneous deposition and volcanism due to inter action between

extensional tectonics and decompression melting. Furthermore, the study does not support the idea of hot spot related volcanism in pull-apart basins. Upwelling heat from deeper levels, through innumerable upward bifurcating faults, before the volcanism, provided kitchen for distillation of older sediments. Volcanic units have not only provided trapping mechanism as oil seals in favorable conditions, but also they are excellent reservoir rocks due to initial vesicular nature and later cooling joints.

Chapter 3 - Recent analytical advances mainly concerning to the use of the X-Rays Fluorescence (XRF) technique have improved the data acquisition in sedimentary basins. This method consists of the processes of electrons excitation and energy conversion in the region of the X-Rays photons. It has been widely used in Geosciences to determinate the elements concentration in samples of rocks, minerals, soils, sediments, etc. The installation of one S8 Tiger spectrometer from Bruker Co. happened at LARIN (Ionizing Radiations Laboratory), UNESPetro (Geosciences Center Applied to Petroleum), IGCE-UNESP-Rio Claro (SP), Brazil, with financial support from Petrobras. Two software packages came with the equipment: QuantExpress (for powder analysis) and GeoMaj (for fused beads analysis). In this chapter are reported the results obtained from several essays held with aliquots of a sample of the lithostratigraphic formation known as “Batateira Layers” that occurs in the Araripe Sedimentary Basin, Ceará State, Brazil. The tests were realized with powdered aliquots, considering the oxides often used in geochemical investigations: SiO_2, Al_2O_3, TiO_2, Fe_2O_3, MnO, CaO, MgO, Na_2O, K_2O and P_2O_5. The maximum voltage and current were 50 kV and 50 mA, respectively. The following experimental conditions were adopted: analysis method (Fast, Full and Best), aliquot weight (10g, 8g, 6g, 4g and 2g) and boric acid amount (3.5g and 5g). The most striking variation was for SiO_2, Al_2O_3 and MgO among the investigated parameters. It was possible identify that both the readings method and aliquot weight affected the acquired results. Little or none influence was found in the quantity of boric acid used in the pellets preparation as it was obtained a highly significant Pearson correlation coefficient ($r = 0.98$) among the readings realized with 3.5 g and 5 g.

In: Sedimentary Basins
Editor: Sam Brookes
ISBN: 978-1-53613-922-8

Chapter 1

THE SEDIMENTARY BASINS OF THE NORTHERN CAMPANIA TYRRHENIAN MARGIN (SOUTHERN ITALY): GEOLOGIC EVOLUTION AND ADVANCES IN SEISMIC STRATIGRAPHY

Gemma Aiello, PhD
Institute of Marine and Coastal Environment (IAMC), National Research Council of Italy (CNR), Naples, Italy

ABSTRACT

The sedimentary basins of the northern Campania Tyrrhenian margin have been investigated in detail aimed at studying and reconstructing their Quaternary geologic evolution through seismo-stratigraphic data. The seismo-stratigraphic analysis herein presented regards the sedimentary basins located in the northern Campania continental margin from Monte di Procida to Mondragone. This analysis, carried out using multichannel seismic data of the Zone E, has allowed to infer the subsurface volcanism in the Gaeta Gulf through the identification of a

wide buried volcanic edifice, fossilized by the prograding sequences supplied by the Volturno River. This volcanism seems to be related with the oldest phases of volcanism in the Campania Plain, evidenced by the Parete and Villa Literno volcanic complexes, detected in the subsurface of the Campania Plain onshore. Moreover, the interpreted data have inferred the occurrence of the Meso-Cenozoic acoustic basement in the area between Monte di Procida and Mondragone, composed of the tectonic units pertaining to the Campania-Lucania platform *Auct.*, overlain by Miocene siliciclastic sequences. The Volturno delta has been recognized as distinguished by bottomset, foreset and topset sequences, similarly to the delta deposits of the Mediterranean continental margins.

The stratigraphic and tectonic setting of the Napoli basin has been studied based on the geologic interpretation of a multichannel seismic profile. It is a Pleistocene half-graben which can be compared, from a geodynamic point of view, to the other peri-tyrrhenian basins of the Campania Tyrrhenian margin. The Naples Bay, including the Napoli basin, is a significant part of a belt of coastal tectono-stratigraphic depressions, including the Campania Plain, the Volturno Plain and the Sele Plain. The Campania Plain is bounded by important normal faults, whose tectonic activity is concentrated at the margins of the coastal plain. The onshore basin is filled by several thousand of meters of Quaternary sediments and volcanic rocks, emplaced during the eruptive activity of the Vesuvius, Phlegrean Fields and Ischia and Procida volcanic complexes. Different seismo-stratigraphic units have been distinguished, representing the Naples basin filling. The first unit is distinguished by progradational to parallel reflectors, overlying the Meso-Cenozoic carbonates and downthrown by normal faults, probably Early Pleistocene in age. The second unit is represented by a syntectonic wedge, deposited during the tectonic tilting of the carbonate strata pertaining to the acoustic basement and is probably Middle Pleistocene in age. The third unit is distinguished from progradational to parallel seismic reflectors and is probably Late Pleistocene in age. The NE-SW trending horst of the Sorrento Peninsula, which separates the Naples and the Salerno Bays is long (about 20 kilometers) and is characterized by the occurrence of listric faults that down throw some of the main blocks composed of Meso-Cenozoic units of carbonate platform pertaining northward towards the Southern Apennines.

The Naples Bay, including the Napoli basin, is crossed by two main systems of normal faults, both NE-SW and NW-SE trending, along which the Nisida and Pentapalummo volcanic banks are located. A complex fault system with a NNE-SSW trend offshore the Vesuvius has been individuated in correspondence with the Torre del Greco volcanic structure, representing the offshore prolongation of the volcanic complex.

Keywords: sedimentary basins, geological models, buried volcanic structures, Southern Italy

1. INTRODUCTION

One aim of this chapter is to present a study of the sedimentary basins in the northern Campania offshore, giving new insights into the seismic stratigraphy of some selected sedimentary basins (northern Campania continental margin between Monte di Procida and Mondragone and Napoli basin). Another aim of this chapter is to show the occurrence of buried volcanic structures offshore the North Campania aimed at improving the knowledge on the relationships between the emplacement of these structures and the tectonic activity during the Late Quaternary. This study has taken into account previous knowledge on the geophysical aspects of the volcanic systems offshore the Naples and Castelvolturno area, where important volcanic structures have been previously documented based on integrated seismic and magnetic studies (Aiello et al., 2005; de Alteriis et al., 2006; Paoletti et al., 2008; Aiello et al., 2010; 2011; 2012; Aiello and Marsella, 2015; 2016; Aiello et al., 2016; Paoletti et al., 2016; Passaro et al., 2016).

On the Campania-Latium continental margin transfer zones located in an oblique back-arc basin setting have been recently suggested (Conti et al., 2017). Multichannel seismic profiles, which have been recently collected, have highlighted the geometry and the kinematics of the Pontine escarpment, linking the Campania-Latium continental margin with the Vavilov basin (Kastens et al., 1986; 1988), located in the Tyrrhenian bathyal plain. These seismic data have been collected from offshore Anzio and offshore Gaeta within the Pontine Island. In this area, a steep slope joins the Italian continental margin to the Vavilov basin. A chronostratigraphic calibration of the seismic profiles has been carried out using the lithostratigraphic data of the Michela 1 and Mara 1 exploration wells (http://unmig.sviluppoeconomico.gov.it/videpi), respectively located

in the offshore between Anzio and Capo Circeo and in the Gulf of Gaeta. In this paper, three main unconformities have been interpreted based on previous geological literature on the area (Zitellini et al., 1984; Moussat et al., 1986; Aiello et al., 2000; 2011; Bruno et al., 2000), separating four seismic units (U1, U2, U3 and U4).

The lowest seismic unit is represented by Meso-Cenozoic carbonates, characterized by a discontinuous and chaotic seismic facies and by a scarce penetration of the acoustic energy (Aiello et al., 2000; 2011; Conti et al., 2017) Its top corresponds with an unconformity, representing the acoustic substratum of the area. In the corresponding onshore sectors this unit can be correlated with the carbonate units cropping out in the Lepini and Aurunci, Massico, Zannone and Circeo Mts. (D'Argenio et al., 1973; Bigi et al., 1992).

The overlying seismic unit is represented by Miocene flysch deposits, characterized by a chaotic seismic facies, with scattered and discontinuous reflectors. It can be correlated with the internal flysch deposits of Southern Apennines ("Flysch di Frosinone" *Auct*.; "Flysch del Cilento" *Auct*.; D'Argenio et al., 1973; Parotto and Praturlon, 1975). Its top is represented by a regional unconformity corresponding to the top of the evaporites genetically related to the Messinian salinity crisis. This seismic unit is, in turn, overlain by an Early to Middle Pliocene seismic unit, well displayed in correspondence with the morpho-structural highs, correlating with the Pliocene deposits and characterized by a lower sub-unit, conglomeratic in nature with an acoustically transparent seismic facies and by an upper sub-unit, composed of alternating clays and sands. The overlying seismic unit is characterized by progradational reflectors, indicating the occurrence of deltaic environments with bottomset, foreset and topset sequences (Aiello et al., 2000); its age is Pleistocene. Seismic data interpretation has suggested that the NNE-SSW trending escarpment recognized in the southern part of the Pontine escarpment represents a transfer zone with a right strike-slip component, characterized by normal faults having an echelon geometry (Conti et al., 2017).

The Quaternary geologic and geomorphologic evolution of the coastal plains of Southern Apennines, referring, in particular, to the Campania and

Sele Plains has been reconstructed through the integration of stratigraphic and geomorphologic data (Santangelo et al., 2017). During the Early Quaternary these basins were formed as half-graben basins, genetically related to the Tyrrhenian Sea opening. In these plains the migration of coastal environments has been controlled by the relationships between the extensional tectonics, the sedimentary supply and the eustatic sea level fluctuations (Santangelo et al., 2017). The geomorphologic evolution of the Campania Plain has been controlled by a strong volcaniclastic aggradation.

In this paper, five multichannel seismic lines located in the northern offshore of the northern Campania region between Monte di Procida and Mondragone have been analyzed based on the criteria of seismic stratigraphy. Moreover, the geologic interpretation of a multichannel seismic line has been re-examined (D'Argenio et al., 2004) from a critical point of view in order to constrain the stratigraphic architecture of the Gulf of Naples.

2. GEOLOGIC SETTING

The Gulf of Naples, together with the Campania Plain, represents one of the most important Neogene-Quaternary basins of the peri-Tyrrhenian area. It is located in a sector linking the southern Apennines and the Tyrrhenian Sea, whose tectonic setting is strictly related with the geodynamic evolution of the back-arc basin-Apenninic chain-foredeep system during the Late Neogene and the Quaternary. The extensional processes in the Tyrrhenian area were contemporaneous with compressional tectonic phases, leading to the individuation of the Apenninic chain and to the migration of the foredeep-chain system towards the Apulian foreland (Malinverno and Ryan, 1986; Oldow et al., 1993; Ferranti et al., 1996; Casciello et al., 2006; Patacca and Scandone, 2007). Previous studies have evidenced that the peri-Tyrrhenian area, in particular along the Campania-Latium continental margin, is characterized by the occurrence of sedimentary basins, perpendicular to the chain, individuated

in correspondence to normal faults, having a NE-SW trending (Bartole et al., 1983; Mariani and Prato, 1988; Sacchi et al., 1994; Acocella et al., 1999; Aiello et al., 2000; Milia and Torrente, 2003; Moeller et al., 2013; Conti et al., 2017).

The distribution of outcrops and the geologic evolution of depositional environments of the Late Miocene marine deposits cropping out onshore in the Campania plain (Ortolani and Aprile, 1978) have indicated that, during the Late Miocene, wide areas of the Tyrrhenian basin were characterized by a complex coastal morphology, distinguished from shallow water environments. Large areas of continental shelf then individuated along the Southern Tyrrhenian margin, where the deltaic systems were fed by first Apenninic rivers (proto-Tiber, for instance), bounded at their base by a tectonically-controlled unconformity, which fossilizes the syn-rift seismic sequences (Aiello et al., 2000).

A seismic study of the 41st parallel fault system offshore the Campanian-Latial continental margin has been carried out (Bruno et al., 2000). A set of seismic reflection lines, collected in the Southern Tyrrhenian Sea offshore, has been interpreted. The obtained results have shown that the Campania-Latium continental margin is characterized by a set of structural lows and highs, matching the mainland geological structures (Massico Mt, Volturno and Garigliano depressions).

The study area is characterized by ESE-WNW, E-W and NE-SW normal faults. The activity of these faults mainly developed during the Late Pliocene and the Early Pleistocene. ESE-WNW to E-W faults have displayed geological structures consistent with strike-slip movements. These faults, which are located on the maximum gradient of the E-W elongated magnetic alignment of the 41st parallel fault zone. The relationships among the 41st parallel fault system and the Ortona-Roccamonfina (ORL) line have been studied. The seismic data have indicated that the ORL is older than the 41st parallel line. The normal movements along the ORL faults are consistent with a NW-SE extension, which is responsible for the longitudinal extension in the Southern Apennines belt (Bruno et al., 2000).

2.1. The Parete and Villa Literno Volcanic Complexes

Starting from the Late Miocene the Campania plain has been involved by an intense volcanism, which was concentrated on the western border of the coastal plain and was later controlled, during the Pleistocene, by NE-SW (counter-Apenninic) normal faults (Florio et al., 1999; Rolandi et al., 2003).

The volcanic products of the Campania volcanism can be distinguished into two main cycles. The first cycle ranges in age from Miocene to Pleistocene and is characterized by calcalkaline, andesitic and basaltic lavas. These lavas have been drilled by the Parete 2 and Villa Literno 2 wells and correspond to the Parete and Villa Literno volcanic complexes (Baldi et al., 1976; Barbieri et al., 1976; Di Girolamo et al., 1984; Rosi and Sbrana, 1987; Barberi et al., 1991; Brocchini et al., 2001). Alkaline and potassic products pertain to the younger cycle, genetically related to the Plio-Pleistocene extensional tectonics, which has characterized the Roman co-magmatic province, including the Vesuvius volcano and the Phlegrean Fields volcanic complex.

Since the 1970 the Parete-Villa Literno area has been investigated based on gravimetric data (Maino and Tribalto, 1963a; 1963b). This area is characterized by a positive gravimetric maximum, which was interpreted as a thick buried volcanic complex made of lavas. The Parete volcanic complex was distinguished after the drilling of the corresponding well, suggesting the occurrence of a lava complex overlying a carbonate monocline structure, probably Mesozoic in age.

The stratigraphy of these two important lithostratigraphic wells (Parete and Villa Literno) has been later discussed (Ortolani and Aprile, 1978) and is shown in Figure 1 (Aiello et al., 2011). The Villa Literno well is located westwards of the Parete town. From the top of the well recent pyroclastic products have been drilled, overlying andesitic tuffs having a thickness of about 150 m. These tuffs overlie marine and transitional clastic deposits, having a thickness of about 650 m. At depths ranging between 830 m and 2980 m the well has drilled basalts and andesites alternating with tuffs, for an overall thickness of about 2150 m, which have evidenced the

occurrence of a thick volcanic complex. The maximum depth of the well was reached at 2990 m. The volcanic products probably continued at increasing depths. On the other side, the Parete well has drilled alternating basaltic and andesitic lavas, underlying recent pyroclastic products and clastic deposits, which have a thickness of about 300 m.

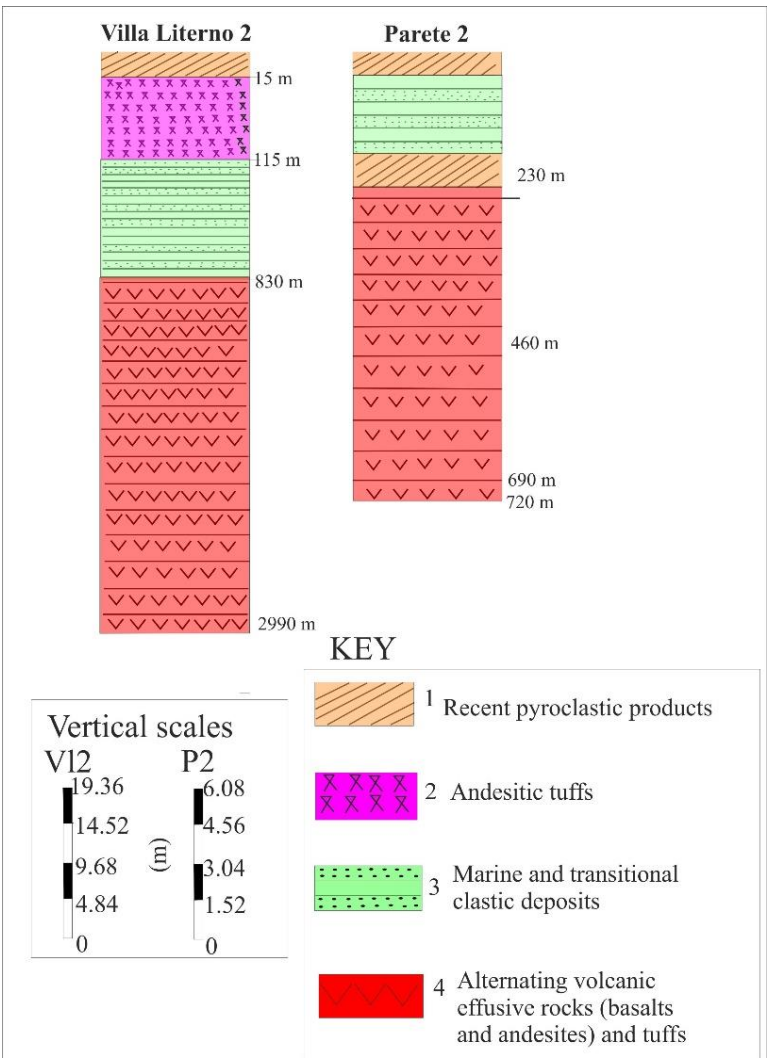

Figure 1. Sketch stratigraphy of the Villa Literno 2 and Parete 2 lithostratigraphic wells (modified after Ortolani and Aprile (1978).

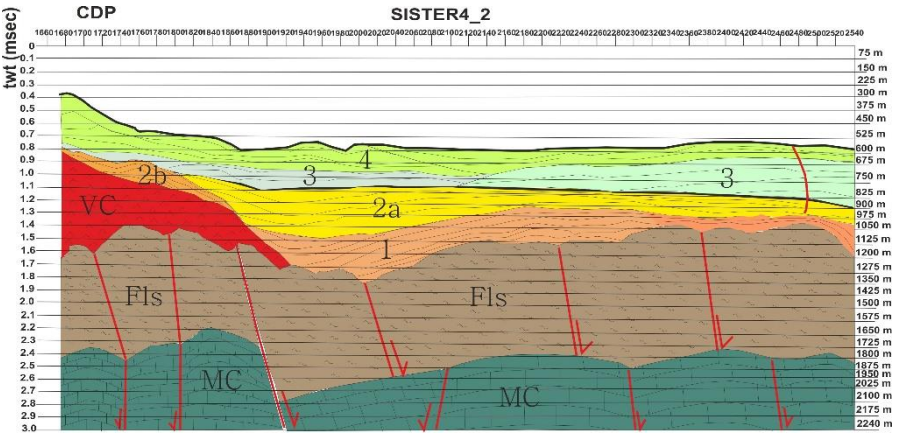

Figure 2. Calibrated geological section in the Volturno basin (modified from Aiello, 2017). Key. MC: Meso-Cenozoic carbonates. FLS: Miocene siliciclastic sequences. VC: Villa Literno volcanic complex. 1, 2a, 2b, 3 and 4: Volturno basin filling.

A calibrated geological section in the Volturno plain has been recently constructed based on seismic and well data (Aiello, 2017; Figure 2). A first group of grounds has been used in order to construct the calibrated geological section, represented by the pyroclastic and alluvial deposits, which have been correlated with the seismic units recognized in the seismic profiles and representing the basin filling of the Volturno Plain. A second group of grounds is represented by andesites and basalts, which have been related with the Villa Literno volcanic complex, previously described and with the seismic unit related to this complex (Aiello, 2017).

Taking into account the lithostratigraphic data of the Cellole Aurunci and Mondragone 1 wells the FLS unit in the calibrated geological section should be related with the Miocene flysch deposits and is composed of alternating shales, sandstones, conglomerates and marly limestones. These deposits are genetically related with the "Flysch di Frosinone" *Auct.* (Parotto and Praturlon, 1975; Bigi et al., 1992).

2.2. The Subsurface Volcanism in the Gaeta Gulf

In the southern Gulf of Gaeta subsurface volcanic edifices have been previously suggested by de Alteriis et al. (2006). A former subaerial

volcanic edifice off the Volturno river, in correspondence with the 41st parallel, where magnetic data constrained by seismic stratigraphy have shown that the whole volcano is fossilized by the prograding wedge supplied by the Volturno river, Middle-Late Pleistocene in age.

Seismic investigation on buried volcanic edifices and on their geophysical aspect is a research theme acquiring an increasing research interest and several studies have been published dealing on these aspects (Herzer, 1995; Sartori et al., 2004; Kerr et al., 2005; Torrente and Milia, 2013; Bischoff et al., 2017; McLean et al., 2017). The seismic stratigraphy of buried volcanic arcs in Northland Peninsula of New Zealand has been deeply studied with respect to its implications on the Neogene subduction. Fifty volcanic edifices, represented both from main volcanoes and small cones have been identified on marine seismic profiles. Volcaniclastic deposits are considered to form distinct seismic sequences, composed of three main elements, including a main body, a sloping apron and a wide and flat ring plain (Herzer, 1995). Accordingly to the methods of the volcanic sequence stratigraphy, the major and intermediate sized volcanic edifices have characteristic morphologies and suites of reflection configurations. In this case, each volcanic sequence is composed of a main body, forming the bulk of the flat topped volcanic cone, of an apron having gently sloping lower flanks and by a ring plain, being the flattest region beyond the apron (Herzer, 1995).

Important volcanic edifices in the Tyrrhenian Sea have been singled out by Sartori et al. (2004) based on multichannel seismic profiles. Two large and elliptical volcanoes are represented by the Magnaghi and Vavilov seamounts, probably Late Pliocene in age and tilted during Late Pleistocene tectonic activity. The Gortani Ridge, located in the Vavilov Basin (Tyrrhenian bathyal plain) is represented by an elongated edifice, emplaced about 4 my ago and composed of basalts of a MORB type, dredged by the ODP site 655 (Beccaluva et al., 1990). Other volcanic edifices are represented by sub-conical volcanoes (Sartori et al., 2004). Volcanic rocks have also been dredged from the Selli Line and the De Marchi seamount, located on both the sides of the Magnaghi Basin and from outcrops located in the North Sicilian Basin and across the Campania margin (Colantoni et al., 1981; Sartori et al., 2004).

The seismic stratigraphy of the Detroit seamount has been characterized with respect to the volcanic edifices occurring at the summit of the seamount (Kerr et al., 2005). Important volcanic edifices have been distinguished in this area, pertaining to the Hawaii islands. They are represented by two peaks or highs in the basement topography and have been interpreted as volcanic cones akin to those documented by Londsdale et al. (1993). Important relationships have been established on the age of the volcanic edifices based on the strata terminations of the surrounding sediments. If the edifices were older than the sediments the seismic horizons are expected to drape or to be concordant with the profile of the volcanic surface (Kerr et al., 2005). This criterion should be considered as valid as a general application to seismo-stratigraphic studies of volcanic edifices.

The volcanic seismic units of the Gaeta Gulf have recently been discussed based on multichannel seismic data (Torrente and Milia, 2013). The chaotic seismic units, interpreted as volcanic in nature, are interstratified with seismic reflectors displaying a good amplitude and continuity and representing the Gaeta basin filling. The geometry of the volcanic units has been analyzed through contour maps of significant seismic horizons and three-dimensional digital models. A volcanic edifice occurs in the central Gaeta Bay. A newly discovered volcanic field has been recognized in the offshore of the Phlegrean Fields and Ischia volcanic complexes, composed of four main volcanic edifices probably emplaced after 0.4 My (Torrente and Milia, 2013).

The size, the elevation and the diameter of the volcanoes detected in the Gulf of Gaeta can be compared with those ones of the Campania margin (Torrente and Milia, 2013). The central edifice recognized in the Gulf of Gaeta corresponds with a two-dimensional mounded edifice, having a three-dimensional geometry of a truncated cone and a height of about 800 m. Its size is comparable with that one of the Vesuvius volcanic edifice (Torrente and Milia, 2013).

The stratigraphy and the architectural elements of a buried volcanic system and their implications for the hydrocarbon exploration have been recently discussed (Bischoff et al., 2017). The emplacement and the burial of volcanoes are controlled by the interactions between the volcanism and

the sedimentation. The fundamental building blocks (*architectural elements*) of a buried volcano and the surrounding sedimentary strata have been studied in order to provide new insights into the knowledge of their relationships with the volcanic systems. Twenty-two individual architectural elements have been characterized and referred to as pre-magmatic, pre-dating the magmatism, syn-magmatic, which are defined by the occurrence of intrusive, eruptive and sedimentary architectural elements and post-magmatic, related with the degradation and the burial of the volcanic structures after the magmatism ceased.

The monogenetic volcanic edifices have been recently studied to understand their feeding systems and the influence of the pre-existing crustal structures on the space and time distribution of these volcanoes (McLean et al., 2017). The seismic data collected on the Ben Nevis structure (Faroe-Shetland Basin, NE Atlantic margin) have shown the occurrence of a laccolith and of a series of branching sills, fed by a central conduit. The monogenetic edifices are distributed around the top of the Ben Nevis structure and have been supplied by a complex network of sills and transgressive sheets (Mclean et al., 2017).

2.3. The Mesozoic Carbonatic Basement

The carbonatic basement, which has been recognized in the interpreted seismic sections, deepens in the western side of the Campania Plain at depths higher than 3 kilometers. Since the age of these deposits ranges from the Miocene and the Quaternary (Cellole Aurunci and Mondragone wells) and taking into account that at the Castelvolturno 1 well Quaternary deposits have been drilled up to a depth of 3 kilometers, it may be supposed that the Miocene sequence, underlying the Meso-Cenozoic carbonates, occur also below the Castelvolturno well (Ippolito et al., 1973; Billi et al., 1997; Aiello et al. 2011, Aiello, 2017). While the carbonate basement has been recognized below the Somma-Vesuvius volcanic complex based on the lithostratigraphic data of the Trecase 1 exploration well (Principe et al., 1997; Brocchini et al., 2001), the geothermal wells

drilled in the Northern Phlegrean Fields have revealed the lacking of this basement.

2.4. The Recent Stratigraphic Studies and Age Dating on the Phlegrean Caldera

The Campi Flegrei Deep Drilling Project (CFDDP) carried out at the INGV- Vesuvius Observatory of Naples has given new insights on the structure of the Phlegrean caldera, its geologic evolution and the corresponding implications in terms of volcanic hazard in the Naples town through the drilling of a new borehole deep about 500 m and the $^{40}Ar/^{39}Ar$ dating of different cores (De Natale et al., 2016). Textural, mineralogical and geochemical data on the cores have been shown by Mormone et al. (2015). The sequence drilled by the well is composed of pyroclastic materials. The first sequence is composed of pumices and scorias coupled with altered lavas and tuffs and has been interpreted as subaerial pyroclastic products including the Agnano-Monte Spina eruption (De Natale et al., 2016). The second sequence, starting to a depth of about 45 m is composed of volcanic materials rich in silica fossils and has been interpreted as a sequence of volcanic and volcaniclastic products deposited in a subaerial and subaqueous environment (De Natale et al., 2016). The third sequence is characterized by a great abundance of gray pumices and gray lithics and has been interpreted as the most recent volcanic products. At depths ranging between 180 m and 250 m a pyroclastic sequence composed of black scorias and glass grains and subordinately of gray pumices and green tuffs has been drilled. It has been interpreted as a pyroclastic sequence overlying the Neapolitan Yellow Tuff (15 ky; Deino et al., 2004). It overlies a level of pumices, dated back to 35.1 ky, which, in turn, overlies a green pyroclastic sequence, extending up to a depth of 450 m. In the basal part of this sequence the Ar-dated feldspars have given an age of 38.5 ky, allowing to interpret this sequence as the Campanian Ignimbrite. The whole lithologic sequence has given radiometric ages ranging between 16.9 +/- 1.1 ky and 47.5 +/- 0.9 ky. These age constraints were useful in order to interpret in detail the collapse of the Phlegrean

caldera and its volcanic evolution. The ages, the microfossil content and the local sea level curve (Antonioli et al., 2004) have been merged to discuss the volcanic evolution. Based on the interpreted data there was a contribution of both the collapse of the CI (Campanian Ignimbrite) and of the NYT (Neapolitan Yellow Tuff). An eruptive vent of the NYT should be located in proximity of the drilling site (De Natale et al., 2016).

2.5. The Neapolitan Yellow Tuff Tephra in the Northern Phlegrean Offshore

The Neapolitan Yellow Tuff (NYT) has been emplaced by a Plinian event happened at Campi Flegrei and dated back to 14.9 +/- 0.4 ky (Deino et al., 2004). The estimated volume of the erupted pyroclastic products is in the order of 45 km^3 DRE (*Dense Rock Equivalent*) and they have overlain a surface of about 1000 km^2. The NYT eruption has determined the formation of a caldera having a diameter of about 10 km. The Gaeta Gulf, at the northern rim of the Campania region, is located northwards of the Campi Flegrei and is comprised in a Plio-Pleistocene basin, related to normal and strike-slip faults genetically related to the evolution of the south-eastern Tyrrhenian Sea (Aiello et al., 2000). In this sector the sedimentation has been strongly influenced by the strong volcanic activity of the Phlegrean Fields during the Late Pleistocene-Holocene. In particular, the volcanic products linked to the NYT eruption have been correlated to a stratigraphic marker correlated in the whole continental shelf (Aiello et al., 2017). Detailed seismo-stratigraphic and tephro-stratigraphic analyses have allowed for the characterization of the examined tephra in the southern sector of the basin located in the Cuma offshore (Aiello et al., 2017). In the studied seismic sections the NYT corresponds to a continuous and parallel seismic reflector on the continental shelf, interlayered in the marine deposits of the transgressive system tract (TST). The depth of the V stratigraphic marker from the sea bottom ranges between 10 and 30 msec (corresponding to 8 to 25 m). The core C1161, drilled at a water depth of 144 m, has recovered 2.62 m of deposits with an estimated compaction of about 15%. The cored sediments

are mainly represented by muds and shales. The seismo-stratigraphic analysis has evidenced that the base of the examined core corresponds to the top of the V reflector. The tephrostratigraphic analysis of the sample drilled at the base of the core has allowed to characterize the upper part of the NYT, both in terms of lithology and chemical composition. Accordingly to the classification of Le Maitre (2005) the composition of the fragments of volcanic glasses extracted from the sample is located along the boundary between trachytes and phonolites and between the tephro-phonolites and the trachytes, forming a continuous compositional trend. The seismo-stratigraphic and tephrostratigraphic analysis of the whole continental shelf is still in course in the whole Gaeta gulf continental shelf. First results regard a core (C9) sampled 30 km seawards of the Garigliano river mouth. The volcanic fraction extracted from a sample cored to 1.60 m from the sea bottom is mainly represented by vesciculated pumices, by fragments of a denser glass and rare lava clasts. The glassy clasts have a composition located along the boundary between the trachytes and the phonolites and between the tephriphonolites and the latites.

3. MATERIALS AND METHODS

Seismic lines interpreted in this chapter has been recorded in the frame of the ViDEPI Project, proposed and directed by the Italian Geological Society (Zone E, Agip Oil Company). The ViDEPI Project has been realized in cooperation with the Ministry of the Economic Development, which has furnished the database and by the Assomineraria (Association of the oil companies active in Italy), which has financed the project.

The ViDEPI project has been carried out accordingly to different steps, listed as it follows. A first step consisted of the finding of the documents deposited in the different offices of the national and regional mineral authority. A second step was the classification and scanning of the founded documents. A third step was the georeferencing of the seismic and well data. During the next step the online publication of the data with a both alpha-numeric and geographic research was carried out. Finally, the

publication of the updating successive than the date of closure of the project was performed.

The seismic data include the seismic profiles progressively realized from the Agip oil company, as an operator funded by the Italian country, when the different areas of the Italian subsurface have been opened to the oil exploration. These zones are indicated with a capital letter from A to G. In particular, in this chapter the seismic lines pertaining to the Zone E have been interpreted (http://unmig.sviluppoeconomico.gov.it/videpi).

The seismic grid interpreted in this chapter consist of 5 seismic lines, whose location has been reported in the following table (Table 1).

Table 1. Seismic lines interpreted in this chapter

Seismic line	Location	Geologic setting
E200	Monte di Procida-Tyrrhenian Sea	Campania continental margin
E198	Marina di Varcaturo– Tyrrhenian Sea	
E196	Marina di Ischitella– Tyrrhenian Sea	
E194	Castelvolturno-Tyrrhenian Sea	
E192	Mondragone-Tyrrhenian Sea	

4. RESULTS

4.1. Geologic Interpretation of the Seismic Line E200

The geologic interpretation of the multichannel seismic profile E200 (Figure 3), having a SE-NW trending and recorded from the Southern Tyrrhenian sea towards the northern Phlegrean offshore has been carried out accordingly to the criteria of seismic stratigraphy (Figure 4). Three main regional unconformities (A, B; C in Figure 4) have been identified and reported on the seismic profile, allowing to distinguish six main seismo-stratigraphic units. These units overlie an undifferentiated acoustic basement, bounded at its top by the A regional unconformity, whose lithologic nature may be only doubtfully inferred based on the time to depth conversion of the observed unconformity and the qualitative correlation of these depths with the lithostratigraphic data of deep

exploration wells onshore. The depths of the A unconformity ranges between 1.4 and 1.8 twt (sec).

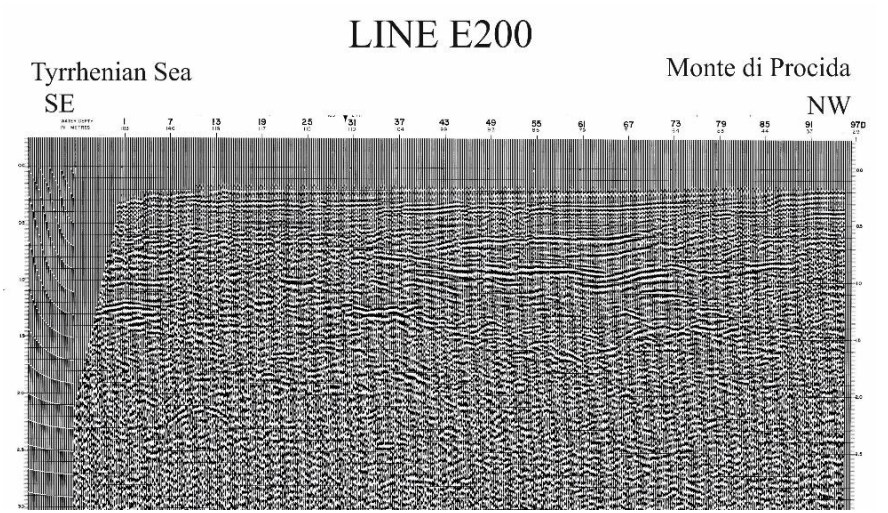

Figure 3. Seismic profile E200, located in the northern Campania offshore from Monte di Procida towards the Tyrrhenian Sea.

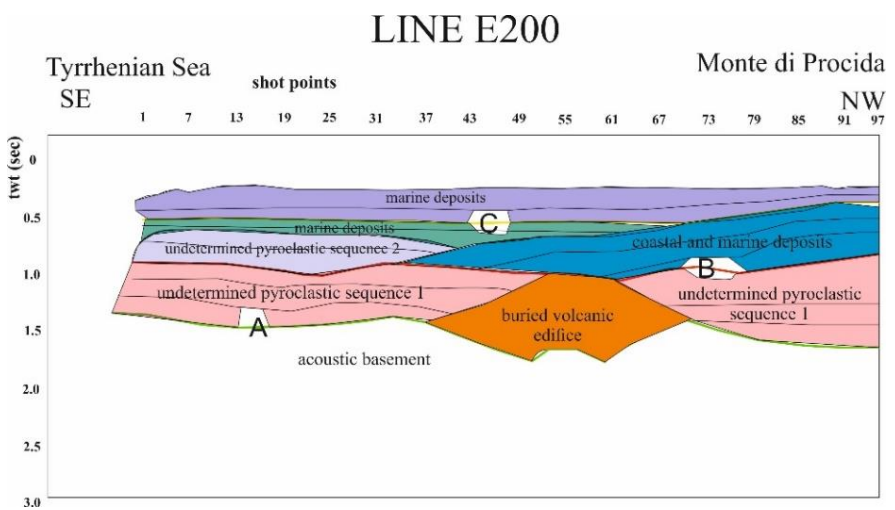

Figure 4. Geological interpretation of the seismic profile E200. Note the occurrence of a buried volcanic edifice, whose flanks are onlapped from an undetermined pyroclastic sequence, which is, in turn, overlain by another pyroclastic sequence and by coastal and marine deposits.

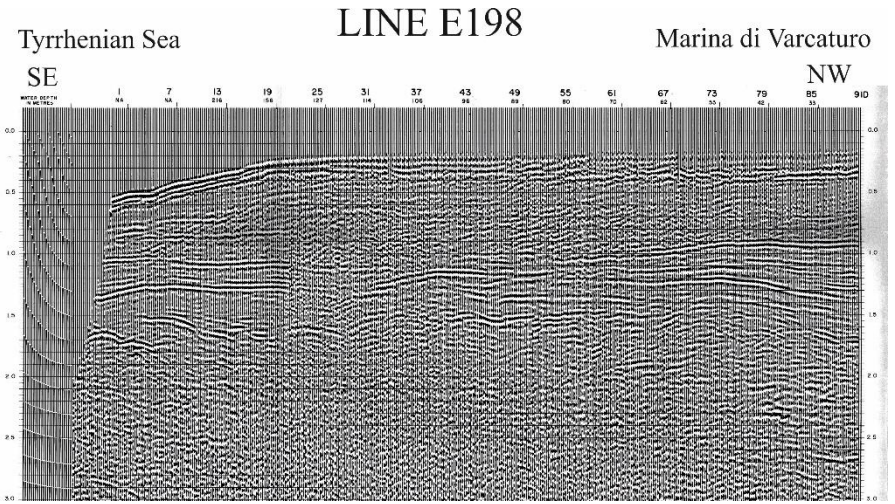

Figure 5. Seismic profile E198 located in the northern Campania offshore from Marina di Varcaturo towards the Tyrrhenian Sea.

Using a inferred velocity of 2500 m/sec the depths have been calculated to be in a depth range between 0,28 km and 0,36 km. These data will be better discussed in the section on the data discussion (see later in the chapter). The first seismic unit is characterized by discontinuous seismic reflectors and by a mounded shaped external geometry. Due to its acoustic characters it has been interpreted as a buried volcanic edifice. The second seismic units is located on both the sides of the first one and is characterized by discontinuous to continuous, sub-parallel seismic reflectors (Figure 3). It has been interpreted as an undetermined pyroclastic unit (Figure 4), the first one (1) detected in the seismic profile. These two units, probably volcanic in nature are bounded above by the second regional unconformity recognized in this seismic profile (B in Figure 4). The B unconformity represents an erosional truncation for the underlying pyroclastic and volcanic sequences, while it represents a downlap surface for the underlying sequence of coastal and marine deposits (Figure 4). On the left in the seismic section a thick seismic unit has been identified, characterized by progradational seismic reflectors, overlying the B unconformity with low angles (Figure 4). This unit is laterally grading into another seismic unit, characterized by a discontinuous and chaotic seismic

facies, which has been interpreted as an undetermined pyroclastic sequence (2). This unit is overlain by another seismic sequence characterized by parallel reflectors, onlapping the underlying unit composed of coastal and marine deposits. The top of this unit is marked by another regional unconformity (C in Figure 4), showing the characteristics of an erosional truncation. The C unconformity is, in turn, overlain by a seismic sequence characterized by parallel reflectors, corresponding with recent marine deposits.

4.2. Geologic Interpretation of the Seismic Line E198

The geologic interpretation of the seismic profile E198 has been performed accordingly to the criteria of seismic stratigraphy- The seismic line crosses the Campania offshore from Marina di Varcaturo (Giugliano in Campania) towards the Tyrrhenian Sea (Figure 5). The interpretation of the multichannel seismic section has allowed to distinguish five main seismic sequences separated by five main regional unconformities (A, B, C, D, E in Figure 6), overlying a Meso-Cenozoic acoustic basement, genetically related with Mesozoic carbonates ("Piattaforma Campano-Lucana" *Auct.*; D'Argenio et al., 1973) and overlying Miocene siliciclastic sequences. This geological structure is characterized by a palaeo-structural high and is laterally down thrown by normal faults having a little throw (Figure 6).

The first seismic sequence is characterized by discontinuous to parallel seismic reflectors. It has been interpreted as an Early Pleistocene marine sequence. It is bounded above by the B unconformity, representing a downlap surface with respect to the overlying seismic sequence. The second seismic sequence is characterized by parallel to slightly inclined seismic reflectors. It has been interpreted as a Middle Pleistocene marine sequence (Figure 6). Similar sequences have been recognized in the Naples Bay based on the geologic interpretation of multichannel seismic profiles (D'Argenio et al., 2004).

The third seismic sequence is characterized by an acoustically-transparent seismic facies. It has been interpreted as an undifferentiated

pyroclastic sequence, which should be genetically related with the eruptive activity of the Phlegrean Fields volcanic complex in the northern Phlegrean Fields offshore. It is bounded at its top by the D unconformity (Figure 6). This sequence is overlain by another seismic sequence, probably pyroclastic in nature, which has been genetically related with the Neapolitan Yellow Tuff (NYT; 15 ky; Deino et al., 2004). The NYT sequence is overlain by another regional unconformity, namely the E unconformity (Figure 6). This unconformity represents the base of another seismic sequence, cropping out at the sea bottom and interpreted as the Holocene marine sequence, characterized by parallel reflectors (Figure 6).

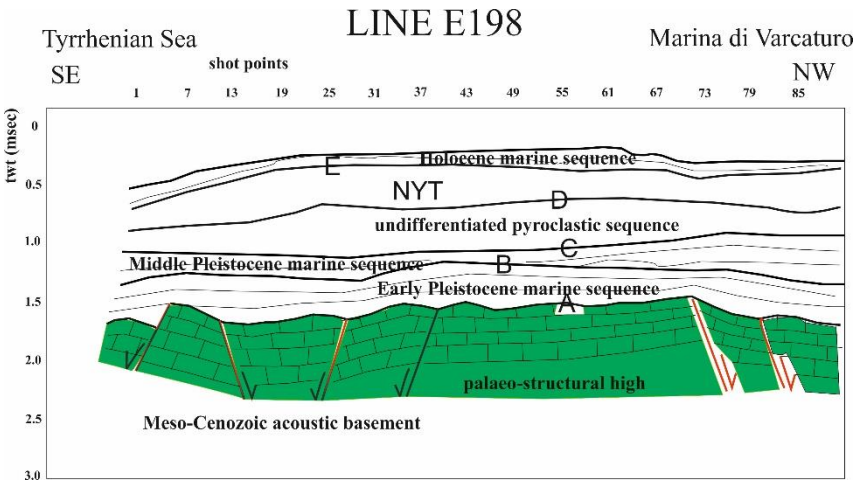

Figure 6. Geological interpretation of the seismic profile E198. Note the occurrence of the Meso-Cenozoic acoustic basement, representing a palaeo-structural high. Early-Middle Pleistocene marine sequences have also been distinguished. They are overlain by an undifferentiated pyroclastic sequence, which is, in turn, overlain by the NYT (Neapolitan Yellow Tuff) deposits. A Holocene marine sequence crops out at the sea bottom.

4.3. Geologic Interpretation of the Seismic line E196

The geologic interpretation of the seismic line E196 has been carried out according to the criteria of seismic stratigraphy. The line is NW-SE trending and runs in the northern Phlegrean offshore from Marina di

Ischitella to the Tyrrhenian Sea (Figure 7). The Meso-Cenozoic carbonate acoustic basement has been identified at depths ranging between 1.3 and 2 sec (twt). It appears to be down thrown by normal faults (Figure 8). The carbonate basement is overlain by a seismic sequence characterized by discontinuous to parallel seismic reflectors, interpreted as an Early-Middle Pleistocene seismic sequence, similar in nature to the sequence already described in the previously mentioned seismic profiles (Figures 7 and 8).

The geological interpretation of this seismic section has clearly shown the Volturno delta system, whose stratigraphic architecture is articulated in four main seismic sequences, such as the bottomset, representing the base of the deltaic complex, two sequences of foreset (foreset 1 and foreset 2), representing the progradational portion of the deltaic system and the topset, representing the upper part of the delta complex (Figure 8).

In the section on the discussion of the data it will be shown that this kind of stratigraphic architecture can be compared with that one of similar deltaic sequences recognized in the Terracina and Gaeta basins (Aiello et al., 2000).

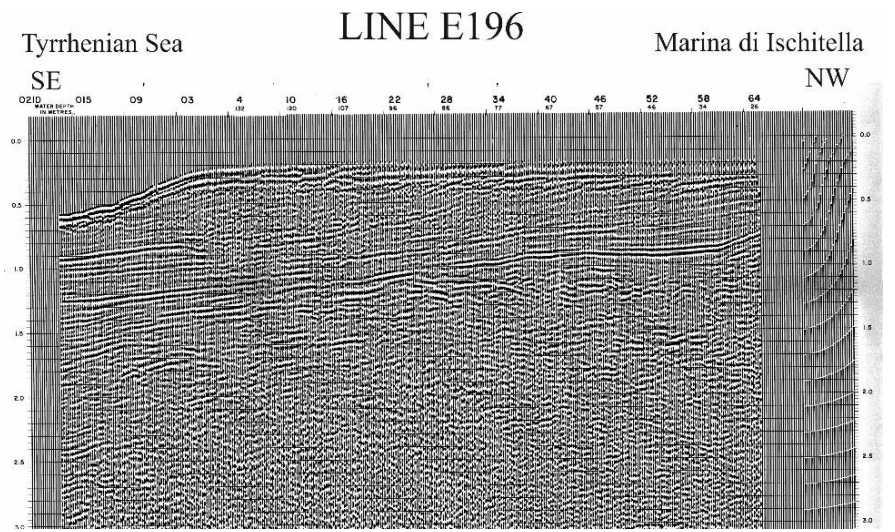

Figure 7. Seismic profile E196 located in the northern Campania offshore from Marina di Ischitella towards the Tyrrhenian sea.

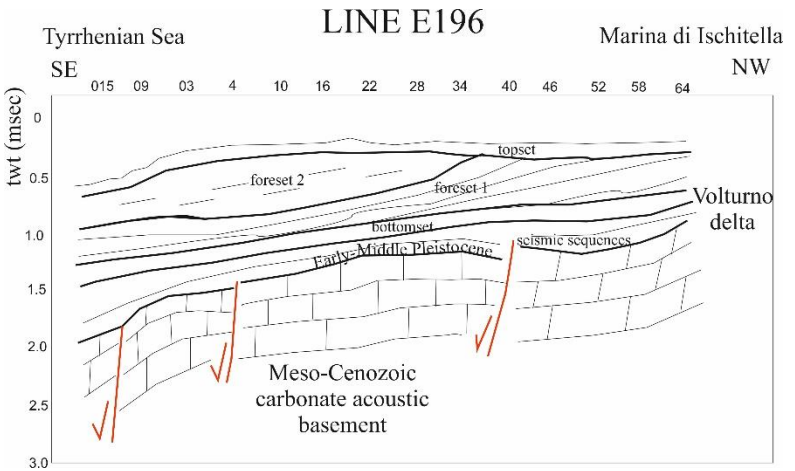

Figure 8. Geological interpretation of the seismic profile E196. Note the occurrence of the Meso-Cenozoic carbonate acoustic basement, overlain by an Early-Middle Pleistocene seismic sequence. The Volturno delta has been interpreted as composed by four main seismic sequences (bottomset, foreset 1, foreset 2, topset).

4.4. Geologic Interpretation of the Seismic Line E194

The geologic interpretation of the seismic line E194 has been carried out accordingly to the criteria of seismic stratigraphy (Figures 9 and 10). The seismic line is located from the Castelvolturno offshore to the Tyrrhenian Sea. A Mesozoic carbonate acoustic basement has been distinguished at depths ranging between 1.2 and 2 sec (twt). This basement, which appears to be strongly down thrown by normal faults is bounded upwards by an erosional unconformity. This erosional unconformity is, in turn, overlain by a syntectonic seismic sequence, whose deposition was probably coeval with the downthrowing of the underlying carbonate basement (Figure 10).

A complete stratigraphic sequence, which is representative of the Volturno delta has been identified based on seismic interpretation. This sequence is composed of a bottomset, of two sequences of foreset (foreset 1 and foreset 2) and finally, by a sequence of topset, which have been distinguished based on the occurring seismic geometries (Figure 10). These

data on the Volturno river delta will be later discussed and compared with the data presented by Amorosi et al. (2012) on the Volturno plain, mainly onshore (Figure 10).

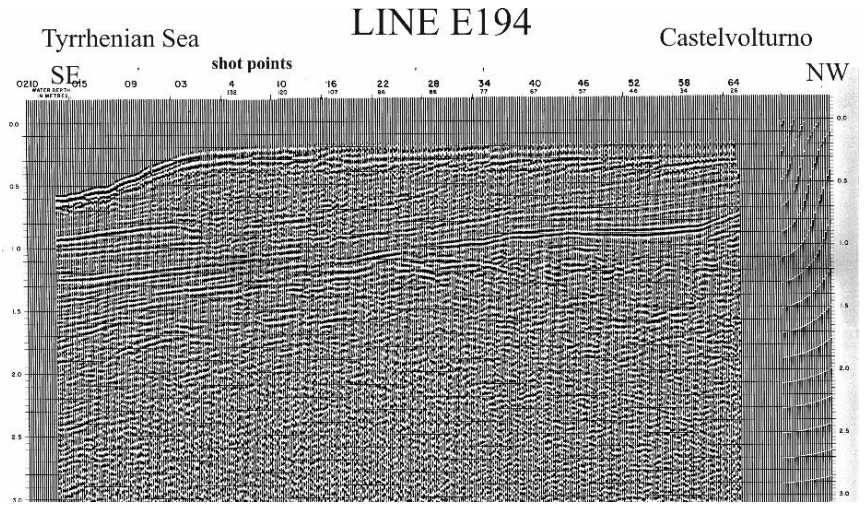

Figure 9. Seismic profile E194 located in the northern Campania offshore from Castelvolturno to the Tyrrhenian Sea.

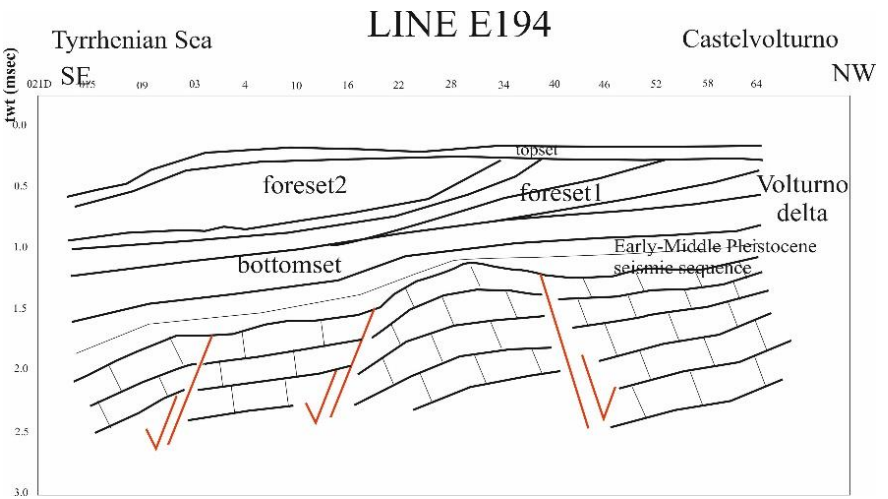

Figure 10. Geological interpretation of the seismic profile E194 (see Figure 8 for the description of the seismo-stratigraphic units).

4.5. Geologic Interpretation of the Seismic Line E192

The seismic line E192 runs from the Mondragone offshore to the Tyrrhenian Sea (Figure 11). Different seismic sequences have been identified on this seismic line accordingly to the criteria of seismic stratigraphy (Figure 12). The Meso-Cenozoic carbonate basement has been distinguished in the seismic section (Figure 12). The acoustic basement is overlain upwards by an erosional unconformity, marking also the base of a syntectonic seismic sequence, characterized by discontinuous seismic reflectors (Figure 12). A buried volcanic edifice has been recognized, which is overlain in onlap by Late Pleistocene marine deposits. The volcanic edifice is characterized by an acoustically transparent seismic unit, related with the occurrence of volcanites and volcaniclastic deposits.

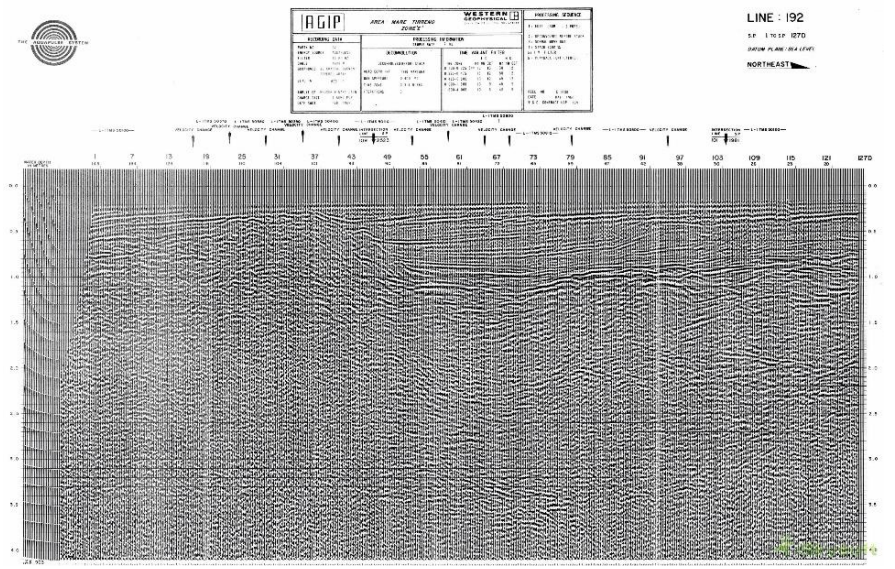

Figure 11. Profilo sismico E192 located in the northern Campania offshore from Mondragone to the Tyrrhenian Sea.

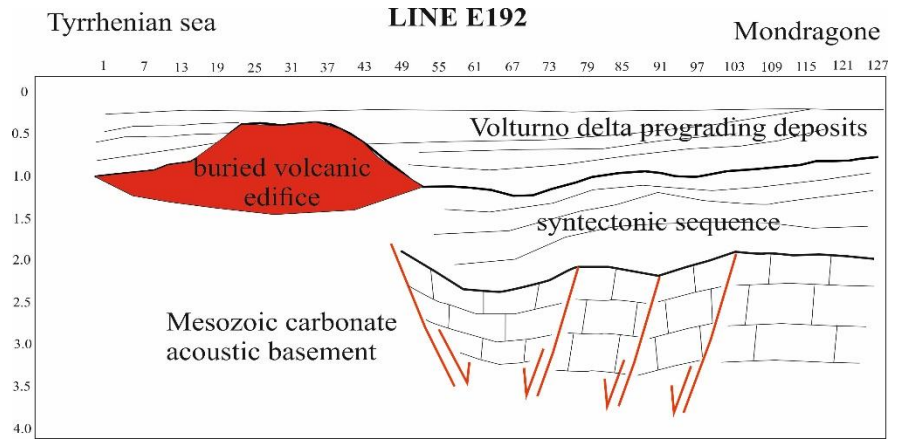

Figure 12. Geological interpretation of the seismic profile E192. A buried volcanic edifice is interstratified in the Volturno delta deposits.

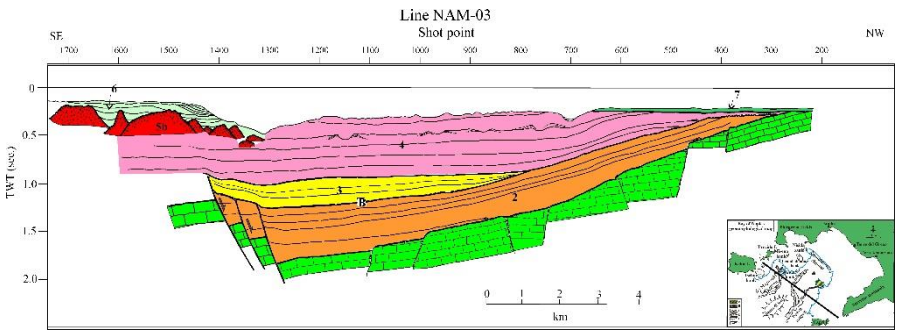

Figure 13. Geological interpretation of the multichannel seismic line NAM3 (see the text for further details).

4.6. Geologic Interpretation of the Multichannel Seismic Line NAM3

Further evidences are given by the interpretation of the regional seismic profile NAM3 (Figure 13), showing the seismo-stratigraphic setting of the area. Several seismic sequences separated by unconformities have been distinguished. The acoustic basement is represented by Meso-Cenozoic platform carbonates (unit 1 in Figure 13), cropping out onshore in the Sorrento Peninsula and in the Capri island and organised as a NW-

dipping monocline. The measured inclinations of the seismic reflectors in the carbonate sequence are of about 6°-7°. Such a values are similar to those shown in outcrops of Meso-Cenozoic carbonates in the Sorrento Peninsula (Perrone, 1988).

The basin filling consists mainly of two prograding wedges (units 2 and 4 in Figure 13), each one characterized by distinctive acoustic patterns and seismic facies. The oldest one (unit 2) is interpreted as a NW dipping relict prograding wedge, formed by siliciclastic deposits, probably Pleistocene in age and occurring offshore the Sorrento Peninsula and the Capri island. Both the Meso-Cenozoic carbonates and the unit 2 have been probably involved by a tectonic tilting during Pleistocene extensional phases of the Sorrento Peninsula, slightly increasing the steepness of the seismic reflectors.

On the continental shelf the seismic reflectors are involved by a main subaerial unconformity (unconformity B in Figure 13), whose areal extension varies from 2-3 kilometres to some hundred of meters proceeding towards the emerged areas. The unconformity B probably indicates a main relative sea-level fall and a strong basinwards shifting of coastal and marine facies, accompanied by sedimentary bypass and strong erosion on the shelf and slope.

Above the unconformity B the clinoforms of the unit 3 (Figure 13) progressively onlaps the slope and basin areas up to the continental shelf. The unit 3 represents a wedge-shaped, transgressive unit, mainly developed in slope and basin settings and probably composed of siliciclastic deposits.

Above the unit 3 a wide prograding wedge (unit 4 in Figure 13) develops: it shows well-preserved offlap breaks and thickens from the shelf towards the slope. This wedge is of notable importance in the study of the stratigraphic architecture of the Bay; it grades laterally, or alternatively is overlain by the volcanic units and is deeply incised by the Dohrn canyon axes. This unit gives origin to relict morphological highs located in the central sector of the Bay, next to the present-day shelf break and northwards of the Dohrn eastern branch. The unit 4 has been probably supplied by the Sarno river mouth during the Middle-Late Pleistocene.

Other feeding sources of the wedge may be represented by siliciclastic deposits produced during erosional phases accompanying the tectonic uplift of the Sorrento Peninsula during Middle-Late Pleistocene.

A wedge-shaped seismic unit, acoustically transparent and volcanic in origin has been recognized (unit 5a in Figure 13). This unit mainly occurs in the eastern sector of the Bay. In particular, it has been well identified offshore the Sorrento Peninsula, where unconformably overlies the Meso-Cenozoic carbonates and/or the seismic unit 2. The same unit has been also identified offshore the Somma-Vesuvius volcanic complex. The top of this unit is often deformed by dome-shaped structures, reaching also kilometric extension. These structures, often corresponding to strong magnetic anomalies are interpreted as buried parasitic vents, genetically related to the Somma-Vesuvius volcanic complex.

5. DISCUSSION

The seismic stratigraphy reconstructed offshore Marina di Varcaturo (Giugliano in Campania) and described in the section on the results is herein compared with a similar seismo-stratigraphic setting, already observed in the Volturno basin (Aiello et al., 2011; Aiello, 2017). The Volturno Basin is filled by four seismic sequences deposited in a marine, coastal and deltaic environment, characterized by frequent intercalations of volcaniclastic levels (Aiello et al., 2011). These sequenze overlie deepest seismic units, genetically related with the Miocene flysch of the central Apennines (“Flysch di Frosinone” Auct.; Aiello et al., 2000) and with the Meso-Cenozoic carbonates of the tectonic units outcropping onshore in the study area (Bigi et al., 1992).

Moreover, the occurrence of a thick seismic unit in the offshore of Marina di Varcaturo, interpreted as the Neapolitan Yellow Tuff (NYT; Deino et al., 2004) may be put in relationships with the new data presented in the Northern Phlegrean offshore with the occurrence of the NYT tephra (Aiello et al., 2017). For the first time, a main volcanic marker has been identified on the continental shelf of the northern Phlegrean Fields in the

Gulf of Gaeta through the geologic interpretation of Subbottom Chirp profiles coupled with the stratigraphic analysis of a core drilled on the continental slope. The geologic interpretation of the seismic lines has shown that the bottom of the core corresponds to a highly continuous seismic reflector (V), which is interstratified within the Transgressive System Tract (TST). In the Northern Phlegrean offshore the TST is thick, if compared with similar deposits of other shelf settings. This high thickness has been probably controlled by the high input of pyroclastic and volcaniclastic deposits controlled by the phases of eruptive activity in the Campania Plain during Late Pleistocene-Holocene (Aiello et al., 2017). The V reflector is located on the continental shelf at different depths, detected from NE to SW and ranging from 10 msec (corresponding to about 8 m) to 30 msec (corresponding to about 25 m) below the sea floor. The seismic reflector may be continuously followed from the continental shelf towards the continental slope. The tephrostratigraphic analysis of this continuous seismic reflector has allowed its correlation with the Neapolitan Yellow Tuff deposits, which was erupted in the Phlegrean Fields 15 ky B.P. (Deino et al., 2004).

Moreover, the volcanic edifice located offshore the Volturno river mouth can be genetically related with the Parete-Villa Literno volcanic complexes, pertaining to the first phases of activity of volcanism in the Campania Plain (Ortolani et al., 1978; Aiello et al., 2011).

CONCLUSION

The Quaternary geologic evolution of some sedimentary basins located on the Tyrrhenian margin offshore the northern Campania has been reconstructed through the techniques of seismic stratigraphy. In particular, the seismo-stratigraphic analysis presented in this chapter deals with the sedimentary basins located in the offshore between the promontory of Monte di Procida and the town of Mondragone.

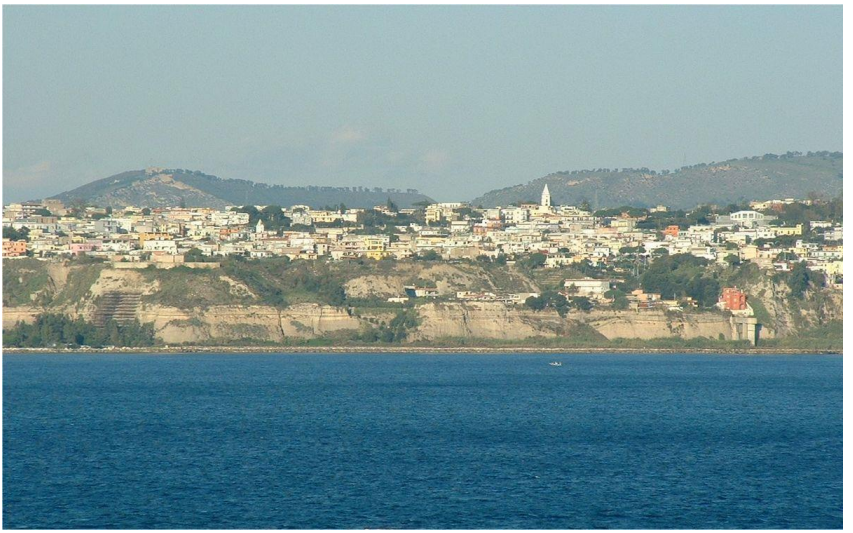

Figure 14. The Promontory of Monte di Procida. Note the occurrence of different paleosols in the volcanic succession cropping out in the corresponding sea cliff.

The Promontory of Monte di Procida (Figure 14) is characterized by the occurrence of a high sea cliff, which exposes a sequence of pyroclastic deposits erupted between 27 and 14 ky by different surrounding eruptive centres (Miliscola, Torrefumo, Torregaveta and S. Martino; Rosi and Sbrana, 1987), as well as by two volcanoes of Procida (Fiumicello and Solchiaro; Fedele et al., 2012). The seismo-stratigraphic setting of the surrounding offshore appears to be dominated by both volcanic, pyroclastic and sedimentary seismic units, as depicted by the interpretation of the seismic line E200 (Figure 4). In particular, a wide buried volcanic edifice, genetically related with the Phlegrean volcanic complex, has been identified (Figure 4). Both the flanks of the volcanic edifice are overlain in onlap by undetermined pyroclastic sequences, probably deposited during the activity of the Phlegrean Fields and Procida island volcanic complexes. These volcanic and pyroclastic sequences are overlain by coastal and marine deposits, characterized by progradational geometries, which have been probably supplied during the eruptive phases occurring in the northern Phlegrean volcanic complex. Perhaps, it should be inferred that

these phases have controlled the stratigraphic architecture of the continental shelf.

Moreover, the seismo-stratigraphic analysis presented in this chapter has confirmed the occurrence of an important subsurface volcanism in the Gaeta Gulf through the identification of a large volcanic edifice, which has been fossilized by the prograding sequences supplied by the Volturno River (Figure 12). This volcanic edifice is located in the Mondragone offshore (Figure 12). This volcanism seems to be related with the oldest phases of volcanism in the Campania Plain and genetically related with the Parete and Villa Literno volcanic complexes, which have been detected in the subsurface of the Campania Plain onshore.

The interpreted seismic data have inferred the occurrence of the Meso-Cenozoic acoustic basement in the area between Monte di Procida and Mondragone, composed of the tectonic units pertaining to the Campania-Lucania platform *Auct.*, overlain by Miocene siliciclastic sequences. The Volturno delta has also been recognized as distinguished by bottomset, foreset and topset sequences, similarly to the numerous delta deposits of the Mediterranean continental margins (Nelson and Maldonado, 1990; Stanley and Warne, 1994; Arnaud Fassetta and Provansal, 1999; Cattaneo et al., 2003; Bruckner et al. 2005; Maselli et al., 2011). The Volturno delta started to individuate at about 6.5 ky, accompanied by the progradation of the adjacent coastal plain, ranging between 3 and 6 km (Barra et al., 1996; Bellotti, 2000; Romano et al., 2004; Amorosi et al., 2012; Sacchi et al., 2014).

The geologic interpretation of a multichannel seismic profile located in the Naples Bay has been re-examined from a critical point of view (Figure 13). This profile has shown the stratigraphic and tectonic setting of the bay, which is characterized by the occurrence of different seismo-stratigraphic units, ranging from the Meso-Cenozoic carbonates and the Late Pleistocene prograding sequences. The Naples Bay is represented by a Pleistocene half-graben and is included in a significant belt of coastal tectono-stratigraphic depressions, including the Campania Plain, the Volturno Plain and the Sele Plain. Significant fault systems bound the Campania Plain, whose tectonic activity is concentrated at the margins of

the bay itself. In the Naples Bay the onshore basin is filled by Quaternary sediments and volcanic rocks, emplaced during the eruptive activity of the Vesuvius, Phlegrean Fields and Ischia and Procida volcanic complexes, thick about several thousand of meters. The Naples basin filling is characterized by different seismo-stratigraphic units. The first unit is distinguished by progradational to parallel reflectors, overlying the Meso-Cenozoic carbonates and downthrown by normal faults, probably Early Pleistocene in age. The second unit is represented by a syntectonic wedge, deposited during the tectonic tilting of the carbonate strata pertaining to the acoustic basement and is probably Middle Pleistocene in age. The third unit is distinguished from progradational to parallel seismic reflectors and is probably Late Pleistocene in age. The NE-SW trending horst of the Sorrento Peninsula, which separates the Naples and the Salerno Bays is long about 20 kilometers and is characterized by the occurrence of listric faults, which downthrow towards north some main blocks composed of Meso-Cenozoic units of carbonate platform pertaining to the Southern Apennines.

REFERENCES

Acocella V., Funiciello R. (1999) The interaction between regional and local tectonics during resurgent doming: the case of the island of Ischia, Italy. *Journal of Volcanology and Geothermal Research*, 88, 109-123.

Aiello G. (2017) The Volturno Basin (Southern Italy): insights into the seismo-stratigraphy and structure of the Campania Plain (Southern Italy). *Horizons in Earth Science Research*, 17, Nova Science Publishers, Hauppauge, New York, USA.

Aiello G., Marsella E. (2015) Interactions between Late Quaternary volcanic and sedimentary processes in the Naples Bay, Southern Tyrrhenian Sea. *Italian Journal of Geosciences*, 134 (2), 367-382.

Aiello G., Marsella E. (2016) Magnetic Theory and Applications in the Naples Bay (Southern Tyrrhenian Sea, Italy): Magnetic Anomaly

Fields and Relationships with Morpho-structural lineaments. *World Journal of Condensed Matter Physics*, 6, 183-216.

Aiello G., Marsella E., Sacchi M. (2000) Quaternary structural evolution of Terracina and Gaeta basins (Eastern Tyrrhenian margin, Italy). *Rendiconti Lincei*, 11, 41-58.

Aiello G., Angelino A., D'Argenio B., Marsella E., Pelosi N., Ruggieri S., Siniscalchi A. (2005) Buried volcanic structures in the Gulf of Naples (Southern Tyrrhenian sea, Italy) resulting from high resolution magnetic survey and seismic profiling. *Annals of Geophysics*, 48 (6), 883-897.

Aiello G., Marsella E., Ruggieri S. (2010) Three-dimensional magneto-seismic reconstruction of the 'Torre del Greco' submerged volcanic structure (Naples Bay, Southern Tyrrhenian Sea, Italy): Implications for Vesuvius's marine geophysics and volcanology. *Near Surface Geophysics*, 8, 17-31.

Aiello G., Cicchella A.G., Di Fiore V., Marsella E. (2011) New seismo-stratigraphic data of the Volturno Basin (northern Campania, Tyrrhenian margin, southern Italy): implications for tectono-stratigraphy of the Campania and Latium sedimentary basins. *Annals of Geophysics*, 54 (3), 265-283.

Aiello G., Marsella E., Passaro S. (2012) Stratigraphic and structural setting of the Ischia volcanic complex (Naples Bay, southern Italy) revealed by submarine seismic reflection data. *Rendiconti Lincei*, 23 (4), 387-408.

Aiello G., Giordano L., Giordano F. (2016) High-resolution seismic stratigraphy of the Gulf of Pozzuoli (Naples Bay) and relationships with submarine volcanic setting of the Phlegrean Fields volcanic complex. *Rendiconti Lincei*, 27 (4), 775-801.

Aiello G., Insinga D.D., Iorio M., Meo A., Senatore M.R. (2017) On the occurrence of the Neapolitan Yellow Tuff tephra in the Northern Phlegraean Fields offshore (Eastern Tyrrhenian margin; Italy). *Italian Journal of Geosciences*, 136 (2), 263-274.

Amorosi A., Pacifico A., Rossi V., Ruberti D. (2012) Late Quaternary incision and deposition in an active volcanic setting: the Volturno valley fill, southern Italy. *Sedimentary Geology*, 282, 307-320.

Antonioli F., Bard E., Potter E.K., Silenzi S., Improta S. (2004) 215-ka history of sea-level oscillations from marine and continental layers in Argentarola Cave speleothems (Italy). *Global and Planetary Change*, 43, 57-78.

Arnaud-Fassetta G., Provansal M. (1999) High frequency variations of water flux and sediment discharge during the Little Ice Age (1586–1725 AD) in the Rhône Delta (Mediterranean France). Relationship to the catchment basin. In: Garnier J., Mouchel JM. (eds) *Man and River Systems. Developments in Hydrobiology*, vol 146. Springer, Dordrecht.

Baldi, P., G.M. Cameli, B. D'Argenio, A. Oliveri Del Castillo, T. Pescatore, L. Puxeddu, A. Rossi and B. Toro (1976) Geothermal research in Western Campania (Southern Italy): a revised interpretation of the Qualiano-Parete structure, In: *Proc. of the Int. Conf. Thermal Waters, Geothermal Energy and Volcanism of the Mediterranean Area*, Athens.

Barberi F., Innocenti L., Lirer L., Munno R., Pescatore T., Santacroce R. (1978) The Campanian Ignimbrite: a major prehistoric eruption in the Neapolitan area (Italy). *Bulletin of Volcanology*, 41 (1), 10-31.

Barberi F., Cassano E., La Torre P., Sbrana A. (1991) Structural evolution of Campi Flegrei caldera in light of volcanological and geophysical data. *Journal of Volcanology and Geothermal Research*, 48 (1-2), 33-49.

Barbieri M., Di Girolamo P., Locardi E., Lombardi G., Stanzione D., Nicoletti M. (1976) Geothermal research in Western Campania (Italy): stratigraphy of the Parete exploratory well and new data on the volcanic sequence. In: *Proceedings of the International Conference Thermal Waters, Geothermal Energy and Volcanism of the Mediterranean area*, Athens.

Barra D., Romano P., Santo A., Campajola L., Roca V., Tuniz C. (1996) The versilian transgression in the Volturno river plain (Campania,

southern Italy): palaeoenvironmental history and chronological data. *Il Quaternario*, 9, 445-458.

Bartole R., Savelli C., Tramontana M., Wezel F.C. (1983) Structural and sedimentary features in the Tyrrhenian margin off Campania, Southern Italy. *Marine Geology*, 55, 163-180.

Beccaluva L., Bonatti E., Dupuy C., et al. (1990) Geochemistry and mineralogy of volcanic rocks from the ODP Sites 650, 651, 655 and 654 in the Tyrrhenian Sea. *Proceedings of the Ocean Drilling Program. Scientific Results* 107, 49 – 74.

Bellotti P. (2000) Il modello morfosedimentario dei maggiori delta tirrenici italiani. *Bollettino della Società Geologica Italiana*, 119, 777-792.

Bigi G., Cosentino D., Parotto M., Sartori R., Scandone P. (1992) *Structural model of Italy Scale 1:500.000*. CNR Progetto Finalizzato Geodinamica, Italy.

Billi A., Bosi V., De Meo A. (1997) Structural characterization of Mount Massico in the framework of the Quaternary evolution of the coastal depressions of the Garigliano and Volturno rivers (northern Campania, Italy). *Italian Journal of Quaternary Sciences*, 10 (1), 15-26.

Bischoff A.P., Nicol A., Beggs M. (2017) Stratigraphy of architectural elements in a buried volcanic system and implications for hydrocarbon exploration. *Interpretation*, Ahead of Print, pp. 1-52.

Brocchini D., Principe C., Castradori D., Laurenzi M.A., Gorla L. (2001) Quaternary evolution of the southern sector of the Campanian Plain and early Somma-Vesuvius activity: insights from the Trecase 1 well. *Mineralogy and Petrology*, 73 (1-3), 67-91.

Bruckner H., Vott A., Schriever A., Handl M. (2005) Holocene delta progradation in the eastern Mediterranean – case studies in their historical context. *Mediterranée*, 104, 95-106.

Bruno P.P.G., Di Fiore V., Ventura G. (2000) Seismic study of the 41st parallel fault system offshore the Campanian-Latial continental margin, Italy. *Tectonophysics*, 324, 37-55.

Bruno P.P.G., de Alteriis G., Florio G. (2002) The western undersea section of the Ischia volcanic complex (Italy, Tyrrhenian sea) inferred

by marine geophysical data. *Geophysical Research Letters*, 29 (9), doi 10.1029/2001GL013904.

Casciello E., Cesarano M., Pappone G. (2006) Extensional detachment faulting on the Tyrrhenian margin of the southern Apennines contractional belt (Italy). *Journal of the Geological Society of London*, 163, 617-629.

Cattaneo A., Correggiari A, Langone L., Trincardi F. (2003) The late-Holocene Gargano subaqueous delta, Adriatic shelf: sediment pathways and supply fluctuations. *Marine Geology*, 193 (1-2), 61-91.

Cinque A., Aucelli P.P.C., Brancaccio L., Mele R., Milia A., Robustelli G., Romano P., Russo F., Russo M., Santangelo N., Sgambati D. (1997) Volcanism, tectonics and recent geomorphological change in the Bay of Napoli. *Supplementi Geografia Fisica Dinamica Quaternaria*, 3, 123-141.

Colantoni P., Fabbri A., Gallignani P., Sartori R., Rehault J.P. (1981) *Carta litologica e stratigrafica dei mari italiani.* [Lithological and stratigraphic map of the Italian seas.] Litografia Artistica Cartografica, Firenze, Italy.

Conti A., Bigi S., Cuffaro M., Doglioni C., Scrocca D., Muccini F., Cocchi L., Ligi M., Bortoluzzi G. (2017) Transfer zones in an oblique back-arc basin setting: Insights from the Latium-Campania segmented margin (Tyrrhenian sea). *Tectonics*, 36, 78-107.

D'Argenio B., Pescatore T., Scandone P. (1973) Schema geologico dell'Appennino meridionale. [Geological scheme of the southern Apennines.] *Atti del Convegno "Moderne vedute sulla geologia dell'Appennino", Accademia Nazionale dei Lincei*, Quaderno 183, 49-72.

D'Argenio B., Aiello G., de Alteriis G., Milia A., Sacchi M. et al. (2004) Digital Elevation Model of the Naples Bay and adjacent areas, Eastern Tyrrhenian Sea. In: *Mapping Geology in Italy* E. Pasquarè & G. Venturini (Eds.), APAT, National Geological Survey of Italy, Spec. Vol. SELCA, Florence, 22-28.

De Alteriis G., Fedi M., Passaro S., Siniscalchi A. (2006) Magneto-seismic interpretation of subsurface volcanism in the Gulf (Italy, Tyrrhenian Sea). *Annals of Geophysics*, 49 (4/5), 929-943.

Deino A.L., Orsi G., Piochi M., De Vita S. (2004) The age of the Neapolitan Yellow Tuff caldera-forming eruption (Campi Flegrei caldera – Italy) assessed by $^{40}Ar/^{39}Ar$ dating method. *Journal of Volcanology and Geothermal Research*, 133, 157-170.

De Natale G., Troise C., Mark D., Mormone A., Piochi M., Di Vito M.A., Isaia R., Carlino S., Barra D., Somma R. (2016) The Campi Flegrei Deep Drilling Project (CFDDP): New insight on caldera structure, evolution and hazard implications for the Naples area (Southern Italy). *Geochemistry, Geophysics, Geosystems*, 17, 4836-4847.

Di Girolamo P., Ghiara M.R., Lirer L., Munno R., Rolandi G., Stanzione D. (1984) Vulcanologia e petrologia dei Campi Flegrei. [Volcanology and petrology of the Phlegraean Fields.] *Bollettino della Società Geologica Italiana*, 103, 349-370.

Fedele L., Morra V., Perrotta A., Scarpati C., Sbrana A., Putignano M.L., Orrù P., Schiattarella M., Aiello G., Budillon F., Conforti A., D'Argenio B. (2012) Note illustrative della carta geologica scala 1:10.000 Fogli 465 e 464 Isola di Procida. [Illustrative notes of the geological map 1: 10.000 scale Sheet 465 and 464 Isola di Procida.] *Note illustrative alla cartografia geologica in scala 1:10.000, ISPRA, Servizio Geologico d'Italia*, Roma.

Ferranti L., Oldow J.S., Sacchi M. (1996) Pre-Quaternary deformation orogen-parallel extension in the Southern Apennine belt, Italy. *Tectonophysics*, 260, 247-325.

Fitsimmons K.E., Hambach U., Veres D., Iovita R. (2013) The Campanian Ignimbrite Eruption: New Data on Volcanic Ash Dispersal and Its Potential Impact on Human Evolution. *PloS One*, 8 (6), e65839.

Florio G., Fedi M., Cella F., Rapolla A. (1999) The Campanian Plain and Phlegrean Fields: structural setting from potential field data. *Journal of Volcanology and Geothermal Research*, 91 (2/4), 361-379.

Forcella F., Gnaccolini L., Vezzoli L. (1981) I depositi piroclastici del settore sud-orientale dell'isola d'Ischia. [Pyroclastic deposits in the

south-eastern area of the island of Ischia.] *Rivista Italiana Paleontologia Stratigrafia*, 89, 1-35.

Gillot P.Y., Chiesa S., Pasquarè G., Vezzoli L. (1982) 33.000 yr. K/Ar dating of the volcano-tectonic horst of the isle of Ischia, Gulf of Naples. *Nature*, 229, 242-245.

Herzer R.H. (1995) Seismic stratigraphy of a buried volcanic arc, Northland, New Zealand and implications for Neogene subduction. *Marine and Petroleum Geology*, 12 (5), 511-531.

Ippolito F., Ortolani F., Russo M. (1973) Struttura marginale tirrenica dell'Appennino Campano: Reinterpretazione di dati di antiche ricerche di idrocarburi. *Memorie della Società Geologica Italiana*, 12, 227–250. [Marginal Tyrrhenian structure of the Campanian Apennines: Reinterpretation of ancient hydrocarbon research data. *Memories of the Italian Geological Society*]

Kastens K., Mascle J., Auroux C., Bonatti E., Broglia C., Channell J., Curzi P., Emeis K.C., Glacon G., Asegawa S., Hieke W., Mascle G., McCoy F., McKenzie J., Mendelson J., Muller C., Rehault J.P., Robertson A., Sartori R., Sprovieri R., Tori M. (1988) ODP Leg 107 in the Tyrrhenian sea: insights into passive margin and back-arc basin evolution. *GSA Bulletin*, 100, 1140-1156.

Kerr B.C., Scholl D.W., Klemperer S.L. (2005) Seismic stratigraphy of Detroit Seamount, Hawaiian-Emperor seamount chain: post-hot-spot shield-building volcanism and deposition of the Meiji drift. *Geochemistry, Geophysics, Geosystems*, 6 (7), doi 10.1029/2004G C000705.

Le Maitre R.W. (2005) *Igneous Rocks: A Classification and Glossary of Terms. Recommendations of the International Union of Geological Sciences Subcommission on the Systematics of Igneous Rocks.* Cambridge University Press, Cambridge.

Maino A., Segre A.G., Tribalto G. (1963a) Risultati ed interpretazioni del rilevamento gravimetrico della zona flegreo-vesuviana e dell'Isola d'Ischia. *Atti XIII Convegno dell'Associazione Geofisica Italiana*, Roma. [Results and interpretations of the gravimetric survey of the

Phlegrean-Vesuvian area and of the Island of Ischia. *Acts XIII Convention of the Italian Geophysical Association*]

Maino A., Segre A.G., Tribalto G. (1963b) Rilevamento gravimetrico dei Campi Flegrei e dell'isola d'Ischia. *Annali dell'Osservatorio Vesuviano*, series 6, vol V. [Gravimetric survey of the Phlegraean Fields and the island of Ischia. *Annals of the Vesuvian Observatory*]

Malinverno A., Ryan W.B.F. (1986) Extension in the Tyrrhenian sea and shortening in the Apennines as a result of arc migration driven by sinking of the lithosphere. *Tectonics*, 5, 227-245.

Mariani M., Prato R. (1988) I bacini neogenici costieri del margine tirrenico: Approccio sismico-stratigrafico. *Memorie della Società Geologica Italiana*, 41, 519-531. [Stratigraphic approach. *Memories of the Italian Geological Society*]

Maselli V., Hutton E.W., Kettner A.J., Syvitski J.P.M., Trincardi F. (2011) High-frequency sea level and sediment supply fluctuations during Termination I: An integrated sequence-stratigraphy and modeling approach from the Adriatic sea (Central Mediterranean). *Marine Geology*, 287 (1-4), 54-70.

McLean C.E., Schofield N., Brown D.J., Jolley D.W., Reid A. (2017) 3D seismic imaging of the shallow plumbing system beneath the Ben Nevis Monogenetic Volcanic Field: Faroe-Shetland Basin. *Journal of the Geological Society*, doi 10.1144/jgs2016-118.

Milia A., Torrente M.M. (2003) Late Quaternary volcanism and transtensional tectonics in the Bay of Naples, Campanian continental margin, Italy. *Mineralogy and Petrology*, 79, 49-65.

Moeller S., Grevemeyer C., Ranero R., Berndt C., Klaeschen D., Sallares D., Zitellini N., De Franco R. (2013) Early stage rifting of the northern Tyrrhenian Sea Basin: results from a combined wide angle and multichannel seismic study. *Geochem. Geophys. Geosyst*., 14, 3032–3052, doi: 10.1002/ggge.20180.

Mormone A., Troise C., Piochi M., Balassone G., Joachimski M., De Natale G. (2015) Mineralogical, geochemical and isotopic features of tuff from the CFDDP 506 m hole: Hydrothermal activity in the eastern

side of the Campi Flegrei volcano (southern Italy). *Journal of Volcanology and Geothermal Research*, 290, 39-52.

Moussat E., Angelier J., Mascle G., Rehault J.P. (1986) L'ouverture de la Mer Tyrrhenienne et la tectonique de faille neogene quaternaire en Calabre. [The opening of the Tyrrhenian Sea and the quaternary neogene fault tectonics in Calabria.] *Giornale di Geologia*, 48, 63-75.

Nelson C.H., Maldonado A. (1990) Factors controlling late Cenozoic continental margin growth from the Ebro Delta to the western Mediterranean deep sea. *Marine Geology* 95 (3-4), 419-440.

Oldow J. S., D'Argenio B., Ferranti L., Pappone G., Marsella E., Sacchi M. (1993) Large-scale longitudinal extension in the southern Apennines contractional belt, Italy. *Geology*, 21, 1123-1126.

Ortolani F., Aprile F., 1978. Nuovi dati sulla struttura profonda della Piana Campana a sud est del fiume Volturno. *Bollettino della Società Geologica Italiana*, 97, 591-608. [New data on the deep structure of the Piana Campana to the southeast of the Volturno River. *Bulletin of the Italian Geological Society*]

Paoletti V., Rapolla A., Secomandi M. (2008) Magnetic signature of submarine volcanoes in the Phlegrean Fields-Ischia Ridge (North-Western side of the Bay of Naples, Southern Italy). *Annals of Geophysics*, 51 (4), 575-584.

Paoletti V., Passaro S., Fedi M., Marino C., Tamburrino S., Ventura G. (2016) Sub-circular conduits and dikes offshore the Somma-Vesuvius volcano revealed by magnetic and seismic data. *Geophysical Research Letters*, doi 10.1002/2016GL070271.

Parascandola A. (1924) I crateri dell'Isola di Procida. *Bollettino Società Naturalisti in Napoli*, 40, 36, 57-60. [The craters of the Island of Procida. *Bulletin Naturalists Society in Naples*]

Parotto M., Praturlon A. (1975) *Geological summary of Central Apennines*. CNR; Quaderni De la Ricerca Scientifica, Roma, 90, 257-311.

Passaro S., Tamburrino S., Vallefuoco M., Gherardi S., Sacchi M., Ventura G. (2016) High-resolution morpho-bathymetry of the Gulf of Naples, Eastern Tyrrhenian Sea. *Journal of Maps*, 12, 203-210.

Patacca E., Scandone P. (2007) Geology of the Southern Apennines. In: Mazzotti, A., Patacca, E., Scandone, P. (Eds.), Results of the CROP Project Sub-project CROP-04 Southern Apennines (Italy), *Bollettino della Società Geologica Italiana* [*Italian Journal of Geoscience*] special issue 7, 75-119.

Rolandi G., Bellucci F., Heizler M.T., Belkin H.E., De Vivo B. (2003) Tectonic controls on the genesis of ignimbrites from the Campanian Volcanic Zone, southern Italy. *Mineralogy and Petrology*, 79, 3-31.

Romano P., Santo A., Voltaggio M. (2004) L'evoluzione geomorfologica della pianura del fiume Volturno (Campania) durante il tardo Quaternario (Pleistocene medio-superiore-Olocene). *Il Quaternario*, 7 (1), 41-58. [The geomorphological evolution of the Volturno river plain (Campania) during the late Quaternary (Middle-upper-Holocene Pleistocene). *The Quaternary*]

Rosi M., Sbrana A. (1987) *Phlegrean Fields*. CNR, Quaderni de la Ricerca Scientifica, Roma, Italy, 114, 9.

Sacchi, M., Infuso, S., Marsella, E., 1994. Late Pliocene–Early Pleistocene compressional tectonics in offshore Campania (eastern Tyrrhenian Sea). *Bollettino di Geofisica Teorica Applicata*, 36, 141–144. [Late Pliocene-Early Pleistocene compressional tectonics in offshore Campania (eastern Tyrrhenian Sea). *Bulletin of Applied Theoretical Geophysics*]

Sacchi M., Molisso F., Pacifico A., Vigliotti M., Sabbarese C., Ruberti D. (2014) Late-Holocene recent evolution of Lake Patria, South Italy: An example of a coastal lagoon within a Mediterranean delta system. *Global and Planetary Change*, 117, 9-27.

Santangelo N., Romano P., Ascione A., Russo Ermolli E. (2017) Quaternary evolution of Southern Apennines coastal plains: a review. *Geologica Carpathica*, 68 (1), 43-56.

Sartori R., Torelli L., Zitellini N., Carrara G., Magaldi M., Mussoni P. (2004) Crustal features along a W–E Tyrrhenian transect from Sardinia to Campania margins (Central Mediterranean). *Tectonophysics*, 383 (2004) 171 – 192.

Stanley D.J., Warne A.G. (1994) Worldwide initiation of Holocene marine deltas by deceleration of sea-level rise. *Science*, 265, 5169, 228-231.

Torrente M.M., Milia A. (2013) Volcanism and faulting of the Campania margin (Eastern Tyrrhenian Sea, Italy): a three-dimensional visualization of a new volcanic field off Campi Flegrei. *Bulletin of Volcanology*, 75, 719- 732.

VIDEPI Project. http://unmig.sviluppoeconomico.gov.it/videpi.

Zitellini N., Marani M., Borsetti A. (1984) Post-orogenic tectonic evolution of Palmarola and Ventotene basins (Pontine Archipelago). *Memorie della Società Geologica Italiana*, 27, 121-131. [*Memories of the Italian Geological Society*]

In: Sedimentary Basins
Editor: Sam Brookes
ISBN: 978-1-53613-922-8

Chapter 2

FORMATION OF PULL-APART BASINS, CRETACEOUS VOLCANO-SEDIMENTARY SEQUENCE, HYDROCARBON POOLS AND SUB-VOLCANIC EXPLORATION: CASE STUDIES FROM PENINSULAR INDIA AND ADJOINING INDIAN OCEAN

K. S. Misra[1,*] and Anshuman Misra[2,†]
[1]University of Petroleum and Energy Studies, Dehradun, India
[2]Kumaun University, Nainital, India

ABSTRACT

Presence of volcano-sedimentary sequence in pull-apart basins has intrigued the geologists for several decades. We explain that the

[*]Correspondence Author Email:drksmisra@gmail.com.
[†]Email:anshumanmisra22@gmail.com.

extensional tectonic processes are not only responsible for formation of these basins but also eruption of volcanic units and emplacement of dykes swarms. High resolution seismic data, processed by Pre-Stacking and Depth Migration (PSDM) and Pre-Stacking and Time Migration (PSTM) techniques and hundreds of drill-hole logs have made on eloquent exposition of basin forming tectonics in different regions of India. Several case studies have also illustrated that the Pre-Cretaceous period is characterized by prolonged extensional tectonics, development of nearly vertical faults, subsidence and formation of basins and sedimentation. With progressive downward continuation, the faults reached to critical limits to cause decompression melting and rampant outpouring of lava units. These units are inter-layered with fossil bearing sediments from the beginning to the end of Cretaceous. This volcano-sedimentary sequence is logged invariably from different basins in and around peninsular India. It is also logged in Andaman, Male and Lakshadweep basins of Indian Ocean. This sequence also covers entire Bay of Bengal and the Arabian Sea and also forms technical basement for the deposition of uninterrupted Tertiary succession. Processing by PSDM and PSTM techniques have also made it possible to get information about the thickness of volcanic units as well as the sediments below them. Improved resolution has helped to identify several basins with thick Pre-Cretaceous Mesozoic succession and differentiate various litho-units of Tertiary succession. These litho-units have various proportions of limestone, shale and sandstone and are some of the finest source rocks of hydrocarbons.

Mesozoic rocks are more severely deformed mainly by nearly vertical faults and the effects gradually diminish in successive overlying younger Tertiary succession. Most of these faults show upward or downward convergence, intersecting each other in the Oligocene stratigraphic horizon, thus forming an hour-glass structure. The basal portions of these structures are often occupied by oceanic ridges while prolific growth of corals reefs in upper portions. These reef complexes are most favorable for hydrocarbon accumulation and also suggest gradual subsidence of blocks. The study of thickness pattern and facie changes, have also suggested continued extensional tectonics. The tectonic grain of these ocean basins is defined by elongated basins and ridges which have originated at K-T boundary. These sheltered basins were most appropriate sites for deposition of sediments rich in good quality organic matter, as source rock for hydrocarbon generation.

Valuable seismic and drilling data obtained at very high cost, makes it clear that there was long duration extensional tectonic activity, during which sedimentation and spasmodic volcanism gave rise to unique volcano-sedimentary sequence. This study enumerates the mechanism of simultaneous deposition and volcanism due to inter action between extensional tectonics and decompression melting. Furthermore, the study does not support the idea of hot spot related volcanism in pull-apart

basins. Upwelling heat from deeper levels, through innumerable upward bifurcating faults, before the volcanism, provided kitchen for distillation of older sediments. Volcanic units have not only provided trapping mechanism as oil seals in favorable conditions, but also they are excellent reservoir rocks due to initial vesicular nature and later cooling joints.

Keywords: pull-apart basins, rift and grabens, Cretaceous volcanism, dyke swarms, volcano-sedimentary sequence, K-T boundary, hydrocarbon exploration

1. PREVIOUS STUDIES AND METHODOLOGY

The Cretaceous volcanic event and development of coal bearing Gondwana successions have been engaging the attention of geologists for over a century. In early part, the study was confined to Deccan Region of western India and was based on field mapping and associated physical volcanic features. Absence of volcanic vents and fissures has intrigued the earlier workers. Only Lonar carter was believed to be of volcanic origin (Medlicott and Blanford, 1879; La touché and Christie, 1910). Geochemical studies Washington (1922) established that the majority of flows are quartz normative tholeiites. In vast volcanic terrain only interesting igneous complexes were studied. The important study areas were Pavagadh, (Chatterjee, 1961). Girnar, (Subbarao, 1972). A variety of rocks were located on the basis of geochemical analysis and models for the parent magma were proposed. Relationship between major tectonic structures and volcanism has started to emerge when Misra (1981) demonstrated that most of the large igneous complexes are located along lineaments. Later mapping of Kutch and Saurashtra regions by Misra (1999), suggested multi-central volcanic eruption where volcanic fields with innumerable plugs, cones, craters and calderas were located. Satellite imagery was extremely useful in recognizing these features. An integrated system of lava channels and tubes has been brought out by Misra (2002). The remnants are often found emanating from common effusive centers. Major breakthrough has come with the finding of Cretaceous volcanic

units in all the Phanerozoic basins in and around Indian sub-continent (Misra, 2008a; Misra and Misra, 2010). Since several of these basins are producing hydrocarbons and others have very high possibility, availability of seismic profiles and borehole logs substantiated the findings.

For regional study, field mapping assisted by aerial photographs and satellite imagery has formed the backbone of study. Several large scale structures such as lineaments are surface expressions of nearly vertical faults. Mapping of dyke swarms has helped in identification of regions which experienced extensional tectonics (Misra, 2008b). Available aeromagnetic data of Gujarat has helped in demarcation of subsurface basin boundaries and basement blocks below the volcanic units. For mapping dyke swarms in areas covered by alluvium, vertical gradient derivative of aeromagnetic data was exceptionally useful. Drill hole logs generated for exploration of hydrocarbons, are utilized to map the extent of Phanerozoic basins, volcano-sedimentary succession in subsurface and offshore regions. The information gathered in land areas is integrated with the details obtained from the offshore and oceanic regions, to get the complete picture. Similarly seismic data processed by PSDM and PSTM techniques, are interpreted for understanding tectonics and stratigraphy. Here we present a consolidated account of all the findings from rift and grabens; occurrences of Cretaceous volcanic units from land, off-shore and oceanic regions; along with the related dyke swarms from different areas. These findings have helped to remove several miss-conceptions and present a coherent geological history.

It has also emerged that all the petroliferous basins of peninsular India have invariably formed by extensional tectonics and are associated with basalt flows and transected by dykes. Several units of basalts are inter-layered with sediments and form a unique fossil bearing volcano-sedimentary succession, ranging in age from the beginning to the end of Cretaceous. Hydrocarbons are produced, not only from the under lying older Mesozoic and overlying Tertiary sequences but also from the volcanic units. These units are fairly good reservoir rocks because of primary vesicular nature and secondary cooling columnar joints. Apart

from this the successive units of basalt have acted as epoxy to seal the cracks in older sediments to make them prolific producers of hydrocarbons. Up welling heat pre-ceding volcanism provided heat to distillate older sediments.

2. REGIONAL TECTONIC SETTING AND DISTRIBUTION OF PULL-APART BASINS

A number of major tectonic features, which are commonly described as rift, grabens, tectonic and lineament zones are transecting Indian `peninsula. (Figure 1). Evidences of extensional tectonism are present along all these features. Furthermore, lineaments interpreted from satellite imagery also show remarkable parallelism with these features (Misra, 2001). Narmada-Tapti Tectonic Zone trends in ENE-WSW, Koel-Damoder Graben in E-W, Mahanadi Graben in ESE-WNW and Pranhita-Godavari Graben in NW-SE direction. A gradual fanning out pattern is exhibited by these grabens, which host most of the Gondwana coal seams. On the western side, curvilinear Kutch Rift has E-W trend in west and attains NE-SW trend in the east. This rift is unique and has deformed marine Jurassic and Cretaceous volcanic succession. Narmada-Tapti Tectonic Zone is the oldest rift and divides Indian sub-continent into two tectonic entities. It has emerged that nearly straight course of Narmada River for over thousand kilometers is mainly controlled by the trend of dykes. West (1962) considered it as Precambrian deep crustal fracture zone. Radhakrishna (1989) described Proterozoic mobile belt activity along this zone in central India. Misra (2008 b) found geological evidences to suggest that along this zone extensional tectonics continued, a dyke swarm was emplaced and acted as major effusive zone during the eruption of Cretaceous volcanism. This graben has been identified and found to extend in oceanic region (Misra and Misra, 2010). In land it is marked by contrasting geology on either sides and is filled by Proterozoic sediments, while in oceanic

extension it exhibits rapid rate of subsidence during Cenozoic era with Cretaceous volcanic units at the top. Cambay Structure has NNW trend in north and attains N-S orientation in the south. These basement features have long geological history; have deformed Proterozoic successions in shoulder belts. Geological evidences suggest that they experienced dominant extensional tectonics from the beginning of the Phanerozoic times. Normal faults gave rise to progressively subsiding elongated basins, filled by Gondwana sedimentary rocks. The curvilinear East Coast Fault Zone runs mostly parallel to the coast. Successive blocks have faulted down in a cascading manner in SE direction. A few of these structures such as Kukdi-Ghod Lineament Zone and Manjeera Tectonic Zone did not develop as graben, but kept on experiencing extension tectonics (Misra, 2007, 2008a).

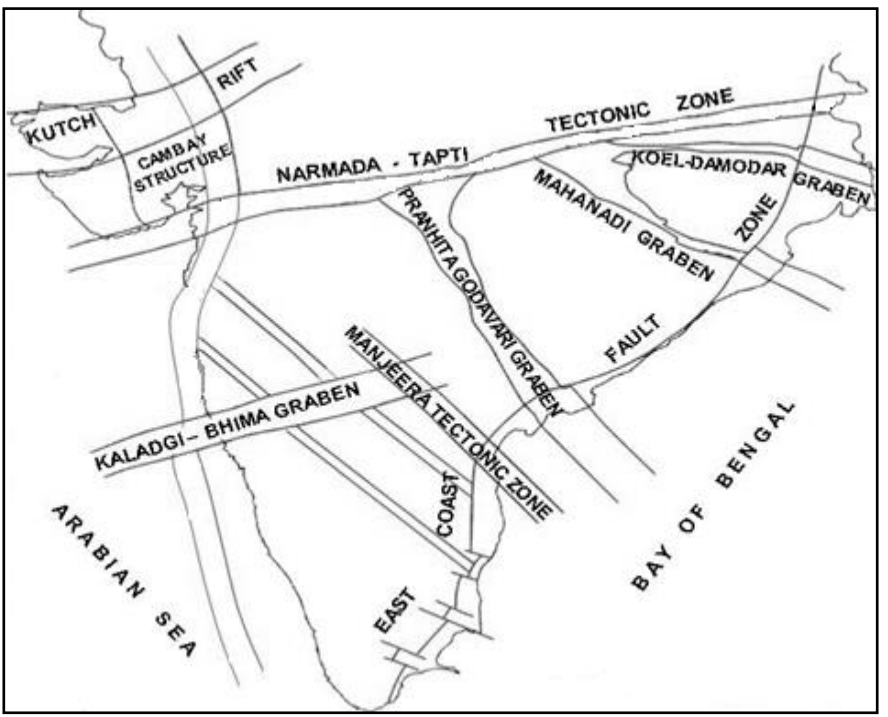

Figure 1. Outline map of peninsular India showing disposition of major rift and grabens (Misra et al. 2016).

3. DEVELOPMENT OF RIFT AND GRABENS AND FORMATION OF PULL APART SEDIMENTARY BASINS

The rift and grabens are of continental significance, as they are several hundred km long. Nearly 70% of energy resources of the country are located along these structures, either in the form of coal or hydrocarbons. The coal seams as well as coal bed methane are mainly of the Gondwana time. The study of thickness patterns and facies change, have also suggested continued extensional tectonics. These structures extend to the offshore regions where enormous sedimentary sequences host hydrocarbon pools of both Cenozoic and Mesozoic Era. They have long geological history beginning with the first cycle started in early Proterozoic times. They came into existence due to extensional tectonics when nearly vertical faults have given rise to generally elongated basins due to subsidence and accompanying sedimentation. This was terminated with the effusion of lava sequences due to decompression melting and magma generation during later part of Proterozoic (Misra, 2007). The volcano-sedimentary sequence of Proterozoic Era was deformed and metamorphosed and presently exposed in shoulder regions of most of the rift and grabens. With continued extensional regime, the second cycle started during which central parts of these structures experienced further subsidence to accommodate Gondwana sediments and finally culminating in enormous Cretaceous igneous activity. In certain cases such as Cambay structure renewed subsidence of central part marks the third cycle and provided basin for deposition of Tertiary succession. Furthermore, accumulation of thick Quaternary (>400) sediments, along with many other geological and geomorphologic features suggest prevailing extensional tectonics. Geomorphologic characters include rugged topography with straight river channels in large sections. Most of the major rivers flow along these structures as they have provided the path of least resistance. Rift and grabens are also characterized by high density of lineaments, which represent surface expression of nearly vertical faults (Misra, 2001). Furthermore, development of depo-centers in the inter-sectional regions of these major structures provided rapidly subsiding basins with organically

charged sediments, upwelling heat along fracture planes provided suitable kitchen for generation of hydrocarbons. Continuing tectonics provided necessary trapping mechanism and development of hydrocarbon pools. Remarkable correspondence between rift and grabens and sedimentary bsinsa has emerged (Figure 2).

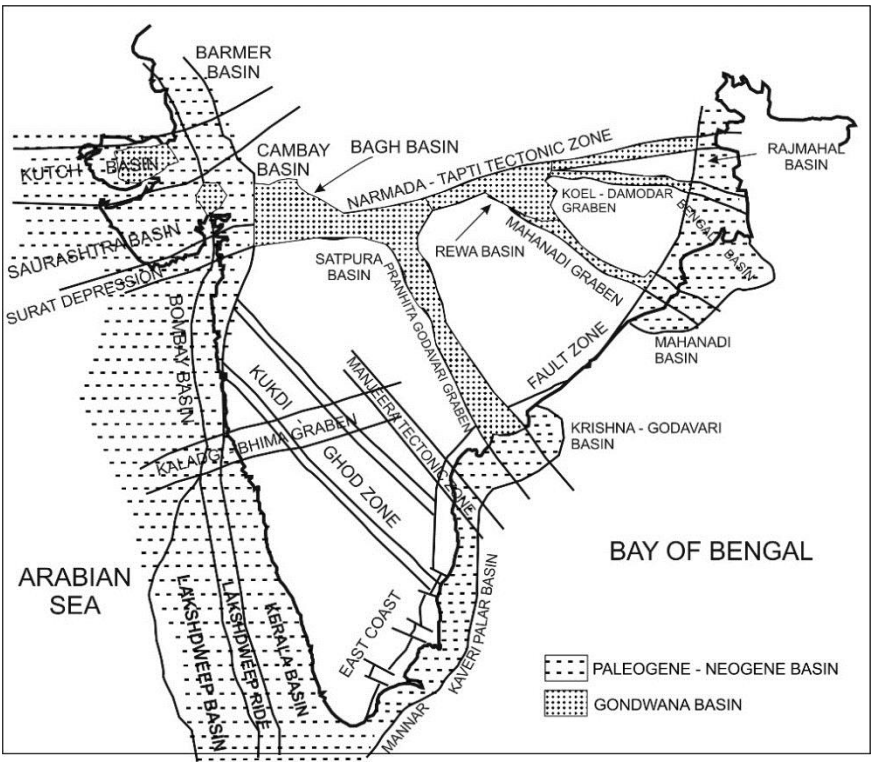

Figure 2. Map of peninsular India showing rift and grabens and their relationship with the pull apart sedimentary basins. Basins have formed along the rift and grabens, however, in intersectional regions they are modified due to compounding affect.

Lineaments laterally extend from exposed shield, to the areas covered by volcanic rocks. Geothermal mapping as well as presence of hot springs associated with these features, reveal high heat flow and connection with the deeper parts of the fragmented lithosphere (Shankar, R., 1995). In geophysical data sets, these tectonic features are characterized by elongated gravity highs and lows and substantiate the presence of

successive horst and grabens. Regional magnetic linears are also seen abruptly ending along these structures. Seismic data and aftershock study of past earthquakes has suggested that these structures outline different crustal blocks which are having both vertical and horizontal strike-slip components (Misra et al. 2004). Higher seismicity along these structures, particularly in their intersectional regions indicates movement, nucleation of stresses and sudden release causing seismic events. These rift and grabens are characterized by high density of lineaments, which represent surface expression of nearly vertical faults (Misra, 2001, 2007). Evidences suggest that extensional tectonics prevailed, during which rift and grabens have developed and accompanying normal faults gave rise to elongated basins. These basins formed locales for deposition of thick sedimentary sequences with coal seams in land areas, and petroliferous marine sediments were they laterally extend to the sea. Satpura and Rewa basins are dumbbell shaped, and have developed in the intersectional areas located along ENE-WSW trending Narmada-Tapti tectonic zone with the Pranhita-Godavari and Mahanadi grabens respectively. Both these basins are triangular in shape with base parallel to Narmada-Tapti tectonic zone and the vertex pointing towards south-east. On the other end of these two grabens the Krishna-Godavari and Mahanadi petroliferous basins are located. The Koel-Damodar valley graben hosts most of the largest Gondwana coal seams, however, oil and gas is yet to be found at its eastern end.

Continued extensional tectonics also resulted in downward propagation of faults and commencement of decompression melting during the Cretaceous period. Several pulses of enormous volcanism are inter-layered with sediments and form volcano-sedimentary succession. This succession, presents fossil record of approximately 90 million years, from the beginning to the end of Cretaceous. It is logged in all the petroliferous basins in and around peninsular India and forms the re-laid floor over which complete sequence of Tertiary rocks has been deposited. Cretaceous period also experienced widespread emplacement of dyke swarms. Parallel disposition of dyke swarms with the rift and grabens illustrates genetic relationship.

4. Cretaceous Volcanic Event in Peninsular India and Adjacent Oceanic Regions

Cretaceous period is conspicuously marked by rampant and spasmodic volcanism in the entire Phanerozoic history of peninsular India. Several units of volcanic flows ranging in age from the beginning to the end of Cretaceous are identified. In land areas the inter-layered sediments are subordinate and deposited as fresh water continental facies. On the other hand in sedimentary basins as well as in off-shore and oceanic regions the fossiliferous marine sediments together form a well-defined volcano-sedimentary succession. Earlier the study of Cretaceous volcanism was confined to the Deccan region of western Maharashtra, where they were described as Deccan Traps. In this region, only certain units are exposed and neither lower nor upper stratigraphic controls are present. It has also been difficult to estimate the thickness of volcanic units which would have been eroded off. Models were made based on study in limited areas and sections. Assumptions were also made that the entire volcanism has taken place either from single central type of activity or a hot spot located below the northerly moving Indian plate.

4.1. Distribution of Volcano-Sedimentary Sequence in Time and Space

This sequence was identified in far off regions such as Saurashtra, Kutch and other parts of Gujarat; Malwa and Mandla regions of Madhya Pradesh, Rajmahal in West Bengal, Sylhet in Meghalaya, Rajahmundry in Andhra Pradesh and St. Mary's island in Karnataka. Drill hole and seismic data sets have revealed that the volcano-sedimentary succession occupies extensive areas of Bengal, Barmer, Cambay basins as well as offshore regions of Kutch, Saurashtra, Bombay, Konkan, Kerala, Mannar-Kaveri, Krishna-Godaveri and Mahanadi basins (Misra, 2005). Later work identified in Kaveri basin and also found that the sequence laterally extends to cover entire Bay of Bengal and eastern half of Arabian Sea.

Comprehensive spatial distribution, brought out during this study is presented here, (Figure 3).

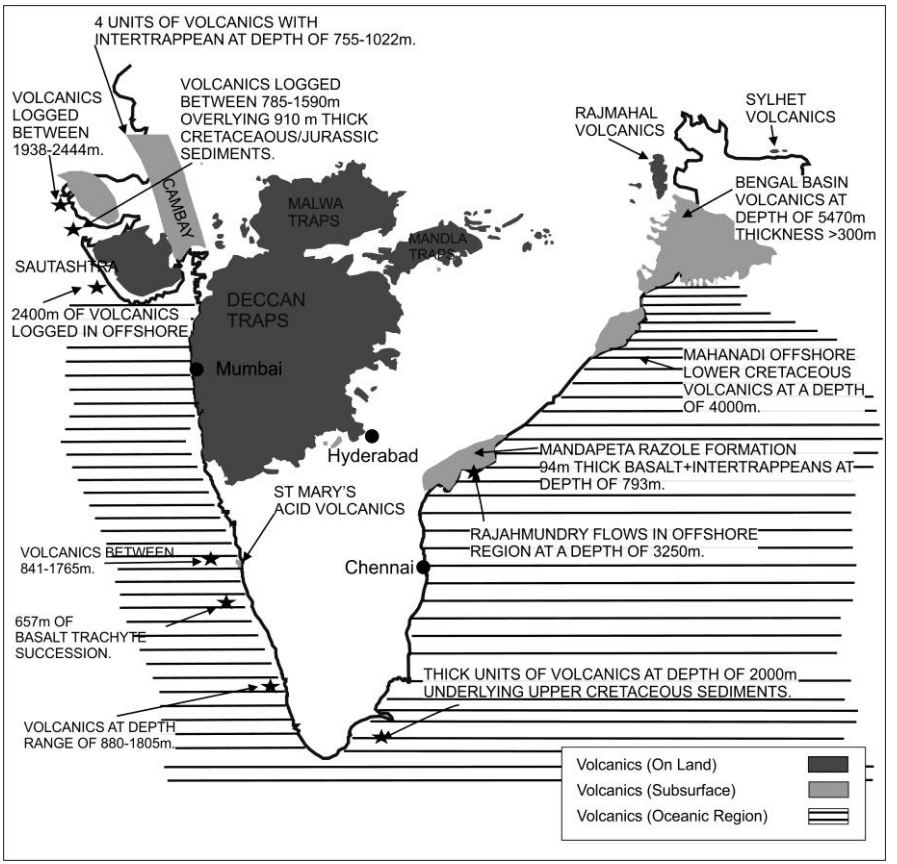

(Modified after Misra and Misra, 2010).

Figure 3. Map of peninsular India and surrounding oceanic region, showing distribution of Cretaceous volcano-sedimentary succession on land, subsurface, off-shore and oceanic region.

The distribution pattern of Cretaceous volcanic units, has not only contributed to our understanding of their origin, but also points to enormous scope for, hydrocarbon exploration in vast sub-basalt regions. Earlier, volcanic units were known only from the land areas. Exploration of hydrocarbons in Cambay and other rift and grabens has brought out their presence below the Tertiary sequence in subsurface. Drilling has

established their presence in offshore regions also. Furthermore, recent seismic surveys and drilling has shown that they occupy almost entire Bay of Bengal and vast regions of Arabian Sea. These interpretations have not only confirmed their lateral continuation from land areas to the oceanic regions, but also the entire succession of underlying and overlying sediments (Misra and Misra 2010). These unambiguous details of distribution from drilling logs have established that in all the basins volcanic units are inter-layered with Cretaceous sediments. These sediments have very good fossil content and provide excellent stratigraphic control from beginning to the end of Cretaceous period. The top most unit of volcano-sedimentary succession is thicker in all the sections and thus suggests long duration volcanism. Reliable radiometric ages have come from detailed logging of forty eight volcanic flows (West, 1958) in Dhandhuka bore well. Alexander (1981) dated samples from this well and got 62.7±2.05 Ma for top units and 101 3.3 for the bottom unit at a depth of 488 meters. This has also suggested a longer duration of the volcanic event. Seismic profiles from the offshore and oceanic areas have shown that the volcano-sedimentary succession has rather uniform thickness, ranging between 250 to 350m. Very distinct relationship has emerged by the interpretation of high resolution PSDM profile in Bombay off-shore region. This suggests that the offshore and ocean basin areas were less affected by tectonics, in comparison with the land areas. Entire succession is deformed by extensional tectonics, however, the Mesozoic rocks are more severely deformed than the Tertiary. The effect of these faults progressively diminishes in overlying younger rocks. The thickness of Cretaceous volcano-sedimentary succession varies greatly in different areas. The thickest pile on land is noted along the western face of the Sahyadri mountain ranges. In Kutch on land, the thickness varies from 125 to 350m. In offshore region of Kutch the thickness increases from north to south. Within Cambay basin, the thickness increases from a few meters in the shoulder areas to nearly 2500m in the central part. Maximum thickness (>3000m) is logged in Ankaleshswar area, below the Tertiary succession. This enormous thickness in believed by Misra (2008a) to be due to compounding effect of subsidence in the intersectional area of Narmada-

Tapti Tectonic Zone and Cambay structure during volcanism. Total subsidence (>7km) in this area is attributed to the room created by the decompression melting and effusion of Cretaceous volcanic units. Generalized logs of different basins are presented here (Figure 4).

The Rajahmundry volcanic units and their subsurface equivalents the Rajol formation, located in the Krishna-Godavari basin are receiving lot of attention in recent years because they are reservoir rocks and are producing hydrocarbons. New world class hydrocarbon findings below the volcano-sedimentary succession, within the older Mesozoic sediments in Kutch and Kaveri basins, are highly encouraging. On land the volcanic outcrops are trending in NE-SW direction, parallel to the East Coast Fault Zone, However, the effusive centers are oriented in NW-SE direction parallel to the Pranhita-Godavari Graben. Dyke emplacement in this volcanic succession is also very interesting. Dykes intersect only up to the top of basaltic rocks and are not transecting overlying Tertiary sediments The very presence of dykes cutting through the volcanic sequence and presence of volcanic vents has confirmed that the eruption was in-situ and they have not been transported to several hundred kilometers from Deccan region, as suggested by some earlier workers (Baksi. et al. 1994).

Rajmahal and Sylhet volcanic units represent land component of enormous and spasmodic volcanism, which has taken place in Bengal Basin (Roybarman, 1983). Pascoe (1964) dealt the problem of the age of these volcanic units and believed them to be from the top of Jurassic to the base of Cretaceous. Radiometric dating has yielded an age of around 116 Ma (Pringle et al. 1994) Vijaya (1997) on the basis of paleontological studies, assigned base of Cretaceous. Related tholeiitic dykes transecting Rajmahal volcanic units have, however yielded an age of 65±3 Ma by 40Ar-39Ar. (Kent et al. 2002). The emplacement of dyke in this region thus suggests that from the beginning of volcanism to the terminal phase of dyke emplacement, it took almost entire Cretaceous period, which has also been observed from the logging of several hundred drill holes from different regions.

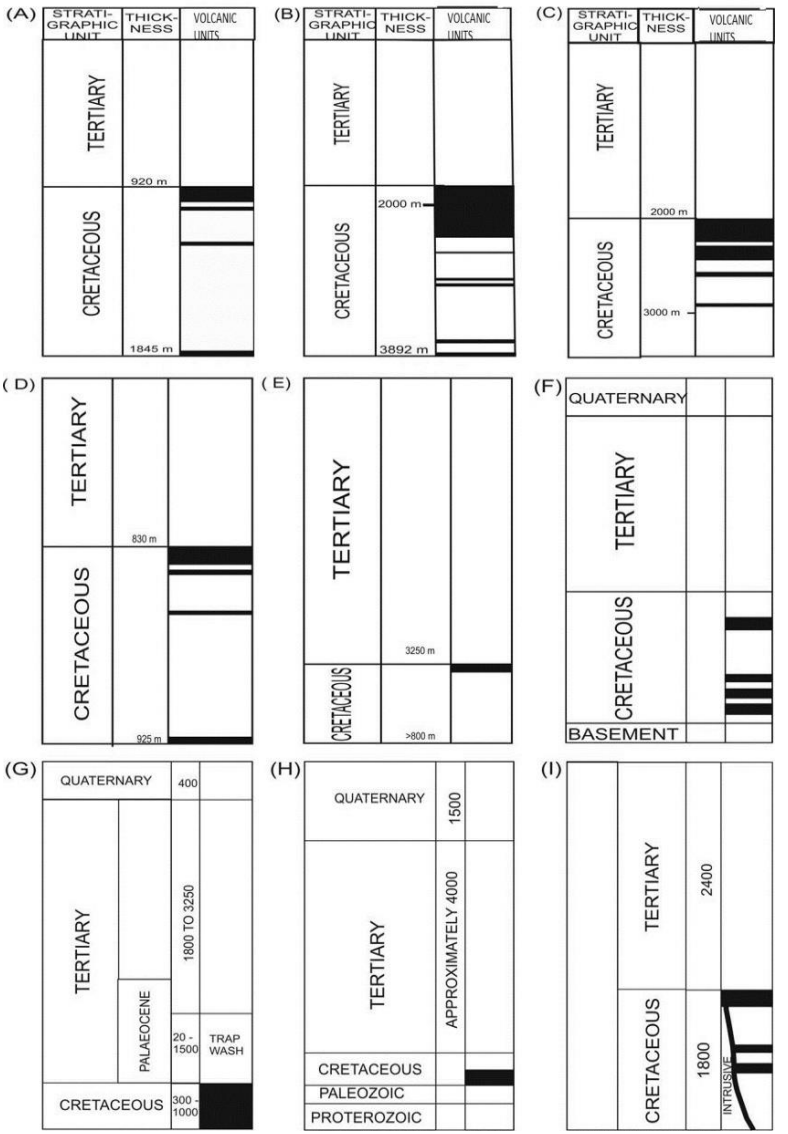

Figure 4. Information about volcanic units extracted from generalized well logs of certain basins (3D, 3E 3G, 3H and 3I after Berger, et al. 1983). 4A Off-shore Kutch, 4B On-land Kutch, Figure 4C. Off-shore Saurashtra, Figure 4D. Lakshadweep basin, Figure 4E Krishna-Godavari basin, 4F. Off-shore Mahanadi basin, 4G. Cambay basin, 4H Bengal basin, 4I Andaman basin. For remaining basins logs are prepared from description in published literature.

Mahanadi off-shore basin volcanic units are logged in drilling logs for the hydrocarbon exploration (Jagannathan et al. 1983). Here they are inter-layered with the early Cretaceous sediments. Lisker and Fachmann (2001) dated volcanics as well as NE-SW trending dyke near Naraj by step heating analysis and found ages of 108±0.8 Ma and 110.6±3.8 Ma respectively. Here dyke emplacement seems to have taken place soon after the volcanism.

4.2. Effusion of Volcanic Units and Formation of Volcano - Sedimentary Sequence

The non-recognition of volcanic cones, craters, calderas has intrigued the earlier workers, for over a century. During which only a few were identified by field mapping by their characteristic shape. Satellite imagery interpretation and verification in field was extremely useful in recognizing these features. They have been recognized not only from the Deccan volcanic terrain, but also in other regions such as Kutch, Saurashtra and Rajahmundri (Misra, 2002, 2005, 2008a and Misra and Misra, 2010). Field studies in entire region have also established that the initial volcanism was of felsic nature and dominated by rhyolite, obsidian and was of explosive nature. These older felsic components are overlain by younger tholeiitic lava. These findings are contrary to established Bowen's reaction series, where felsic components erupt last after magmatic differentiation. Later acquisition of geophysical data did not find any evidences in favor of huge magma chamber. It was also believed earlier that the volcanism was uni-central and lot of efforts was made to develop unified lava stratigraphy and locate huge volcano. Absence of evidences in favor of such a volcano, led several workers to suggest that it is located somewhere in Arabian Sea. Attempts to make unified stratigraphy also did not succeed. Continued studies by present authors have brought out interesting results, which suggest that volcanism was multi central. Volcanic fields with innumerable volcanoes kept on popping up at different levels and had local stratigraphy around them. Such fields are identified not only from Deccan region but

also from Kutch, Saurashtra and Rajahmundri volcanic regions. The age of volcanism and dyke emplacement that has emerged is quite interesting. As described earlier the volcanism was of long duration covering entire Cretaceous period. The basalt units are inter-layered with sediments and together form volcano-sedimentary succession. The thickness and number of individual units varies in different basins. However, These basaltic units are often prolific producers of hydrocarbons, particularly natural gas. The disposition of basaltic units has played significant role in movement and preferential accumulation of hydrocarbons, both in underlying Mesozoic and overlying Tertiary sequences. It has also been concluded that the basin forming and basin modifying tectonics, as well as volcanism has profound influence of prolonged extensional tectonics.

They are best exposed in several parts of Kutch areas where overlying Tertiary Gaj Beds which protected them, and are eroded off in recent times. These centers are incised in the center and are aligned along the structural grain of Jurassic sequence. Multiple centers forming volcanic fields at different levels have thus emerged from the study.

Fossil assemblage in the sediments of unique volcano-sedimentary sequence ranges in age from beginning to the end of Cretaceous period. Furthermore, both underlying older Mesozoic and overlying Tertiary successions are full of fossils, thus provide excellent bio-stratigraphic control.

Volcanic units have erupted along developing rift and grabens, because of extensional tectonics and lava was generated due to decompression melting. Cretaceous period is also marked by rampant vertical tectonics which decreased with the termination of volcanism. Uninterrupted Tertiary succession overlies this Cretaceous-Tertiary boundary in continental and oceanic regions. Upwelling heat through the vertical fractures helped to generate hydrocarbons and volcanic units provided sealing mechanism. These units are themselves prolific producers of hydrocarbons in Raageshwari field of Barmer basin, Padhra and Ingoli fields in Cambay basin and both oil and gas from Rajol volcanic flows in Krishna-Godavari basin. The production is due to primary, secondary and tertiary porosity and permeability developed in them. The primary one is basically due to

presence of vesicles, the secondary is mainly because of cooling cracks and tertiary is associated with development of closely spaced vertical fractures. Dyke swarms emplaced along extensional fractures related to the major structures such a Narmada-Tapti Tectonic Zone and Cambay Graben also control the preferential accumulation of hydrocarbons.

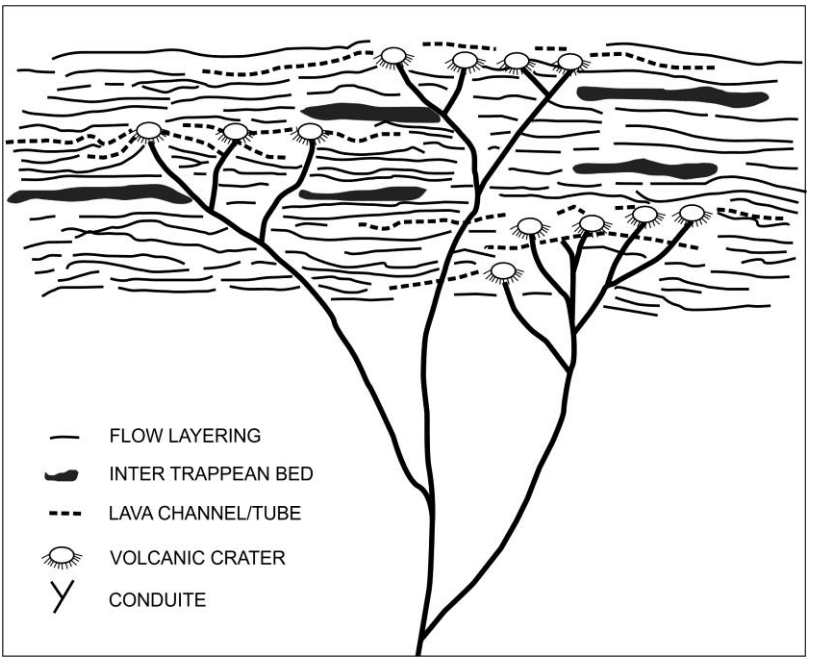

Figure 5. Typical volcanic units and their mode of eruption can be seen. Upward bifurcating conduits have given rise to volcanic fields at different levels.

Present study further elaborates overwhelming evidences to suggest that the volcanism at all the places is rift related. It incorporates findings of seismic surveys and drilling logs to notify several new occurrences of Cretaceous volcanic units from widely separated land, subsurface, offshore and oceanic regions. Integration of findings from each of these occurrences has helped to present a comprehensive tectonic history. Manifestations of extensional tectonics, such as development of rift and grabens, decompression melting, magma generation, effusion and emplacement of dykes, match with observations. Evidences suggest that the lavas were

generated by the decompression melting and it might be possible that some faults would have reached to critical limits earlier and would have also continued for longer period. This would have also been controlled by the thickness of lithosphere and rate of propagation of faults in downward direction. Disposition of volcanic units, igneous complexes and dykes along rift and grabens, particularly in their intersectional areas suggest genetic relationship. Convergence of several rift and grabens below the main Deccan volcanic region, where largest activity has taken place is very interesting. Furthermore, these units are logged in all the petroliferous basins, where large amount of expensive data is collected. These units also laterally continue uninterrupted in entire Bay of Bengal and eastern half of the Arabian Sea. This significant observation indicates that the ocean basins are covered by Cretaceous volcano-sedimentary succession and are not oceanic basalt as believed earlier. Apart from this the recognition of pre-Cretaceous sedimentary succession below the volcanic units has further substantiated this observation. These findings do not support the idea of hot spot volcanism associated with the northerly movement of Indian plate. The trail of this hot spot is generally believed to pass from Deccan region to the ocean via Lakshadweep-Maldives ridge system, crosses the Carlsberg ridge and continues up to the Reunion volcanic Islands in southern Indian Ocean. However, no evidences of remnant trail are found by interpretation of geomorphologic, geological, aeromagnetic data sets during this study, rather continuance of all older rift and grabens on its path are noticed. To explain the presence of Cretaceous volcanic units associated with the sedimentary basins along the east coast of India, one more hot spot was conjectured. Apart from this, the uninterrupted and continuous sedimentary succession along both western and eastern offshore does not show any corridor through which hot spots would have passed.

5. Extensional Tectonics, Emplacement of Dyke Swarms and Orientation of Hydrocarbon Fields

The Cretaceous igneous activity is also genetically related with the emplacement of dyke swarms. The dykes within the swarms are similar to the quartz normative tholeiite of typical middle and upper volcanic sequences. Several major dyke swarms transect the Peninsular India. The most important one is trending in ENE-WSW direction and is parallel to the Narmada –Tapti Tectonic Zone of central India. The dykes belonging to this swarm are more profuse and thicker in the western part, and their number and width decreases gradually in eastern direction. The second dyke swarm is oriented in N-S direction and is directionally parallel to the west coast, which is largely shaped by the southerly extension of the Cambay structure. Both these dyke swarms are seen to be emanating from the general area of Gulf of Cambay. The other dyke swarm is parallel to the Pranhita-Godavari graben (Figure 6). Most credible evidence to suggest the rift related volcanism has come from the mapping of dyke swarms. The parallelism between rift and grabens and dyke swarms emerged during present study, unambiguously explains genetic relationship. Emplacement of successive dyke swarms is associated with each volcanic pulse and complete directional orientation with rift and grabens is very strong evidence to suggest that Cretaceous volcanism is also rift related. Furthermore, emplacement of dyke swarms represents ephemeral period, during prolonged Mesozoic and Tertiary extensional tectonics.

There are also dykes intruding the Gondwana succession and are mainly confined within the rift and grabens. These dykes are of either lamprophyre or dolerite composition. Mapping of dyke swarms has been very rewarding for exploration of hydrocarbon pods. The emplacement of swarms represent only a short duration within prolonged phase of extensional tectonics, during which Mesozoic and Tertiary depo-centers have formed. Furthermore, the chronology of tectonic events which led to the development of Mesozoic depo-centers, heat flow, volcanism and deposition of Tertiary sequences has provided new approach for exploration.

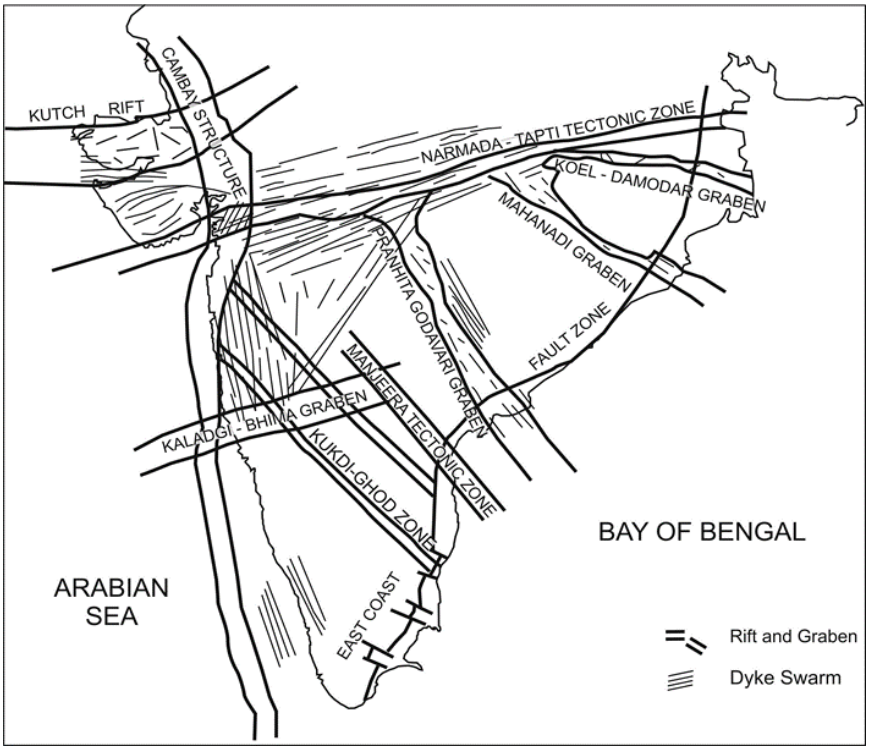

Figure 6. Map of peninsular India showing transecting rift and grabens along with Cretaceous dyke swarms. The swarms are parallel to the rift and grabens while local dykes are confined mainly within them.

Availability of aeromagnetic data has further opened new vista for not only understanding the volcano-sedimentary basins but also in hydrocarbon exploration. It was earlier believed that aeromagnetic data will be off little use in knowing the details of either volcanic units or the sedimentary rocks below them and therefore, the entire region covered by basalt was not flown for aeromagnetic surveys. Very recently, the aeromagnetic data collected over Gujarat region has brought out intricate details of basement tectonics and presence of horst and grabens, disposition and limits of sedimentary basins, thickness of basaltic and sedimentary units, dyke swarms and intrusive bodies (Figure 7). In this figure a large square shaped region is bounded by basement faults. It is interpreted that the Dharanghadhra-Wadhawan basin located in the NE part

of Saurashtra is extending below the basalt, into this region. Furthermore, the horst and grabens on both southern and western sides of Saurashtra can also be seen as elongated magnetic high and lows. The recently discovered oil and gas fields are located in this region and their elongation coincides with the rift and grabens. The vertical gradient derivative of aeromagnetic data shows better defined horst and graben structures. The western boundary of Cambay structure is also very conspicuous. Details of these dyke swarms and dykes have been reported by Misra (2008b).

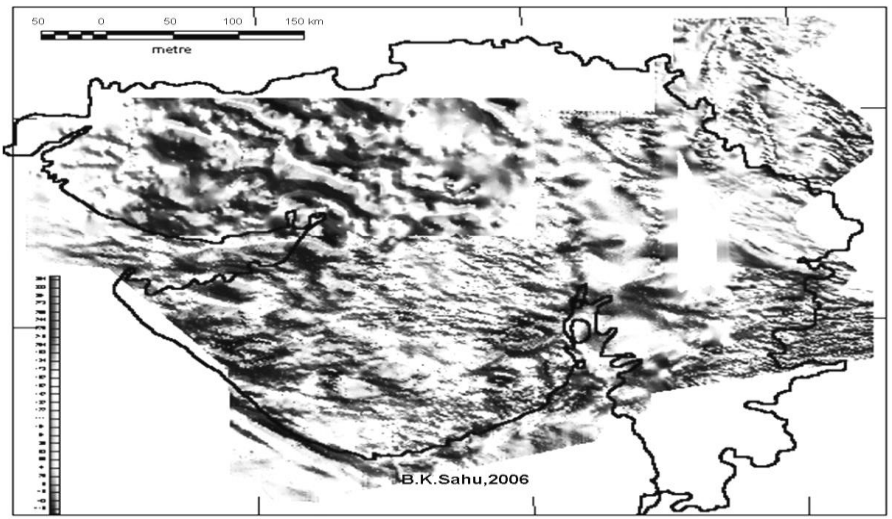

Figure 7. Total field aeromagnetic data of Gujarat The dyke swarm regions were extensional areas during Mesozoic as well as Tertiary times.

The present study has enumerated that the emplacement of dyke swarms represents an ephemeral portion of long extensional tectonic phase. The extensional tectonics preceding and postdating the dyke swarm emplacement was largely responsible for the development of older Mesozoic and Tertiary basin. Thick hydrocarbon bearing sedimentary sequences have been located along the ENE-WSW trending dyke swarm. The best examples of control in hydrocarbon pools are Ankeleshwar, Hazira, Ambe, Gandhar and Lakshmi. The Ankeleshwar field is the largest on-land field in India, producing hydrocarbons for over half a century is

located right in the bifurcation region of this major dyke swarm (Figure 8). Similarly the recently discovered hydrocarbon field in Gulf of Kutch is also located in the extension of dyke swarm.

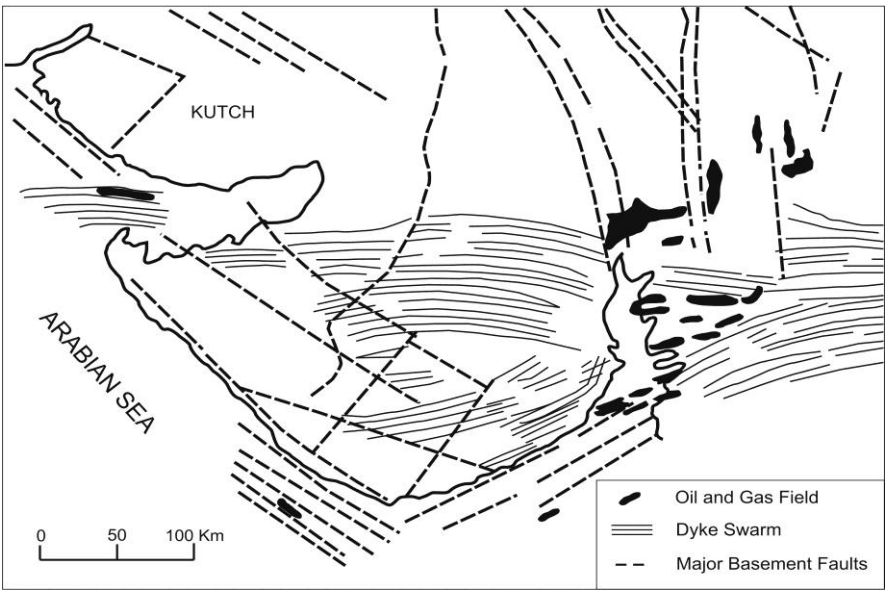

Figure 8. Map showing interpretation of total field aeromagnetic data along with disposition of oil and gas fields in Gujarat. Major dyke swarm and its relation with hydrocarbon pools can be seen.

Nearly E-W trending dolerite dyke swarm located between Narmada and Tapti River bifurcates in Ankeleshwar region and one arm proceeds to the Gulf of Kutch, through the Central Saurastra and southern arm to southern Saurastra. The dyke swarm regions were extensional areas during Mesozoic as well as Tertiary periods. Preliminary results in and around Saurashra have shown, that the depth of the basement can be estimated (Figure 9). A change in the pattern of depth of basement very well matches with the rifts hidden below the volcanic units. In offshore areas it corresponds with the successive horst and graben structures.

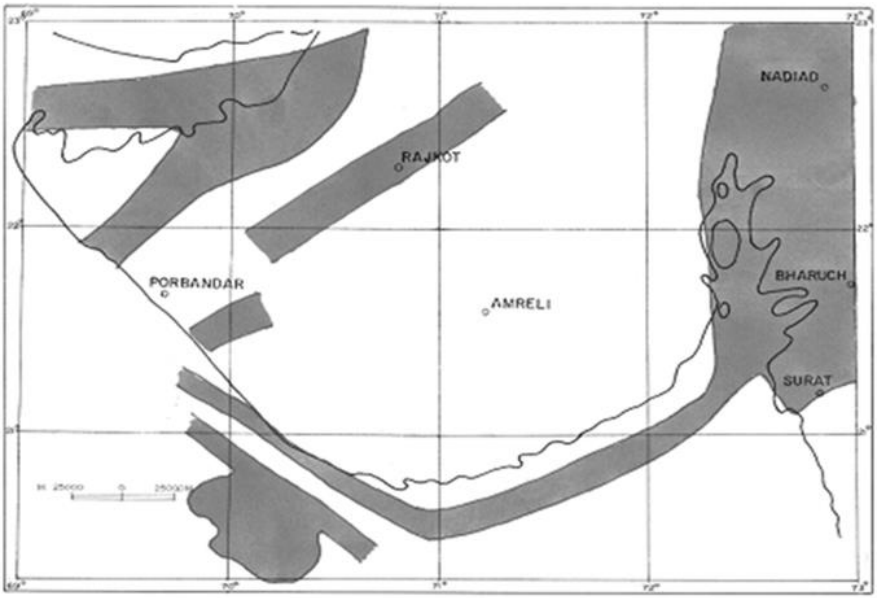

Figure 9. Euler depth perception map of Saurashtra and Cambay graben. The regions depicted in grey are showing areas where the depth of basement in more than 5 Km. Hidden rifts below the basaltic flows are interpreted by elongated nature of basement subsidence.

6. Exploration of Hydrocarbons in Sub-Volcanic Regions

Apart from the aeromagnetic data, the developments in seismic data processing have made significant contribution to exploration in sub-volcanic regions. The most significant one is PSDM and PSTM, data processed by these techniques has potential to not only estimate the thickness of volcanic units, but also interpret the sediments below them (Figure 10).

The basalt lavas are sandwiched between older Mesozoic and younger Tertiary sequences. It was earlier impossible to explore hydrocarbons in sub-basalt basins, because no geological or geophysical methods could provide required information. Last two decades have significantly

contributed to our understanding of volcanic units and mapping of geological features below the basalt by interpretation of seismic profiles generated by PSDM and PSTM techniques. The basalt units are inter-layered with sediments and together form volcano-sedimentary succession. The thickness and number of individual units varies in different basins, however, they are present from beginning to the end of Cretaceous period. These basaltic units are often prolific producers of hydrocarbons, particularly natural gas.

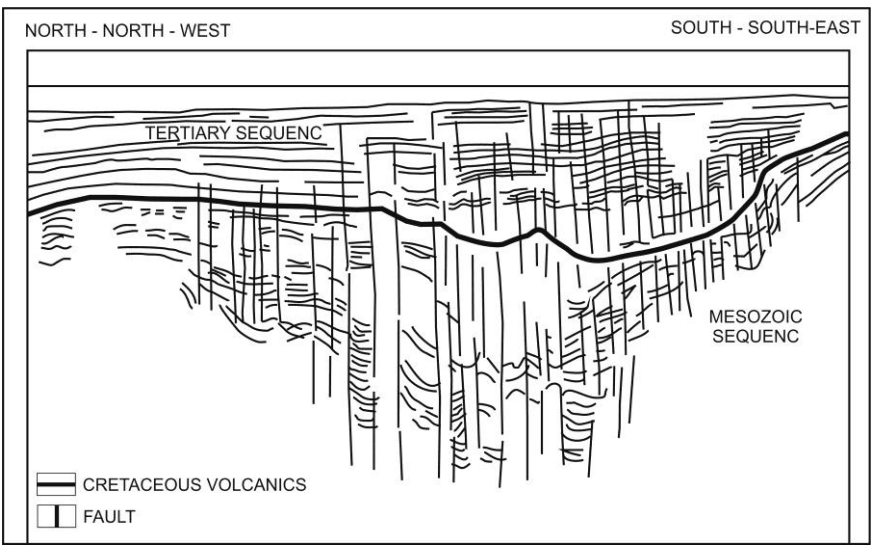

Figure 10. Interpretation of Seismic profile across Kaladgi-Bhimagraben in off-shore region

The disposition of basaltic units has also played significant role in movement and preferential accumulation of hydrocarbons, both in underlying Mesozoic and overlying Tertiary sequences. It has also been concluded that the basin forming and basin modifying tectonics, as well as volcanism has profound influence of prolonged extensional tectonics. It has been possible to map geological details below the Cretaceous volcanic sequence. The basin can be seen to have formed due to vertical tectonics, where successive blocks have faulted down towards the center of the

grabens. The extensional tectonics was rampant during Mesozoic and migrated towards SSE direction later during the Tertiary period.

7. SYNTHESIS

Peninsular India has been experiencing largely extensional tectonics across major geological structures. This has resulted in development of rift and grabens and associated vertical gravity faults, subsidence along them formed elongated basins. The compounding effect of subsidence along intersecting rift and grabens has been responsible for the development of depo-centers. Four prominent sedimentary basins are located along the east coast of India. They are commonly known as Kaveri-Mannar, Krishna-Godavari, Mahanadi and Bengal basins. These basins are nearly parallel to the coast line which is largely controlled by the East Coast fault zone. This directional parallelism suggests that the formation and development of basins is governed by the enechelon faults. These faults are mainly responsible for development of parallel horst and grabens due to relative gravity faulting, although the sum total of this faulting has given cascading effect in easterly direction. Various sedimentological evidences suggest that the faulting was contemporaneous with the sedimentation.

The rift and grabens radiate out from the continental region and extend in offshore areas. Geological conditions favored development of Gondwana coal in continental areas while in delta and offshore regions the conditions were more congenial for development of hydrocarbon pools. Due to compounding effects of subsidence these areas experienced rapid sedimentation. These sediments were highly charged with the organic material brought by the rivers which was sufficient to attract enormous quantity of it from the oceanic regions. Upwelling heat from deeper levels, through innumerable upward bifurcating faults, provided kitchen for distillation of hydrocarbons. The Cretaceous volcanic units which are also known as “Traps” seem to have provided oil trapping mechanism in favorable conditions. Very high pressures are encountered in the Cretaceous sedimentary sequences underlain by the volcanic units in

certain areas such as Krishna-Godavari basin. This is because fractures were sealed by the successive volcanic units and continued upwelling heat in these regions, is also demonstrated by the presence of hot springs in the vicinity of intersectional areas.

The temperatures of the lavas were also not very high as it is generally believed. The presence of fossilized tree trunks by the vesicular basalt (Misra, 2005) and low temperature zeolites suggest that the lava temperatures were close to 6500C. Mesozoic and older rocks have not received required attention due to the overlying volcanic units. It was difficult to image subsurface rocks because of attenuation problems in seismic surveys. Similarly it was presumed that high magnetic susceptibility of volcanic rocks will not provide any useful information. However, due to significant improvement in processing of data, lot of valuable information has emerged regarding the thickness of volcanic units and sedimentary rocks. Aeromagnetic data products have provided data about basement tectonics, dykes and limits of sedimentary basins. Furthermore, finding of gas hydrates in offshore regions and coal bed methane in the Gondwana rocks covered by the volcanic units makes this study of tectonics and Cretaceous volcanism relevant for associated hydrocarbon exploration.

CONCLUSION

The most important finding of the study is that, during the entire Phanerozoic history of peninsular India, volcanism has taken place only during the Cretaceous period. Drilling logs from different basins thus have a unique sequence, within which several volcanic units are inter-layered with sediments. The sediments have very good fossil content and provide excellent stratigraphic control from beginning to the end of Cretaceous period, suggesting long duration volcanism.

The study has also led us to believe that the Cretaceous volcanism was rampant in spatially wide spread areas, sedimentary basins and oceanic regions. Continued extensional tectonics resulted in development of rift

and grabens, decompression melting, magma generation and multi-central eruption. Large scale transportation has taken place by system of lava channels and tubes. Emanating pattern of these channels and tubes has helped to recognize several effusive centers.

It has emerged that the Cretaceous igneous activity encompasses not only colossal outpouring of lava flows but also emplacement of huge igneous complexes and dyke swarms. The prominent effusive zones are linear and parallel to major rift and grabens. Volcanism was more rampant in intersectional areas of these structures. During the initial phase volcanism was felsic in nature, due to melting of shallower sialic lithosphere. With progressive downward movement of nearly vertical faults it became quartz normative tholeiitic. Alkaline phase is found in areas where faults could reach to further deeper levels. Individual dolerite and lamprophyre dykes are confined within the rift and grabens where they transect coal bearing Gondwana sequences.

Identification of Cretaceous volcano-sedimentary succession in all the petroliferous basins and its lateral continuance to the oceanic regions indicates very extensive spread. It has also emerged that there are thick pre-Cretaceous sediments underlie this succession. These findings have helped to remove the misconception of oceanic basalt. The ocean basins are gradually subsiding while land areas are rising. The study does not support the idea of hot spot volcanism related to the northerly movement of Indian plate.

Major dyke swarms associated with volcanic activity are parallel to Narmada-Tapti Tectonic Zone, Cambay structure and Phanhita-Godavari graben. The dykes are emplaced along nearly vertical fractures created by the extensional tectonics. The exact similarity of chemical composition of dykes forming the swarms and volcanic units indicates genetic relationship and does not show any characters of lavas which could have originated in hot spot or mantle plume conditions.

Exploration in sub-basalt regions can better be achieved by integrated interpretation of satellite imagery, aeromagnetic and seismic data. Processing of aeromagnetic data to obtain vertical gradient/ depth perceptions and seismic data by PSDM/PSTM techniques has great

potential in sub-basalt prospecting. The case studies presented formulate technique to develop better understanding of complex basins and exploration, which can be applied, be other comparable basins.

ACKNOWLEDGMENTS

We will like to profusely thank Nova Publishers for invitation to submit this manuscript for publication in "Sedimentary Basins: Evolution, Methods of Formation and Recent Advances" volume. Seismic profiles processed by PSDM and PSTM techniques were provided by Ms. Sujata Venketraman, Program Director G X Technologies, Houston, Texas, were of great value in understanding sedimentary basins. The authors also wish to thank Dr. S. J. Chopra, Chancellor, University of Petroleum and Energy Studies, Dehradun, for providing all possible help in research and preparation of manuscript. Innumerable anonymous well site geologists who have meticulously logged hundreds of drill holes from different basins are thankfully acknowledged.

REFERENCES

Alexander, P. O. (1981) Age and duration of Deccan Volcanism. (1981) *Geol. Soc. Ind. Mem*. 3. pp 244-253.

Baksi, A.K., Byerly, G.R. Chan, L-H and Farrar, E., (1994) Intracanyon flows in the Deccan Province, India? *Case history of the Rajahmundry Traps: Geology*, v.22, pp. 605-608.

Berger, P., Cerny, P., Hook, J.V., Jaffex, Kabir, C.S., Kumar, R., Minne, J.C., Pinningtou, D.J., Serra, O., Shukla, S.N., Sibbit And Visvanath, S.N., (1983), Petroleum Geology of India in Schlumberger, *Well Evaluation Conference*, pp 1-36.

Chatterjee, S.C., 1961. Petrology of the lavas of Pavagad Hill, Gujarat. *J. Geol. Soc. India*, 2, pp.61-77.

Jagannathan, C.R. Ratnam, C., Baishya and Das Gupta, U. (1983) Geology of the shore Mahanadi basin. *Petroleum Asia Journal. Spl. Issue Petroliferous Basins of India*, pp. 101-104.

Kent, R.W., Pringle, M.S. Muller, R.D., Saunders, A.D., Ghosh, N.C., (2002) 40Ar/39Ar Geochronology of the Rajmahal basalts, India and their relationship to the Kerguelan plateau, *Jour. Petrology* 43, pp 1141-1153.

La touché, J. H. D. and Christie (1910) The Geology of the Lonar Lake. *Rec. Geol. Surv. India*. v. 14, pp266-285.

Lisker, F. and Fachmann, S., 2001. Phanerozoic history of the Mahanadi region, India. *Journal of Geophysical Research: Solid Earth*, 106(B10), pp. 22027-22050.

Medlicott, H. B. and Blanford, W. T. (1879) *A Manual of the Geology of India Part 1*: *Peninsular India*, pp379-380.

Misra, K. S. (1981) The Tectonic Setting of Deccan Volcanics in Southern Saurashtra and northern Gujarat.) *Geol. Soc. Ind. Mem*. 3. pp 81-86.

Misra K.S., (1999) Deccan volcanics in Saurashtra and Kutch, Gujarat India. *Mem. Geol. Soc. India* No. 43, pp 352-334.

Misra, K.S., 2001. Lineament fabric and its relation to the eruption of Deccan volcanics and seismicity of westcentral India. *Geol. Surv. India,* pp.209-221.

Misra K.S., (2002) Arterial system of lava tubs and channels within Deccan Volcanics of western India, *Jour. Geol. Soc. India*, v.59, pp 115-124.

Misra, K.S., Bhutani, R. and Sonp, R., 2004. Seismogeology of the Kutch and Adjoining Region, with Special Reference to 26th January 2001 Earthquake in the Vicinity of Bachau, Gujarat. *Journal-Geological Society of India,* 64(2), pp.153-164.

Misra K.S., (2005) Distribution Pattern, Age and Distribution Pattern, Age and Duration and Mode of Eruption of Deccan and Associated Volcanics Gong. *Geol. Mag. Spl.* v. 8, pp 53-60.

Misra, K.S. (2007) Tectonic history of major geological structures of peninsular India and development of petroliferous basins and eruption

of Deccan and associated volcanics, *Jour. Geophysics*, v. 27, No.3, pp 3-14.

Misra, K. S. (2008a). Cretaceous Volcanic Sequences and Development of Hydrocarbon Pools in and Around Peninsular India. *Petroview*, Vol-2, No.3, September, 2008, pp.3-20.

Misra, K.S. (2008b) Dyke Swarms and Dykes within the Deccan Volcanic Province, India. *Indian Dykes*, Narosa Publishing House Pvt. Ltd. New Delhi, India, pp 57-72.

Misra, K.S. (2009). *Geological evidences suggesting volcanic origin of Lonar Crater, Deccan Volcanological Society*, Special Publication, April, 2009.

Misra, K. S., Misra, Anshuman (2010) Tectonic Evolution of Sedimentary Basins and development of Hydrocarbon Pools along the Off-shore and Oceanic Regions. *Gondwana Geol. Magazine*, Spl. V 12, pp 165-176.

Misra, K. S., Shukla, A. and Niyogi, S., 2016. Possibility of CO2 Sequestration in Basalt and Sub-Basalt Sediments in and Around Peninsular India. *Journal of Indian Geophysical Union*, pp.16-19.

Pringle, M. S., Storey, M., Wijbans, J., (1994) 40Ar/ 39Ar geochronology of Mid- Cretaceous Indian Ocean basalts: constrains of the origin of large basalt provinces, *EOS Transactions American Geophysical Union* 75 (abstract).

Pascoe, E. H. (1964) *The Geology of India and Burma*, V.III, Government of India Publication.

Radhakrishna, B.P., 1989. Suspect tectono-stratigraphic terrane elements in the Indian subcontinent. *J. Geol. Soc. India*, 34(1), p. 24.

Shankar, R., 1995. Fragmented Indian shield and recent earthquake. *Geol. Surv India Special Publ*, 27, pp. 41-48.

Roybarman, A. (1983) *Geology and Hydrocarbon Prospects of West Bengal. Petroleum Asia Journal*, Spl. Issue Petroliferous Basins of India, pp. 51-56.

Subba Rao, S. 1971. Petrogenesis of the acid igneous rocks of the Deccan Traps. *Bull. volcan.* 35, 983–97.

Vijaya (1997) Palynological dating of infra and intertrappean sediments in the Mesozoic succession of borehole PGD-6, Domra sub basin, West Bengal, India. *Cretaceous Research*, v.18, pp 833-848.

Washington, H. S. (1922) Deccan Traps and other plateau basalts. *Geol.Soc. Amer. Bull*. v.33, pp 765-804.

West, W. D. (1958) *The Stratigraphy and petro genesis of forty-eight flows of Deccan Traps*.Penetrated by boring in Western India. *Trans. Nat. Inst. Sci. India*, v. 4. pp 1-56.

West, W.D., 1962. The line of the Narmada and Son valleys. *Cur. Sci., 31,* pp.143-144.

In: Sedimentary Basins
Editor: Sam Brookes
ISBN: 978-1-53613-922-8

Chapter 3

XRF ANALYSIS APPLIED TO THE BATATEIRA RIVER FORMATION (ARARIPE SEDIMENTARY BASIN, CEARÁ STATE, BRAZIL)

Gabrielle Roveratti[1] and Daniel Marcos Bonotto[2]
[1]Claretiano Faculdade, Rio Claro, São Paulo, Brasil
[2]Departamento de Petrologia e Metalogenia, Universidade Estadual Paulista (UNESP), Câmpus de Rio Claro, Rio Claro, São Paulo, Brasil

ABSTRACT

Recent analytical advances mainly concerning to the use of the X-Rays Fluorescence (XRF) technique have improved the data acquisition in sedimentary basins. This method consists of the processes of electrons excitation and energy conversion in the region of the X-Rays photons. It has been widely used in Geosciences to determinate the elements concentration in samples of rocks, minerals, soils, sediments, etc. The installation of one S8 Tiger spectrometer from Bruker Co. happened at LARIN (Ionizing Radiations Laboratory), UNESPetro (Geosciences Center Applied to Petroleum), IGCE-UNESP-Rio Claro

(SP), Brazil, with financial support from Petrobras. Two software packages came with the equipment: QuantExpress (for powder analysis) and GeoMaj (for fused beads analysis). In this chapter are reported the results obtained from several essays held with aliquots of a sample of the lithostratigraphic formation known as "Batateira Layers" that occurs in the Araripe Sedimentary Basin, Ceará State, Brazil. The tests were realized with powdered aliquots, considering the oxides often used in geochemical investigations: SiO_2, Al_2O_3, TiO_2, Fe_2O_3, MnO, CaO, MgO, Na_2O, K_2O and P_2O_5. The maximum voltage and current were 50 kV and 50 mA, respectively. The following experimental conditions were adopted: analysis method (Fast, Full and Best), aliquot weight (10g, 8g, 6g, 4g and 2g) and boric acid amount (3.5g and 5g). The most striking variation was for SiO_2, Al_2O_3 and MgO among the investigated parameters. It was possible identify that both the readings method and aliquot weight affected the acquired results. Little or none influence was found in the quantity of boric acid used in the pellets preparation as it was obtained a highly significant Pearson correlation coefficient (r = 0.98) among the readings realized with 3.5 g and 5 g.

INTRODUCTION

The analysis by the X-rays fluorescence (XRF) technique is widely used in Geosciences to provide the elements concentration in samples of rocks, minerals, ores, soils, sediments, etc. This technique reaches the electromagnetic spectrum region between 0.1 and 100 Å. The XRF purpose consists on determining qualitatively and quantitatively the elements concentration by measuring the emitted radiations when the chemical elements in a sample forcedly emit X-rays as detailed elsewhere [1-3].

This technique was applied to "Batateira" layers located at Araripe Basin (Fig 1), which is included in a set of small basins belonging to the "Northeast interior basins" [4]. It is a complex sequence located in the extreme south of Ceará State, also comprising parts of Pernambuco and Piauí states (Figure 1). Araripe basin has a total area of about 8,000 km^2, limited by the following geographic coordinates: longitude - 38º30´W up to 40º55´W; latitude - 07º07´S up to 07º49´S (Figure 2). The "Northeast interior basins" geotectonic set is formed by sedimentary basins with

typical young rifts structures filled by terrigenous sediments of Eo-Jurassic to Neo-Cretaceous ages embedded in Borborema Province basement and associated to great Pre-Cambrian lineaments [4].

The origin of Araripe Basin directly links to the South Atlantic Ocean opening event, which involved the entire east portion of the South-American Platform (Wealdenian Reactivation), which is responsible by the Gondwana paleo-continent fragmentation and by the Mesozoic rifts formation from Brazilian Northeast [4]. The intense activity of the South-American Platform created large taphrogenic depressions, allowing the formation of deposition centers of Meso-Cenozoic sequences that comprise today the Araripe Sedimentary Sequence [5].

Ponte and Appi [6] gave the name of Batateira River Formation to the Abaiara Formation [5]. All Mesozoic sedimentary records after the Wealdenian Reactivation in the "Northeast interior basins" are included in the Post-Rift sequence [7, 8]. Batateira River Formation is located in the basis of the Post-Rift Tectonic-Sequence of Araripe Basin, also composed by Santana, Arajara and Exú formations.

Batateira River Formation consists from the basis to the top of thick white and yellow sandstone banks, with mean and coarse badly selected grains exhibiting crossed stratification and irregular bedding, also displaying frequent allochthonous clastic sediments of red claystones, cut and filling structures and ferruginous crusts (Figure 3). Medium to thin interlayered sandstones also occur together with yellow, reddish and grayish stratified clayey siltstones. Fine, well-selected and laminated white sandstones possessing large crossed stratification are of less frequent occurrence. The section displays a clear enhancement of the grain size decrease, gradually prevailing the fine clayey sandstones, siltstones and shales together with bituminous, papyraceous and fossiliferous shales. Above starts a new grain size decreasing depositional cycle, beginning with conglomerates and mean laminated sandstones in the transition of Crato Member of Santana Formation. This lithological succession illustrates two cycles of a fluvial-lacustrine depositional system [6].

Batateira River Formation records only occur in Cariri Valley structural depressions and in the rift buried under Araripe Chapada. 2-AR-

1-CE well crosses it in a 198-m section of the 514-712 m depth interval from this unity [6]. The dark shales, mainly the betuminous, are very fossiliferous (fragments of fish, conchostraceous, ostracods and biozones pollen from the upper part of Alagoas Floor). The final portion of Batateira Formation correlates to Trairi Layers (Ceará Basin) and Ponta do Tubarão Layers (Potiguar Basin), both representing the Transitional Supersequence in their respective basins [9]. The Aptian/Albian transition at Araripe basin occurs between the dark shales and laminated limestones of Santana Formation basis.

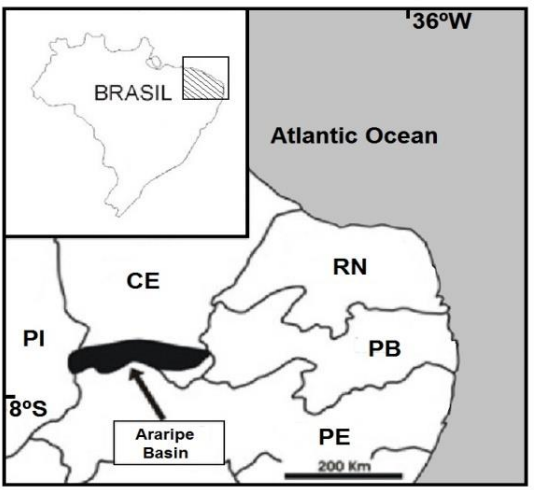

Figure 1. Location of Araripe Basin, Ceará State, Brazil.

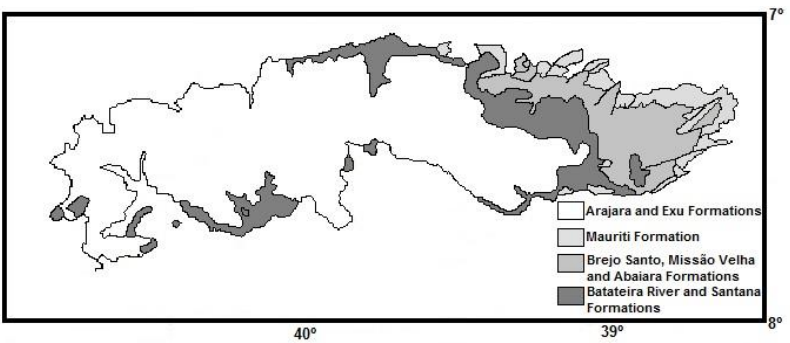

Figure 2. Major formations comprising the Araripe Basin. Modified from [9].

Figure 3. Some features of the Batateira River Formation. Adapted from [10].

MATERIALS AND METHODS

The installation of the XRF spectrometer used in this study (S8 Tiger from Bruker Co.) was at LARIN (Ionizing Radiations Laboratory), UNESPetro (Geosciences Center Applied to Petroleum), IGCE-UNESP-Rio Claro (SP), Brazil, with financial support from Petrobras. It realizes the elements quantification since beryllium (Be) up to uranium (U). Its maximum power is 1 kW, maximum current is 50 mA and maximum voltage is 50 kV. The machine does not require the use of external refrigeration with water, as adopted by other instruments. Two analytical software packages came with the equipment: QuantExpress, aimed to pressed samples (powder); GeoMaj, dedicated to fused samples.

This chapter presents the results acquired from several experiments performed with a sample of the Batateira River Formation by the pressed powder method. It was used the *QuantExpress* software and it was considered the eight abundant rock-forming elements (oxygen, silicon, aluminum, iron, calcium, sodium, potassium and magnesium) in their

oxide forms: SiO_2, Al_2O_3, Na_2O, K_2O, CaO, MgO, and Fe_2O_3 [11]. In addition, the oxides TiO_2, MnO and P_2O_5 that are often relevant in geochemical studies were also included in this study. The operational conditions corresponded to 30 kV and 5 mA of voltage and current, respectively.

Figure 4. Sample of the Batateira River Formation after the milling process.

Figure 5. General view of the Herzog stamping machine (left-outside; right-inside).

The pressed powder method consisted on mixing an amount of the powdered sample (<74 μm) (Figure 4) with the binding agent Oregon CAS9002-88-4 wax (~1.5g). After that, the mix was put in a stamping machine (Herzog Model HTP40-MA15277-1-1) together with an amount (3.5g-"Bat" or 5g-"Bat1") of boric acid (H_3BO_3) (Figures 5 and 6). The final pellet was a 40-mm diameter disc (Figure 7).

Initially, the sample's weight changed in the analyses, from 2g up to 10g. Then, it was changed the analysis time, according to three readings of the *QuantExpress* software: Fast (3 minutes), Full (8 minutes) e Best (15 minutes). The data considered here corresponded to those normalized by the software.

Figure 6. Crushed sample (left) and detail of the sample exit (right).

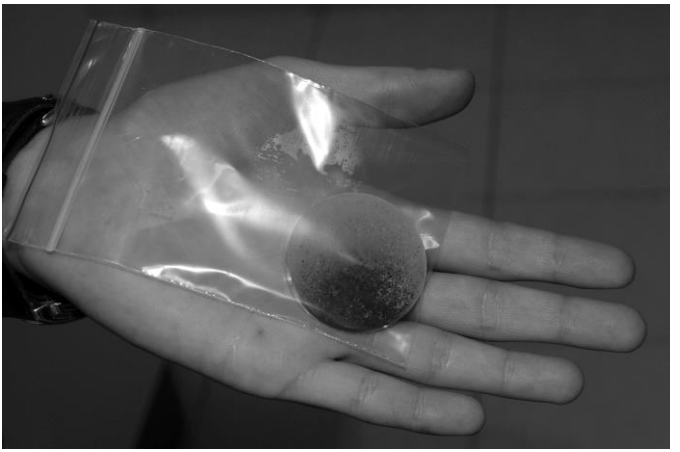

Figure 7. Pellet of the Batateira River Formation sample for XRF analysis.

RESULTS AND DISCUSSION

Table 1 reports the results of the readings obtained from all experiments, indicating quite variable concentrations, according to the aliquot weight, counting time (analysis mode), and boric acid quantity (3.5g or 5g). Plots of such database are in Figures 8 and 9 in order to identify possible trends related to the parameters investigated, which allowed construct Table 2 for their preliminary check. It was adopted YES (Y) for the reading that yielded the lowest concentration value, whereas NO (N) for others. The adoption of scores 0.5 or 0.3 to each reading happened if more than one analysis mode provided the lowest one. This procedure was used in order to evaluate the initial hypothesis that the Best mode would provide the lowest concentrations as the system operation during a longer counting time would allow the identification of elements remaining "invisible" in other faster readings. This was confirmed for 3.5g of boric acid, whereas the Fast mode yielded the more reliable results for the amount of boric acid corresponding to 5g.

Table 1. Analytical results (in %) obtained by XRF spectrometry applied to the Batateira River Formation sample

Oxide	2g			4g			6g			8g			10g		
	Fast	Full	Best	Fast	Full	Best	Fast	Full	Best	Fast	Full	Best	Fast	Full	Best
SiO_2	37.80[1]	39.12[1]	38.77[1]	40.09[1]	40.22[1]	39.51[1]	38.36[1]	39.31[1]	38.94[1]	39.80[1]	40.19[1]	39.57[1]	40.69[1]	39.07[1]	38.97[1]
(%)	39.51[2]	40.16[2]	39.86[2]	39.33[2]	40.22[2]	40.10[2]	40.50[2]	40.49[2]	39.89[2]	38.78[2]	39.19[2]	39.18[2]	38.83[2]	39.67[2]	39.91[2]
Al_2O_3	16.67[1]	16.32[1]	16.23[1]	16.74[1]	16.69[1]	16.98[1]	16.51[1]	16.77[1]	16.74[1]	16.59[1]	17.06[1]	16.76[1]	16.92[1]	16.62[1]	16.70[1]
(%)	16.52[2]	17.04[2]	17.16[2]	16.98[2]	17.25[2]	17.16[2]	17.02[2]	17.02[2]	17.08[2]	16.32[2]	16.63[2]	16.81[2]	17.21[2]	16.99[2]	17.10[2]
Fe_2O_3	8.44[1]	8.72[1]	8.62[1]	7.93[1]	8.72[1]	8.63[1]	7.68[1]	8.57[1]	8.59[1]	8.61[1]	8.54[1]	8.63[1]	8.34[1]	8.65[1]	8.66[1]
(%)	8.03[2]	8.46[2]	8.77[2]	8.26[2]	8.67[2]	8.66[2]	8.07[2]	8.52[2]	8.66[2]	8.09[2]	8.57[2]	8.61[2]	8.19[2]	8.48[2]	8.66[2]
K_2O	3.32[1]	3.35[1]	3.24[1]	3.48[1]	3.38[1]	3.37[1]	3.36[1]	3.35[1]	3.33[1]	3.67[1]	3.34[1]	3.35[1]	3.09[1]	3.30[1]	3.32[1]
(%)	3.29[2]	3.30[2]	3.30[2]	3.29[2]	3.40[2]	3.34[2]	3.22[2]	3.33[2]	3.35[2]	3.33[2]	3.32[2]	3.27[2]	3.27[2]	3.36[2]	3.35[2]
MgO	2.67[1]	2.61[1]	2.58[1]	2.68[1]	2.71[1]	2.69[1]	2.61[1]	2.62[1]	2.62[1]	2.52[1]	2.70[1]	2.71[1]	2.62[1]	2.58[1]	2.57[1]
(%)	2.72[2]	2.73[2]	2.69[2]	2.73[2]	2.68[2]	2.68[2]	3.51[2]	2.70[2]	2.76[2]	2.64[2]	2.68[2]	2.67[2]	2.72[2]	2.65[2]	2.71[2]
TiO_2	0.95[1]	0.86[1]	0.88[1]	0.99[1]	0.90[1]	0.85[1]	0.86[1]	0.85[1]	0.89[1]	0.85[1]	0.85[1]	0.87[1]	0.86[1]	0.89[1]	0.85[1]
(%)	0.97[2]	0.84[2]	0.88[2]	0.96[2]	0.92[2]	0.85[2]	0.83[2]	0.90[2]	0.87[2]	0.95[2]	0.90[2]	0.86[2]	0.80[2]	0.84[2]	0.84[2]
CaO	0.67[1]	0.59[1]	0.59[1]	0.58[1]	0.56[1]	0.59[1]	0.65[1]	0.58[1]	0.58[1]	0.62[1]	0.60[1]	0.58[1]	0.59[1]	0.59[1]	0.59[1]
(%)	0.64[2]	0.61[2]	0.58[2]	0.51[2]	0.58[2]	0.58[2]	0.49[2]	0.59[2]	0.57[2]	0.66[2]	0.60[2]	0.60[2]	0.56[2]	0.62[2]	0.58[2]
P_2O_5	0.15[1]	N/D[1]	0.11[1]	N/D[1]	0.11[1]	0.09[1]	N/D[1]	0.12[1]	0.09[1]	N/D[1]	0.10[1]	0.11[1]	0.10[1]	0.11[1]	0.10[1]
(%)	0.17[2]	0.08[2]	0.10[2]	0.14[2]	0.12[2]	0.11[2]	0.16[2]	0.10[2]	0.11[2]	0.13[2]	0.09[2]	0.13[2]	0.18[2]	0.12[2]	0.11[2]
Na_2O	N/D[1]	0.06[1]	0.06[1]	N/D[1]	N/D[1]	0.05[1]	N/D[1]	N/D[1]	0.04[1]	N/D[1]	N/D[1]	0.05[1]	N/D[1]	N/D[1]	0.04[1]
(%)	N/D[2]	N/D[2]	0.05[2]	N/D[2]	N/D[2]	0.04[2]	0.10[2]	0.07[2]	0.04[2]	N/D[2]	N/D[2]	0.05[2]	N/D[2]	N/D[2]	0.06[2]
MnO	0.03[1]	0.03[1]	0.03[1]	0.02[1]	0.03[1]	0.03[1]	0.03[1]	0.03[1]	0.04[1]	0.03[1]	0.03[1]	0.03[1]	0.02[1]	0.03[1]	0.03[1]
(%)	0.03[2]	0.03[2]	0.03[2]	0.03[2]	0.03[2]	0.03[2]	N/D[2]	0.03[2]	0.03[2]	0.03[2]	0.03[2]	0.03[2]	N/D[2]	0.04[2]	0.03[1]

[1]Bat = 3.5g; [2]Bat1 = 5g.

Table 2. Scores of the lowest concentrations obtained by the different analysis modes of the XRF spectrometry applied to the Batateira River Formation sample. Y = YES; N = NO

	Mode	2g	4g	6g	8g	10g	Scores	Scores (%)
SiO_2 (%)	Fast	$Y^{(1)}$ $N^{(2)}$	$N^{(1)}$ $N^{(2)}$	$N^{(1)}$ $N^{(2)}$	$N^{(1)}$ $Y^{(2)}$	$N^{(1)}$ $N^{(2)}$	$1^{(1)}$ $1^{(2)}$	$6.25^{(1)}$ $6.80^{(2)}$
	Full	$N^{(1)}$ $N^{(2)}$	$N^{(1)}$ $N^{(2)}$	$N^{(1)}$ $N^{(2)}$	$N^{(1)}$ $N^{(2)}$	$N^{(1)}$ $N^{(2)}$	$0^{(1)}$ $0^{(2)}$	$0^{(1)}$ $0^{(2)}$
	Best	$N^{(1)}$ $N^{(2)}$	$N^{(1)}$ $N^{(2)}$	$N^{(1)}$ $N^{(2)}$	$N^{(1)}$ $N^{(2)}$	$N^{(1)}$ $N^{(2)}$	$0^{(1)}$ $0^{(2)}$	$0^{(1)}$ $0^{(2)}$
Al_2O_3 (%)	Fast	$N^{(1)}$ $N^{(2)}$	$N^{(1)}$ $N^{(2)}$	$N^{(1)}$ $N^{(2)}$	$N^{(1)}$ $Y^{(2)}$	$N^{(1)}$ $N^{(2)}$	$0^{(1)}$ $1^{(2)}$	$0^{(1)}$ $6.80^{(2)}$
	Full	$N^{(1)}$ $N^{(2)}$	$N^{(1)}$ $N^{(2)}$	$N^{(1)}$ $N^{(2)}$	$N^{(1)}$ $N^{(2)}$	$N^{(1)}$ $N^{(2)}$	$0^{(1)}$ $0^{(2)}$	$0^{(1)}$ $0^{(2)}$
	Best	$Y^{(1)}$ $N^{(2)}$	$N^{(1)}$ $N^{(2)}$	$N^{(1)}$ $N^{(2)}$	$N^{(1)}$ $N^{(2)}$	$N^{(1)}$ $N^{(2)}$	$1^{(1)}$ $0^{(2)}$	$6.25^{(1)}$ $0^{(2)}$
Na_2O (%)	Fast	$N^{(1)}$ $N^{(2)}$	$N^{(1)}$ $N^{(2)}$	$N^{(1)}$ $N^{(2)}$	$N^{(1)}$ $N^{(2)}$	$N^{(1)}$ $N^{(2)}$	$0^{(1)}$ $0^{(2)}$	$0^{(1)}$ $0^{(2)}$
	Full	$N^{(1)}$ $N^{(2)}$	$N^{(1)}$ $N^{(2)}$	$N^{(1)}$ $N^{(2)}$	$N^{(1)}$ $N^{(2)}$	$N^{(1)}$ $N^{(2)}$	$0^{(1)}$ $0^{(2)}$	$0^{(1)}$ $0^{(2)}$
	Best	$N^{(1)}$ $N^{(2)}$	$N^{(1)}$ $Y^{(2)}$	$Y^{(1)}$ $Y^{(2)}$	$N^{(1)}$ $N^{(2)}$	$Y^{(1)}$ $N^{(2)}$	$2^{(1)}$ $2^{(2)}$	$12.50^{(1)}$ $13.60^{(2)}$
K_2O (%)	Fast	$N^{(1)}$ $N^{(2)}$	$N^{(1)}$ $N^{(2)}$	$N^{(1)}$ $Y^{(2)}$	$N^{(1)}$ $N^{(2)}$	$Y^{(1)}$ $N^{(2)}$	$1^{(1)}$ $1^{(2)}$	$6.25^{(1)}$ $13.60^{(2)}$
	Full	$N^{(1)}$ $N^{(2)}$	$N^{(1)}$ $N^{(2)}$	$N^{(1)}$ $N^{(2)}$	$N^{(1)}$ $N^{(2)}$	$N^{(1)}$ $N^{(2)}$	$0^{(1)}$ $0^{(2)}$	$0^{(1)}$ $0^{(2)}$
	Best	$N^{(1)}$ $N^{(2)}$	$N^{(1)}$ $N^{(2)}$	$N^{(1)}$ $N^{(2)}$	$N^{(1)}$ $N^{(2)}$	$N^{(1)}$ $N^{(2)}$	$0^{(1)}$ $0^{(2)}$	$0^{(1)}$ $0^{(2)}$
CaO (%)	Fast	$N^{(1)}$ $N^{(2)}$	$N^{(1)}$ $N^{(2)}$	$N^{(1)}$ $Y^{(2)}$	$N^{(1)}$ $N^{(2)}$	$N^{(1)}$ $N^{(2)}$	$0^{(1)}$ $1^{(2)}$	$0^{(1)}$ $6.80^{(2)}$
	Full	$N^{(1)}$ $N^{(2)}$	$Y^{(1)}$ $N^{(2)}$	$N^{(1)}$ $N^{(2)}$	$N^{(1)}$ $N^{(2)}$	$N^{(1)}$ $N^{(2)}$	$1^{(1)}$ $0^{(2)}$	$6.25^{(1)}$ $0^{(2)}$
	Best	$N^{(1)}$ $N^{(2)}$	$N^{(1)}$ $N^{(2)}$	$N^{(1)}$ $N^{(2)}$	$N^{(1)}$ $N^{(2)}$	$N^{(1)}$ $N^{(2)}$	$0^{(1)}$ $0^{(2)}$	$0^{(1)}$ $0^{(2)}$
MgO (%)	Fast	$N^{(1)}$ $N^{(2)}$	$N^{(1)}$ $N^{(2)}$	$N^{(1)}$ $N^{(2)}$	$Y^{(1)}$ $Y^{(2)}$	$N^{(1)}$ $N^{(2)}$	$1^{(1)}$ $1^{(2)}$	$6.25^{(1)}$ $6.80^{(2)}$
	Full	$N^{(1)}$ $N^{(2)}$	$N^{(1)}$ $N^{(2)}$	$N^{(1)}$ $N^{(2)}$	$N^{(1)}$ $N^{(2)}$	$N^{(1)}$ $N^{(2)}$	$0^{(1)}$ $0^{(2)}$	$0^{(1)}$ $0^{(2)}$
	Best	$N^{(1)}$ $N^{(2)}$	$N^{(1)}$ $N^{(2)}$	$N^{(1)}$ $N^{(2)}$	$N^{(1)}$ $N^{(2)}$	$N^{(1)}$ $N^{(2)}$	$0^{(1)}$ $0^{(2)}$	$0^{(1)}$ $0^{(2)}$
Fe_2O_3 (%)	Fast	$N^{(1)}$ $Y^{(2)}$	$N^{(1)}$ $N^{(2)}$	$Y^{(1)}$ $N^{(2)}$	$N^{(1)}$ $N^{(2)}$	$N^{(1)}$ $N^{(2)}$	$1^{(1)}$ $1^{(2)}$	$6.25^{(1)}$ $6.80^{(2)}$
	Full	$N^{(1)}$ $N^{(2)}$	$N^{(1)}$ $N^{(2)}$	$N^{(1)}$ $N^{(2)}$	$N^{(1)}$ $N^{(2)}$	$N^{(1)}$ $N^{(2)}$	$0^{(1)}$ $0^{(2)}$	$0^{(1)}$ $0^{(2)}$
	Best	$N^{(1)}$ $N^{(2)}$	$N^{(1)}$ $N^{(2)}$	$N^{(1)}$ $N^{(2)}$	$N^{(1)}$ $N^{(2)}$	$N^{(1)}$ $N^{(2)}$	$0^{(1)}$ $0^{(2)}$	$0^{(1)}$ $0^{(2)}$
TiO_2 (%)	Fast	$N^{(1)}$ $N^{(2)}$	$N^{(1)}$ $N^{(2)}$	$N^{(1)}$ $N^{(2)}$	$Y^{(1)}$ $N^{(2)}$	$N^{(1)}$ $Y^{(2)}$	$0.5^{(1)}$ $1^{(2)}$	$3.125^{(1)}$ $6.80^{(2)}$
	Full	$N^{(1)}$ $N^{(2)}$	$N^{(1)}$ $N^{(2)}$	$Y^{(1)}$ $N^{(2)}$	$Y^{(1)}$ $N^{(2)}$	$N^{(1)}$ $N^{(2)}$	$1.5^{(1)}$ $0^{(2)}$	$15.625^{(1)}$ $0^{(2)}$

	Mode	2g	4g	6g	8g	10g	Scores	Scores (%)
	Best	N[(1)] N[(2)]	Y[(1)] N[(2)]	N[(1)] N[(2)]	N[(1)] N[(2)]	Y[(1)] N[(2)]	2[(1)] 0[(2)]	12.50[(1)] 0[(2)]
MnO (%)	Fast	N[(1)] Y[(2)]	Y[(1)] Y[(2)]	N[(1)] N[(2)]	N[(1)] Y[(2)]	Y[(1)] N[(2)]	2[(1)] 0.9[(2)]	12.50[(1)] 6.19[(2)]
	Full	N[(1)] Y[(2)]	N[(1)] Y[(2)]	N[(1)] Y[(2)]	N[(1)] Y[(2)]	N[(1)] N[(2)]	0[(1)] 1.4[(2)]	0[(1)] 9.52[(2)]
	Best	N[(1)] Y[(2)]	N[(1)] Y[(2)]	N[(1)] Y[(2)]	N[(1)] Y[(2)]	N[(1)] Y[(2)]	0[(1)] 2.4[(2)]	0[(1)] 16.32[(2)]
P_2O_5 (%)	Fast	N[(1)] N[(2)]	N[(1)] N[(2)]	N[(1)] N[(2)]	N[(1)] N[(2)]	N[(1)] N[(2)]	0[(1)] 0[(2)]	0[(1)] 0[(2)]
	Full	N[(1)] Y[(2)]	N[(1)] N[(2)]	N[(1)] N[(2)]	N[(1)] N[(2)]	N[(1)] N[(2)]	0[(1)] 1[(2)]	0[(1)] 6.80[(2)]
	Best	N[(1)] N[(2)]	Y[(1)] N[(2)]	Y[(1)] N[(2)]	N[(1)] N[(2)]	N[(1)] N[(2)]	2[(1)] 0[(2)]	12.50[(1)] 0[(2)]
Total	Fast	1[(1)]	1[(1)]	1[(1)]	1.5[(1)]	2[(1)]	6.5[(1)]	40.6[(1)]
		1.3[(2)]	0.3[(2)]	2[(2)]	3.3[(2)]	1[(2)]	7.9[(2)]	53.7[(2)]
Scores	Full	0[(1)]	1[(1)]	1[(1)]	0.5[(1)]	0[(1)]	2.5[(1)]	15.6[(1)]
		1.3[(2)]	0.3[(2)]	0.5[(2)]	0.3[(2)]	0[(2)]	2.4[(2)]	16.3[(2)]
	Best	1[(1)]	2[(1)]	2[(1)]	0[(1)]	2[(1)]	7[(1)]	43.7[(1)]
		0.3[(2)]	1.3[(2)]	1.5[(2)]	0.3[(2)]	1[(2)]	4.4[(2)]	30[(2)]

[(1)] Bat = 3.5g; [(2)] Bat 1 = 5g.

Table 3. The difference (DIF) of each reading relative to the average value (AVE) obtained by XRF spectrometry applied to the Batateira River Formation sample, as well the DIF/AVE ratios. All data are in percentage

	Mode	SiO_2	Al_2O_3	Na_2O	K_2O	CaO	MgO	Fe_2O_3	TiO_2	MnO	P_2O_5
AVE		39.534(1)	16.687(1)	0.020(1)	3.350(1)	0.597(1)	2.633(1)	8.489(1)	0.880(1)	0.029(1)	0.084(1)
		39.708(2)	16.953(2)	0.027(2)	3.315(2)	0.585(2)	2.685(2)	8.447(2)	0.881(2)	0.025(2)	0.119(2)
		2g									
DIF	Fast	1.560(1)	0.017(1)	0.020(1)	0.030(1)	0.073(1)	0.037(1)	0.049(1)	0.070(1)	0.001(1)	0.066(1)
		0.198(2)	0.433(2)	0.027(2)	0.025(2)	0.055(2)	0.035(2)	0.417(2)	0.089(2)	0.025(2)	0.051(2)
	Full	0.240(1)	0.367(1)	0.040(1)	0.00(1)	0.007(1)	0.023(1)	0.231(1)	0.020(1)	0.001(1)	0.004(1)
		0.452(2)	0.087(2)	0.027(2)	0.015(2)	0.025(2)	0.045(2)	0.013(2)	0.041(2)	0.005(2)	0.119(2)
	Best	0.590(1)	0.457(1)	0.040(1)	0.110(1)	0.007(1)	0.053(1)	0.131(1)	0.00(1)	0.001(1)	0.026(1)
		0.152(2)	0.207(2)	0.023(2)	0.015(2)	0.005(2)	0.005(2)	0.323(2)	0.001(2)	0.005(2)	0.019(2)
DIF/AVE	Fast	0.040(1)	0.001(1)	1.00(1)	0.009(1)	0.123(1)	0.014(1)	0.006(1)	0.079(1)	0.034(1)	0.786(1)
		0.005(2)	0.025(2)	1.00(2)	0.007(2)	0.094(2)	0.013(2)	0.049(2)	0.101(2)	1.00(2)	0.429(2)
	Full	0.006(1)	0.022(1)	2.00(1)	0.00(1)	0.012(1)	0.009(1)	0.027(1)	0.023(1)	0.035(1)	0.048(1)
		0.011(2)	0.005(2)	1.00(2)	0.004(2)	0.043(2)	0.017(2)	0.001(2)	0.046(2)	0.200(2)	1.00(2)
	Best	0.015(1)	0.027(1)	2.00(1)	0.033(1)	0.012(1)	0.020(1)	0.015(1)	0.00(1)	0.035(1)	0.309(1)
		0.004(2)	0.012(2)	0.852(2)	0.004(2)	0.008(2)	0.002(2)	0.038(2)	0.001(2)	0.200(2)	0.160(2)
		4g									
DIF	Fast	0.730(1)	0.053(1)	0.020(1)	0.130(1)	0.017(1)	0.047(1)	0.559(1)	0.110(1)	0.009(1)	0.084(1)
		0.378(2)	0.027(2)	0.027(2)	0.025(2)	0.075(2)	0.045(2)	0.187(2)	0.079(2)	0.005(2)	0.021(2)
	Full	0.860(1)	0.003(1)	0.020(1)	0.030(1)	0.037(1)	0.077(1)	0.231(1)	0.020(1)	0.001(1)	0.036(1)
		0.512(2)	0.297(2)	0.027(2)	0.085(2)	0.005(2)	0.005(2)	0.223(2)	0.039(2)	0.005(2)	0.009(2)
	Best	0.150(1)	0.293(1)	0.030(1)	0.020(1)	0.007(1)	0.057(1)	0.141(1)	0.030(1)	0.001(1)	0.006(1)
		0.392(2)	0.207(2)	0.013(2)	0.025(2)	0.005(2)	0.005(2)	0.213(2)	0.031(2)	0.005(2)	0.009(2)

	Mode	SiO_2	Al_2O_3	Na_2O	K_2O	CaO	MgO	Fe_2O_3	TiO_2	MnO	P_2O_5
DIF/AVE	Fast	$0.019^{(1)}$	$0.003^{(1)}$	$1.00^{(1)}$	$0.039^{(1)}$	$0.028^{(1)}$	$0.018^{(1)}$	$0.066^{(1)}$	$0.125^{(1)}$	$0.310^{(1)}$	$1.00^{(1)}$
		$0.009^{(2)}$	$0.002^{(2)}$	$1.00^{(2)}$	$0.007^{(2)}$	$0.128^{(2)}$	$0.017^{(2)}$	$0.022^{(2)}$	$0.090^{(2)}$	$0.200^{(2)}$	$0.176^{(2)}$
	Full	$0.022^{(1)}$	$0.0002^{(1)}$	$1.00^{(1)}$	$0.009^{(1)}$	$0.062^{(1)}$	$0.029^{(1)}$	$0.027^{(1)}$	$0.023^{(1)}$	$0.034^{(1)}$	$0.429^{(1)}$
		$0.013^{(2)}$	$0.017^{(2)}$	$1.00^{(2)}$	$0.026^{(2)}$	$0.008^{(2)}$	$0.002^{(2)}$	$0.026^{(2)}$	$0.044^{(2)}$	$0.200^{(2)}$	$0.076^{(2)}$
	Best	$0.004^{(1)}$	$0.018^{(1)}$	$1.50^{(1)}$	$0.006^{(1)}$	$0.012^{(1)}$	$0.022^{(1)}$	$0.017^{(1)}$	$0.034^{(1)}$	$0.034^{(1)}$	$0.071^{(1)}$
		$0.010^{(2)}$	$0.012^{(2)}$	$0.481^{(2)}$	$0.007^{(2)}$	$0.008^{(2)}$	$0.002^{(2)}$	$0.025^{(2)}$	$0.035^{(2)}$	$0.200^{(2)}$	$0.076^{(2)}$
		6g									
DIF	Fast	$1.00^{(1)}$	$0.177^{(1)}$	$0.020^{(1)}$	$0.010^{(1)}$	$0.053^{(1)}$	$0.023^{(1)}$	$0.809^{(1)}$	$0.020^{(1)}$	$0.001^{(1)}$	$0.084^{(1)}$
		$0.792^{(2)}$	$0.067^{(2)}$	$0.073^{(2)}$	$0.095^{(2)}$	$0.095^{(2)}$	$0.175^{(2)}$	$0.377^{(2)}$	$0.051^{(2)}$	$0.025^{(2)}$	$0.041^{(2)}$
	Full	$0.050^{(1)}$	$0.083^{(1)}$	$0.053^{(1)}$	$0.00^{(1)}$	$0.017^{(1)}$	$0.013^{(1)}$	$0.081^{(1)}$	$0.030^{(1)}$	$0.001^{(1)}$	$0.016^{(1)}$
		$0.782^{(2)}$	$0.067^{(2)}$	$0.043^{(2)}$	$0.015^{(2)}$	$0.005^{(2)}$	$0.015^{(2)}$	$0.073^{(2)}$	$0.019^{(2)}$	$0.005^{(2)}$	$0.001^{(2)}$
	Best	$0.420^{(1)}$	$0.053^{(1)}$	$0.020^{(1)}$	$0.020^{(1)}$	$0.017^{(1)}$	$0.013^{(1)}$	$0.101^{(1)}$	$0.010^{(1)}$	$0.011^{(1)}$	$0.006^{(1)}$
		$0.182^{(2)}$	$0.127^{(2)}$	$0.013^{(2)}$	$0.035^{(2)}$	$0.015^{(2)}$	$0.075^{(2)}$	$0.213^{(2)}$	$0.011^{(2)}$	$0.005^{(2)}$	$0.009^{(2)}$
DIF/AVE	Fast	$0.025^{(1)}$	$0.011^{(1)}$	$1.000^{(1)}$	$0.003^{(1)}$	$0.089^{(1)}$	$0.009^{(1)}$	$0.095^{(1)}$	$0.023^{(1)}$	$0.035^{(1)}$	$1.000^{(1)}$
		$0.020^{(2)}$	$0.004^{(2)}$	$2.704^{(2)}$	$0.029^{(2)}$	$0.162^{(2)}$	$0.065^{(2)}$	$0.045^{(2)}$	$0.058^{(2)}$	$1.000^{(2)}$	$0.344^{(2)}$
	Full	$0.001^{(1)}$	$0.005^{(1)}$	$1.00^{(1)}$	$0.00^{(1)}$	$0.028^{(1)}$	$0.005^{(1)}$	$0.009^{(1)}$	$0.034^{(1)}$	$0.034^{(1)}$	$0.190^{(1)}$
		$0.020^{(2)}$	$0.004^{(2)}$	$1.592^{(2)}$	$0.004^{(2)}$	$0.008^{(2)}$	$0.006^{(2)}$	$0.009^{(2)}$	$0.022^{(2)}$	$0.200^{(2)}$	$0.008^{(2)}$
	Best	$0.011^{(1)}$	$0.003^{(1)}$	$1.00^{(1)}$	$0.006^{(1)}$	$0.028^{(1)}$	$0.005^{(1)}$	$0.012^{(1)}$	$0.011^{(1)}$	$0.379^{(1)}$	$0.071^{(1)}$
		$0.005^{(2)}$	$0.007^{(2)}$	$0.481^{(2)}$	$0.010^{(2)}$	$0.026^{(2)}$	$0.028^{(2)}$	$0.025^{(2)}$	$0.013^{(2)}$	$0.200^{(2)}$	$0.076^{(2)}$
		8g									
DIF	Fast	$0.440^{(1)}$	$0.097^{(1)}$	$0.020^{(1)}$	$0.320^{(1)}$	$0.023^{(1)}$	$0.113^{(1)}$	$0.121^{(1)}$	$0.030^{(1)}$	$0.001^{(1)}$	$0.084^{(1)}$
		$0.928^{(2)}$	$0.633^{(2)}$	$0.027^{(2)}$	$0.015^{(2)}$	$0.075^{(2)}$	$0.045^{(2)}$	$0.357^{(2)}$	$0.069^{(2)}$	$0.005^{(2)}$	$0.011^{(2)}$
	Full	$0.830^{(1)}$	$0.373^{(1)}$	$0.020^{(1)}$	$0.010^{(1)}$	$0.003^{(1)}$	$0.067^{(1)}$	$0.051^{(1)}$	$0.030^{(1)}$	$0.001^{(1)}$	$0.006^{(1)}$
		$0.518^{(2)}$	$0.323^{(2)}$	$0.027^{(2)}$	$0.005^{(2)}$	$0.015^{(2)}$	$0.005^{(2)}$	$0.123^{(2)}$	$0.019^{(2)}$	$0.005^{(2)}$	$0.019^{(2)}$
	Best	$0.210^{(1)}$	$0.073^{(1)}$	$0.030^{(1)}$	$0.000^{(1)}$	$0.017^{(1)}$	$0.077^{(1)}$	$0.141^{(1)}$	$0.010^{(1)}$	$0.001^{(1)}$	$0.026^{(1)}$
		$0.528^{(2)}$	$0.143^{(2)}$	$0.023^{(2)}$	$0.045^{(2)}$	$0.015^{(2)}$	$0.015^{(2)}$	$0.163^{(2)}$	$0.021^{(2)}$	$0.005^{(2)}$	$0.011^{(2)}$

Table 3. (Continued)

	Mode	SiO_2	Al_2O_3	Na_2O	K_2O	CaO	MgO	Fe_2O_3	TiO_2	MnO	P_2O_5
DIF/AVE	Fast	0.011[(1)]	0.006[(1)]	1.000[(1)]	0.095[(1)]	0.038[(1)]	0.043[(1)]	0.014[(1)]	0.034[(1)]	0.034[(1)]	1.000[(1)]
		0.023[(2)]	0.037[(2)]	1.000[(2)]	0.004[(2)]	0.128[(2)]	0.017[(2)]	0.042[(2)]	0.078[(2)]	0.200[(2)]	0.092[(2)]
	Full	0.021[(1)]	0.022[(1)]	1.000[(1)]	0.003[(1)]	0.005[(1)]	0.025[(1)]	0.006[(1)]	0.034[(1)]	0.034[(1)]	0.071[(1)]
		0.013[(2)]	0.019[(2)]	1.000[(2)]	0.001[(2)]	0.026[(2)]	0.002[(2)]	0.015[(2)]	0.022[(2)]	0.200[(2)]	0.160[(2)]
	Best	0.005[(1)]	0.004[(1)]	1.500[(1)]	0.000[(1)]	0.028[(1)]	0.029[(1)]	0.017[(1)]	0.011[(1)]	0.034[(1)]	0.310[(1)]
		0.013[(2)]	0.008[(2)]	0.852[(2)]	0.014[(2)]	0.026[(2)]	0.006[(2)]	0.019[(2)]	0.024[(2)]	0.200[(2)]	0.092[(2)]
		10g									
DIF	Fast	1.330[(1)]	0.233[(1)]	0.020[(1)]	0.260[(1)]	0.007[(1)]	0.013[(1)]	0.149[(1)]	0.020[(1)]	0.009[(1)]	0.016[(1)]
		0.878[(2)]	0.257[(2)]	0.027[(2)]	0.045[(2)]	0.025[(2)]	0.035[(2)]	0.257[(2)]	0.081[(2)]	0.025[(2)]	0.061[(2)]
	Full	0.290[(1)]	0.067[(1)]	0.020[(1)]	0.050[(1)]	0.007[(1)]	0.053[(1)]	0.161[(1)]	0.010[(1)]	0.001[(1)]	0.036[(1)]
		0.038[(2)]	0.037[(2)]	0.027[(2)]	0.045[(2)]	0.035[(2)]	0.035[(2)]	0.033[(2)]	0.041[(2)]	0.015[(2)]	0.099[(2)]
	Best	0.390[(1)]	0.013[(1)]	0.020[(1)]	0.030[(1)]	0.007[(1)]	0.063[(1)]	0.171[(1)]	0.030[(1)]	0.001[(1)]	0.016[(1)]
		0.202[(2)]	0.147[(2)]	0.033[(2)]	0.035[(2)]	0.005[(2)]	0.025[(2)]	0.213[(2)]	0.041[(2)]	0.005[(2)]	0.009[(2)]
DIF/AVE	Fast	0.034[(1)]	0.014[(1)]	1.000[(1)]	0.078[(1)]	0.012[(1)]	0.005[(1)]	0.017[(1)]	0.023[(1)]	0.310[(1)]	0.190[(1)]
		0.022[(2)]	0.015[(2)]	1.000[(2)]	0.013[(2)]	0.043[(2)]	0.013[(2)]	0.030[(2)]	0.092[(2)]	1.000[(2)]	0.513[(2)]
	Full	0.007[(1)]	0.004[(1)]	1.000[(1)]	0.015[(1)]	0.012[(1)]	0.020[(1)]	0.019[(1)]	0.011[(1)]	0.034[(1)]	0.429[(1)]
		0.001[(2)]	0.002[(2)]	1.000[(2)]	0.014[(2)]	0.060[(2)]	0.013[(2)]	0.004[(2)]	0.046[(2)]	0.600[(2)]	0.076[(2)]
	Best	0.010[(1)]	0.001[(1)]	1.000[(1)]	0.009[(1)]	0.012[(1)]	0.024[(1)]	0.020[(1)]	0.034[(1)]	0.034[(1)]	0.190[(1)]
		0.005[(2)]	0.009[(2)]	1.222[(2)]	0.010[(2)]	0.008[(2)]	0.009[(2)]	0.025[(2)]	0.046[(2)]	0.200[(2)]	0.076[(2)]

[(1)] Bat = 3.5g; [(2)] Bat1 = 5g.

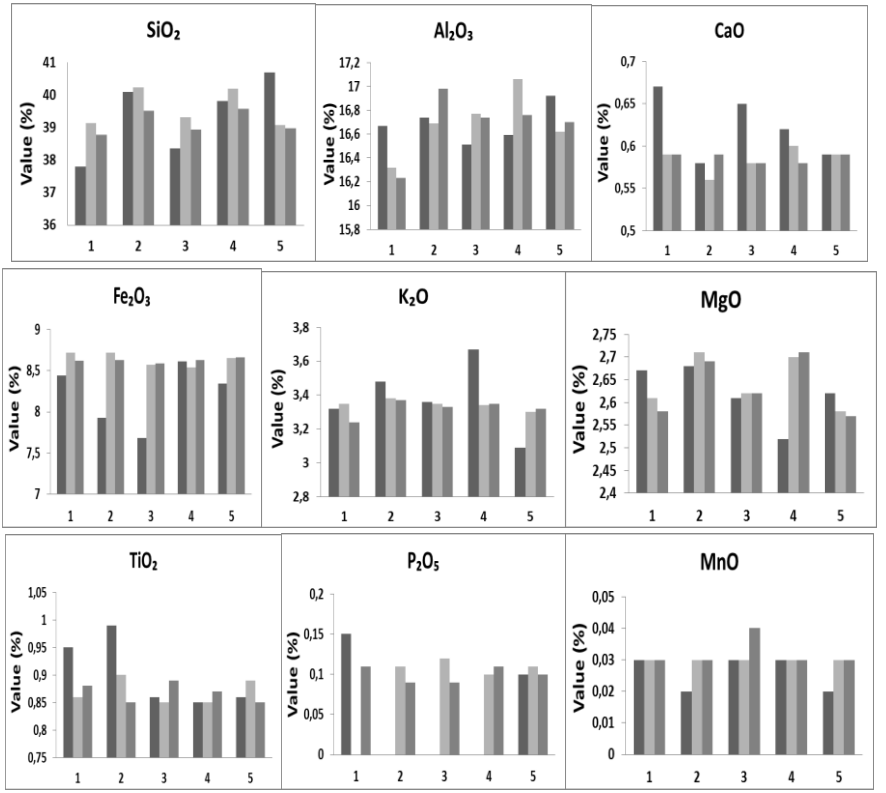

Figure 8. Plots of the XRF analytical data obtained for the Batateira River Formation sample (3.5g). Numbers 1, 2, 3, 4, and 5 correspond to aliquots of 2g, 4g, 6g, 8g, and 10g, respectively. Analysis mode: Fast (dark gray), Full (light gray), and Best (medium gray).

The data reported in Table 1 and plotted in Figure 8 indicate the following range of the concentration values (in %) for the Bat readings: SiO_2 (37.80-40.69), Al_2O_3 (16.23-17.06), Na_2O (0.04-0.06), K_2O (3.09-3.67), CaO (0.56-0.67), MgO (2.52-2.71), Fe_2O_3 (7.68-8,.2), TiO_2 (0.85-0.99), MnO (0.02-0.03) and P_2O_5 (0.09-0.15). Their average (AVE) values correspond to SiO_2 = 39.534%, Al_2O_3 = 16.687%, Na_2O = 0.020%, K_2O = 3.350%, CaO = 0.597%, MgO = 2.633%, Fe_2O_3 = 8.489%, TiO_2 = 0.880%, MnO = 0.029%, and P_2O_5 = 0.084%. The difference (DIF) of each reading relative to the average value is reported in Table 3, as well the DIF/AVE ratio (in percentage) that exhibits the following range: SiO_2

(0.38-3.38), Al_2O_3 (0.02-2.74), Na_2O (100-200), K_2O (0-9.55), CaO (0.50-12.23), MgO (0.49-4.29), Fe_2O_3 (0.58-9.53), TiO_2 (0-7.95), MnO (3.45-31.03) and P_2O_5 (4.76-100).

The data showed in Table 1 and Figure 9 indicate the following range of the concentration values (in %) for the Bat1 readings: SiO_2 (38.78-40.50), Al_2O_3 (16.52-17.25), Na_2O (0.04-0.1), K_2O (3.22-3.40), CaO (0.49-0.66), MgO (2.64-3.51), Fe_2O_3 (8.03-8.77), TiO_2 (0.83-0.97), MnO (0.03-0.04) and P_2O_5 (0.09-0.17). Their average (AVE) values correspond to SiO_2 = 39.708%, Al_2O_3 = 16.953%, Na_2O = 0.027%, K_2O = 3.315%, CaO = 0.585%, MgO = 2.685%, Fe_2O_3 = 8.447%, TiO_2 = 0.881%, MnO = 0.025%, and P_2O_5 = 0.119%. The difference (DIF) of each reading relative to the average value is reported in Table 3, as well the DIF/AVE ratio (in percentage) that exhibits the following range: SiO_2 (0.096-2.36), Al_2O_3 (0.22-3.74), Na_2O (48.15-270.37), K_2O (0.15-2.86), CaO (0.85-16.24), MgO (0.19-6.52), Fe_2O_3 (0.58-9.53), TiO_2 (0.11-10.10), MnO (20-100) and P_2O_5 (0.84-100).

Plots of such database are in Figures 10 and 11 in order to identify possible trends related to the oxides concentration, analysis mode and aliquot weight. The experimental conditions yielding the most suitable concentrations values correspond to those implying in the lowest DIF/AVE ratios. Evaluation of such situation happened from the scores reported in Table 4 as built adopting YES (Y) for the lowest ratios and NO (N) for others. The superscript $^{(1)}$ corresponds to the "Bat" aliquots (typical boric acid weight = 3.5 g), whereas the superscript $^{(2)}$ to the "Bat1" aliquots (5g of boric acid). Analogously to the criteria used in Table 2, adoption of scores 0.5 or 0.3 to each reading happened if more than one analysis mode provided the lowest DIF/AVE ratio. The simple statistical analysis shown in Table 4 indicates a total score of 36-44% for the Best analysis mode, as well that the 2g and 4g-aliquots yielded the highest scores. Therefore, in terms of the statistical point of view and among all tested experimental conditions, the Best analysis mode and the lightest aliquots weight yielded the most appropriate readings for the Batateira River Formation.

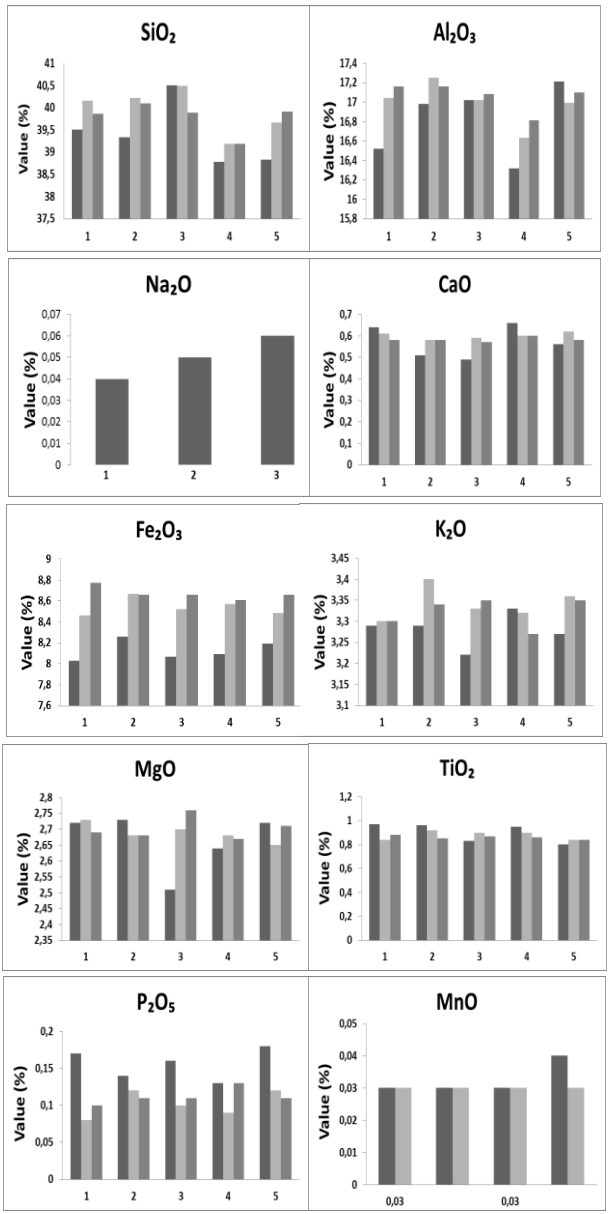

Figure 9. Plots of the XRF analytical data obtained for the Batateira River Formation sample (5g). Numbers 1, 2, 3, 4, and 5 correspond to aliquots of 2g, 4g, 6g, 8g, and 10g, respectively. Analysis mode: Fast (dark gray), Full (light gray), and Best (medium gray).

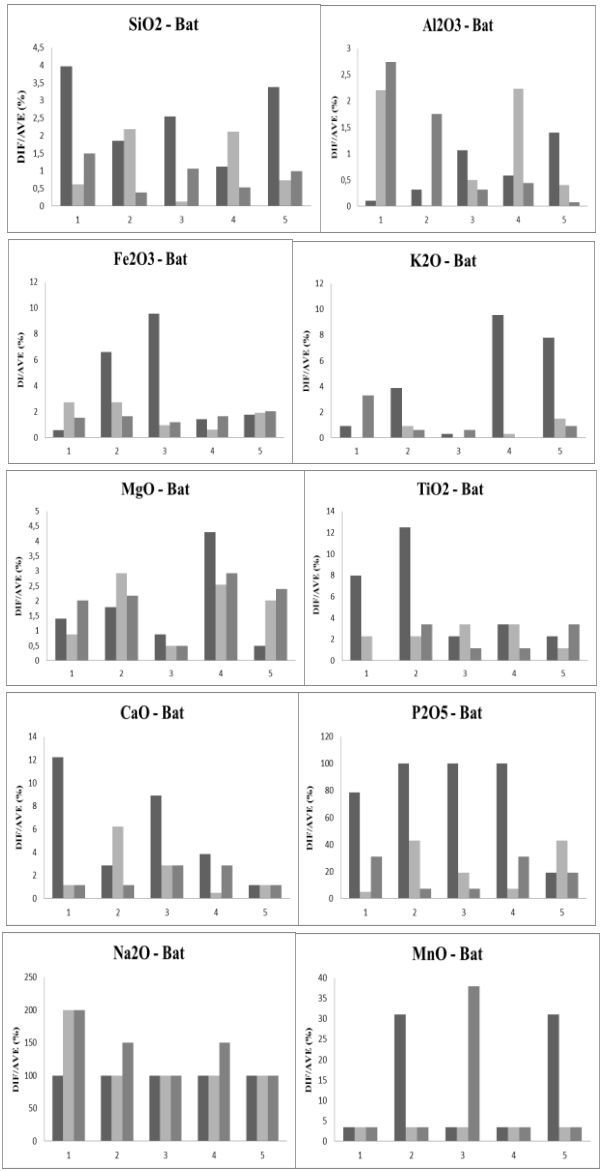

Figure 10. Plots of the DIF/AVE ratios for the XRF analytical data obtained for the Batateira River Formation sample with 3.5g of boric acid. Numbers 1, 2, 3, 4, and 5 correspond to aliquots of 2g, 4g, 6g, 8g, and 10g, respectively. Analysis mode: Fast (dark gray), Full (light gray), and Best (medium gray).

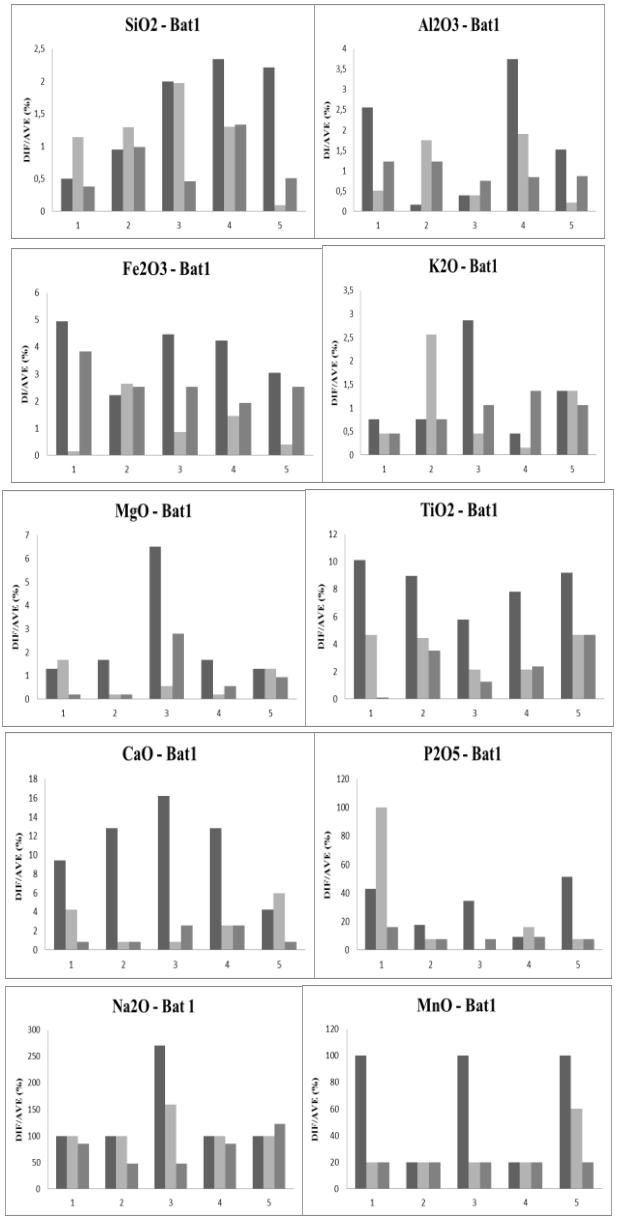

Figure 11. Plots of the DIF/AVE ratios for the XRF analytical data obtained for the Batateira River Formation sample with 5g of boric acid. Numbers 1, 2, 3, 4, and 5 correspond to aliquots of 2g, 4g, 6g, 8g, and 10g, respectively. Analysis mode: Fast (dark gray), Full (light gray), and Best (medium gray).

Table 4. Scores of the lowest DIF/AVE ratios obtained by the different analysis modes as well as the boric acid variations of the XRF spectrometry applied to the Batateira River Formation sample. Y = YES; N = NO

	Mode	2g	4g	6g	8g	10g	Scores	Scores (%)
SiO_2	Fast	$N^{(1)}$	$N^{(1)}$	$N^{(1)}$	$Y^{(1)}$	$N^{(1)}$	$1^{(1)}$	$2.62^{(1)}$
		$Y^{(2)}$	$N^{(2)}$	$N^{(2)}$	$N^{(2)}$	$N^{(2)}$	$1^{(2)}$	$2.40^{(2)}$
	Full	$N^{(1)}$	$N^{(1)}$	$Y^{(1)}$	$N^{(1)}$	$N^{(1)}$	$1^{(1)}$	$2.62^{(1)}$
		$N^{(2)}$	$N^{(2)}$	$N^{(2)}$	$N^{(2)}$	$Y^{(2)}$	$1^{(2)}$	$2.40^{(2)}$
	Best	$N^{(1)}$	$Y^{(1)}$	$N^{(1)}$	$N^{(1)}$	$N^{(1)}$	$1^{(1)}$	$2.62^{(1)}$
		$Y^{(2)}$	$N^{(2)}$	$N^{(2)}$	$N^{(2)}$	$N^{(2)}$	$1^{(2)}$	$2.40^{(2)}$
Al_2O_3	Fast	$Y^{(1)}$	$N^{(1)}$	$N^{(1)}$	$N^{(1)}$	$N^{(1)}$	$1^{(1)}$	$2.62^{(1)}$
		$N^{(2)}$	$Y^{(2)}$	$N^{(2)}$	$N^{(2)}$	$N^{(2)}$	$1^{(2)}$	$2.40^{(2)}$
	Full	$N^{(1)}$	$Y^{(1)}$	$N^{(1)}$	$N^{(1)}$	$N^{(1)}$	$1^{(1)}$	$2.62^{(1)}$
		$N^{(2)}$	$N^{(2)}$	$N^{(2)}$	$N^{(2)}$	$Y^{(2)}$	$1^{(2)}$	$2.40^{(2)}$
	Best	$N^{(1)}$	$N^{(1)}$	$N^{(1)}$	$N^{(1)}$	$Y^{(1)}$	$1^{(1)}$	$2.62^{(1)}$
		$N^{(2)}$	$N^{(2)}$	$Y^{(2)}$	$N^{(2)}$	$N^{(2)}$	$1^{(2)}$	$2.40^{(2)}$
Na_2O	Fast	$Y^{(1)}$	$Y^{(1)}$	$Y^{(1)}$	$Y^{(1)}$	$Y^{(1)}$	$2.6^{(1)}$	$2.812^{(1)}$
		$Y^{(2)}$	$Y^{(2)}$	$N^{(2)}$	$Y^{(2)}$	$Y^{(2)}$	$1.8^{(2)}$	$4.33^{(2)}$
	Full	$N^{(1)}$	$Y^{(1)}$	$Y^{(1)}$	$Y^{(1)}$	$Y^{(1)}$	$1.6^{(1)}$	$4.192^{(1)}$
		$Y^{(2)}$	$Y^{(2)}$	$N^{(2)}$	$Y^{(2)}$	$Y^{(2)}$	$1.8^{(2)}$	$4.33^{(2)}$
	Best	$N^{(1)}$	$N^{(1)}$	$Y^{(1)}$	$N^{(1)}$	$Y^{(1)}$	$0.6^{(1)}$	$1.572^{(1)}$
		$N^{(2)}$	$Y^{(2)}$	$Y^{(2)}$	$N^{(2)}$	$N^{(2)}$	$1.3^{(2)}$	$3.60^{(2)}$
K_2O	Fast	$N^{(1)}$	$N^{(1)}$	$Y^{(1)}$	$N^{(1)}$	$N^{(1)}$	$0.5^{(1)}$	$1.31^{(1)}$
		$N^{(2)}$	$N^{(2)}$	$N^{(2)}$	$Y^{(2)}$	$N^{(2)}$	$0.5^{(2)}$	$1.70^{(2)}$
	Full	$N^{(1)}$	$N^{(1)}$	$N^{(1)}$	$Y^{(1)}$	$N^{(1)}$	$1^{(1)}$	$1.31^{(1)}$
		$N^{(2)}$	$N^{(2)}$	$N^{(2)}$	$Y^{(2)}$	$N^{(2)}$	$0.5^{(2)}$	$1.70^{(2)}$
	Best	$N^{(1)}$	$Y^{(1)}$	$Y^{(1)}$	$N^{(1)}$	$N^{(1)}$	$1.5^{(1)}$	$1.31^{(1)}$
		$Y^{(2)}$	$N^{(2)}$	$N^{(2)}$	$N^{(2)}$	$N^{(2)}$	$1^{(2)}$	$2.40^{(2)}$
CaO	Fast	$N^{(1)}$	$N^{(1)}$	$N^{(1)}$	$N^{(1)}$	$Y^{(1)}$	$1^{(1)}$	$1.31^{(1)}$
		$N^{(2)}$	$N^{(2)}$	$N^{(2)}$	$N^{(2)}$	$Y^{(2)}$	$1^{(2)}$	$2.40^{(2)}$
	Full	$N^{(1)}$	$N^{(1)}$	$N^{(1)}$	$Y^{(1)}$	$N^{(1)}$	$1^{(1)}$	$2.62^{(1)}$
		$N^{(2)}$	$Y^{(2)}$	$Y^{(2)}$	$N^{(2)}$	$N^{(2)}$	$1.5^{(2)}$	$3.60^{(2)}$
	Best	$Y^{(1)}$	$Y^{(1)}$	$N^{(1)}$	$N^{(1)}$	$Y^{(1)}$	$2.5^{(1)}$	$6.55^{(1)}$
		$Y^{(2)}$	$Y^{(2)}$	$N^{(2)}$	$N^{(2)}$	$Y^{(2)}$	$2^{(2)}$	$4.80^{(2)}$
MgO	Fast	$N^{(1)}$	$N^{(1)}$	$N^{(1)}$	$N^{(1)}$	$Y^{(1)}$	$1^{(1)}$	$2.62^{(1)}$
		$Y^{(2)}$	$N^{(2)}$	$N^{(2)}$	$N^{(2)}$	$Y^{(2)}$	$1.5^{(2)}$	$3.60^{(2)}$
	Full	$N^{(1)}$	$N^{(1)}$	$Y^{(1)}$	$N^{(1)}$	$N^{(1)}$	$1^{(1)}$	$2.62^{(1)}$
		$N^{(2)}$	$Y^{(2)}$	$N^{(2)}$	$Y^{(2)}$	$N^{(2)}$	$1.5^{(2)}$	$3.60^{(2)}$

	Best	$Y^{(1)}$	$N^{(1)}$	$N^{(1)}$	$N^{(1)}$	$N^{(1)}$	$1^{(1)}$	$2.62^{(1)}$
		$Y^{(2)}$	$Y^{(2)}$	$N^{(2)}$	$N^{(2)}$	$N^{(2)}$	$1^{(2)}$	$2.62^{(2)}$
Fe_2O_3	Fast	$Y^{(1)}$	$N^{(1)}$	$N^{(1)}$	$N^{(1)}$	$N^{(1)}$	$1^{(1)}$	$2.62^{(1)}$
		$N^{(2)}$	$Y^{(2)}$	$N^{(2)}$	$N^{(2)}$	$N^{(2)}$	$1^{(2)}$	$2.62^{(2)}$
	Full	$N^{(1)}$	$N^{(1)}$	$N^{(1)}$	$Y^{(1)}$	$N^{(1)}$	$1^{(1)}$	$2.62^{(1)}$
		$Y^{(2)}$	$N^{(2)}$	$N^{(2)}$	$N^{(2)}$	$N^{(2)}$	$1^{(2)}$	$2.62^{(2)}$
	Best	$N^{(1)}$	$N^{(1)}$	$Y^{(1)}$	$N^{(1)}$	$N^{(1)}$	$1^{(1)}$	$2.62^{(1)}$
		$N^{(2)}$	$Y^{(2)}$	$Y^{(2)}$	$N^{(2)}$	$Y^{(2)}$	$2.5^{(2)}$	$6.00^{(2)}$
TiO_2	Fast	$N^{(1)}$	$N^{(1)}$	$Y^{(1)}$	$N^{(1)}$	$Y^{(1)}$	$1.3^{(1)}$	$3.406^{(1)}$
		$N^{(2)}$	$N^{(2)}$	$Y^{(2)}$	$N^{(2)}$	$N^{(2)}$	$1^{(2)}$	$1.70^{(2)}$
	Full	$N^{(1)}$	$N^{(1)}$	$N^{(1)}$	$N^{(1)}$	$Y^{(1)}$	$1^{(1)}$	$0.786^{(1)}$
		$N^{(2)}$	$N^{(2)}$	$Y^{(2)}$	$Y^{(2)}$	$N^{(2)}$	$1.5^{(2)}$	$3.60^{(2)}$
	Best	$Y^{(1)}$	$Y^{(1)}$	$N^{(1)}$	$N^{(1)}$	$Y^{(1)}$	$0.9^{(1)}$	$2.358^{(1)}$
		$Y^{(2)}$	$N^{(2)}$	$N^{(2)}$	$N^{(2)}$	$N^{(2)}$	$0.5^{(2)}$	$1.70^{(2)}$
MnO	Fast	$Y^{(1)}$	$N^{(1)}$	$N^{(1)}$	$Y^{(1)}$	$N^{(1)}$	$1.3^{(1)}$	$3.406^{(1)}$
		$Y^{(2)}$	$Y^{(2)}$	$N^{(2)}$	$Y^{(2)}$	$N^{(2)}$	$0.9^{(2)}$	$2.16^{(2)}$
	Full	$N^{(1)}$	$Y^{(1)}$	$Y^{(1)}$	$Y^{(1)}$	$Y^{(1)}$	$2.3^{(1)}$	$6.026^{(1)}$
		$Y^{(2)}$	$Y^{(2)}$	$Y^{(2)}$	$Y^{(2)}$	$N^{(2)}$	$1.4^{(2)}$	$3.36^{(2)}$
	Best	$N^{(1)}$	$Y^{(1)}$	$N^{(1)}$	$Y^{(1)}$	$Y^{(1)}$	$1.3^{(1)}$	$3.406^{(1)}$
		$Y^{(2)}$	$Y^{(2)}$	$Y^{(2)}$	$Y^{(2)}$	$Y^{(2)}$	$2.4^{(2)}$	$5.76^{(2)}$
P_2O_5	Fast	$N^{(1)}$	$N^{(1)}$	$N^{(1)}$	$N^{(1)}$	$Y^{(1)}$	$1^{(1)}$	$2.62^{(1)}$
		$N^{(2)}$	$N^{(2)}$	$N^{(2)}$	$Y^{(2)}$	$N^{(2)}$	$1^{(2)}$	$2.40^{(2)}$
	Full	$Y^{(1)}$	$N^{(1)}$	$N^{(1)}$	$N^{(1)}$	$N^{(1)}$	$1^{(1)}$	$2.62^{(1)}$
		$N^{(2)}$	$N^{(2)}$	$Y^{(2)}$	$N^{(2)}$	$N^{(2)}$	$0.5^{(2)}$	$1.70^{(2)}$
	Best	$N^{(1)}$	$Y^{(1)}$	$Y^{(1)}$	$N^{(1)}$	$N^{(1)}$	$2^{(1)}$	$5.24^{(1)}$
		$N^{(2)}$	$Y^{(2)}$	$Y^{(2)}$	$N^{(2)}$	$Y^{(2)}$	$2.5^{(2)}$	$6.00^{(2)}$
Total	Fast	$4^{(1)}$	$0.5^{(1)}$	$1.8^{(1)}$	$1.8^{(1)}$	$3.1^{(1)}$	$11.2^{(1)}$	$31.8^{(1)}$
		$2.3^{(2)}$	$2.1^{(2)}$	$0.5^{(2)}$	$2.3^{(2)}$	$2^{(2)}$	$9.2^{(2)}$	$26.6^{(2)}$
Scores	Full	$1^{(1)}$	$2^{(1)}$	$3.3^{(1)}$	$3.8^{(1)}$	$1.1^{(1)}$	$11.2^{(1)}$	$31.8^{(1)}$
		$1.8^{(2)}$	$1.6^{(2)}$	$2^{(2)}$	$2.3^{(2)}$	$2.5^{(2)}$	$10.2^{(2)}$	$29.4^{(2)}$
	Best	$2.3^{(1)}$	$4.8^{(1)}$	$2.8^{(1)}$	$0.3^{(1)}$	$2.6^{(1)}$	$11.8^{(1)}$	$36.4^{(1)}$
		$4.3^{(2)}$	$3.1^{(2)}$	$4^{(2)}$	$0.3^{(2)}$	$3.5^{(2)}$	$15.2^{(2)}$	$44.0^{(2)}$

$^{(1)}$ Bat = 3.5g; $^{(2)}$ Bat1 = 5g.

The Full and Best reading modes allow identify some different oxides not characterized in the Fast mode, for instance, BaO, Y_2O_3, V_2O_5, Ga_2O_3, Cr_2O_3 and ZrO_2, among others. This happens because if the system operates during longer counting times, then, the sample irradiation by the X rays allows visualize elements that were "invisible" in the faster readings as shown by data reported in Table 5.

Table 5. Comparison of the reading modes for selected oxides characterized by XRF spectrometry applied to the Batateira River Formation sample

Oxides	2g			4g			6g			8g			10g		
	Fast	Full	Best	Fast	Full	Best	Fast	Full	Best	Fast	Full	Best	Fast	Full	Best
BaO	N/D(1)	N/D(1)	0.04(1)	N/D(1)	N/D(1)	N/D(1)	N/D(1)	N/D(1)	N/D(1)	N/D(1)	0.09(1)	N/D(1)	N/D(1)	0.09(1)	N/D(1)
(%)	N/D(2)	N/D(2)	0.06(2)	N/D(2)	N/D(2)	0.04(2)	N/D(2)	N/D(2)	0.04(2)	N/D(2)	0.10(2)	0.05(2)	N/D(2)	0.12(2)	0.06(2)
ZrO_2	0.02(1)	0.01(1)	0.10(1)	0.02(1)	0.02(1)	0.02(1)	0.04(1)	0.08(1)	0.02(1)	0.01(1)	0.04(1)	0.02(1)	N/D(1)	0.09(1)	0.02(1)
(%)	0.02(2)	0.02(2)	0.01(2)	N/D(2)	0.02(2)	0.02(2)	N/D(2)	0.02(2)	0.03(2)	0.01(2)	0.70(2)	0.05(2)	0.02(2)	N/D(2)	0.02(2)
Cr_2O_3	N/D(1)	0.02(1)	N/D(1)	0.03(1)	0.02(1)	0.02(1)	0.02(1)	N/D(1)	0.02(1)	N/D(1)	0.01(1)	0.02(1)	0.05(1)	0.01(1)	0.02(1)
(%)	N/D(2)	N/D(2)	0.02(2)	0.03(2)	0.01(2)	0.02(2)	N/D(2)	0.02(2)	0.02(2)	N/D(2)	0.02(2)	0.02(2)	N/D(2)	0.02(2)	0.02(2)
Rb_2O	0.02(1)	0.02(1)	N/D(1)	0.01(1)	0.02(1)	0.02(1)	0.02(1)	0.02(1)	0.02(1)	0.02(1)	0.02(1)	0.02(1)	0.02(1)	0.02(1)	0.02(1)
(%)	0.02(2)	0.02(2)	0.02(2)	0.01(2)	0.02(2)	0.02(2)	0.20(2)	0.02(2)	0.02(2)	0.02(2)	0.02(2)	0.02(2)	0.01(2)	0.02(2)	0.02(2)
SrO	0.01(1)	N/D(1)	0.01(1)	0.01(1)	0.01(1)	0.01(1)	0.01(1)	0.01(1)	0.01(1)	0.01(1)	0.01(1)	0.01(1)	0.01(1)	0.02(1)	0.01(1)
(%)	0.01(2)	0.01(2)	0.01(2)	0.01(2)	0.01(2)	0.01(2)	0.02(2)	0.01(2)	0.01(2)	0.009(2)	0.01(2)	0.01(2)	0.008(2)	0.01(2)	0.02(2)
CeO_2	N/D(1)	N/D(1)	N/D(1)	N/D(1)	0.07(1)	N/D(1)	N/D(1)	N/D(1)	N/D(1)	N/D(1)	N/D(1)	N/D(1)	N/D(1)	0.04(1)	N/D(1)
(%)	N/D(2)	N/D(2)	N/D(2)	0.12(2)	N/D(2)	N/D(2)	N/D(2)	N/D(2)	N/D(2)	N/D(2)	N/D(2)	0.02(2)	N/D(2)	N/D(2)	0.01(2)
ZnO	0.01(1)	0.01(1)	0.01(1)	0.02(1)	0.02(1)	0.01(1)	0.02(1)	N/D(1)	0.01(1)	0.01(1)	0.02(1)	0.01(1)	0.02(1)	0.01(1)	0.01(1)
(%)	0.01(2)	0.02(2)	0.01(2)	0.02(2)	0.01(2)	0.01(2)	N/D(2)	0.01(2)	0.01(2)	0.01(2)	0.01(2)	0.01(2)	N/D(2)	0.01(2)	0.01(2)
CuO	N/D(1)	0.02(1)	N/D(1)	0.02(1)	0.01(1)	0.01(1)	0.02(1)	0.02(1)	0.01(1)	N/D(1)	N/D(1)	0.01(1)	N/D(1)	0.02(1)	0.01(1)
(%)	N/D(2)	0.01(2)	N/D(2)	N/D(2)	0.01(2)	0.01(2)	N/D(2)	0.01(2)	0.01(2)	N/D(2)	0.01(2)	0.008(2)	0.03(2)	0.01(2)	0.01(2)
NiO	200(1)	N/D(1)	N/D(1)	N/D(1)	82(1)	72(1)	N/D(1)	N/D(1)	58(1)	100(1)	N/D(1)	N/D(1)	N/D(1)	87(1)	70(1)
(ppm)	200(2)	N/D(2)	66(2)	N/D(2)	100(2)	62(2)	N/D(2)	N/D(2)	78(2)	N/D(2)	72(2)	63(2)	N/D(2)	N/D(2)	60(2)
Ga_2O_3	N/D(1)	60(1)	N/D(1)	N/D(1)	N/D(1)	N/D(1)	N/D(1)	N/D(1)	47(1)	N/D(1)	N/D(1)	N/D(1)	N/D(1)	N/D(1)	N/D(1)
(ppm)	N/D(2)	N/D(2)	38(2)	N/D(2)	N/D(2)	N/D(2)	N/D(2)	N/D(2)	N/D(2)	N/D(2)	N/D(2)	42(2)	N/D(2)	N/D(2)	33(2)
Y_2O_3	N/D(1)	N/D(1)	N/D(1)	N/D(1)	N/D(1)	30(1)	N/D(1)	N/D(1)	N/D(1)	N/D(1)	34(1)	N/D(1)	N/D(1)	N/D(1)	25(1)
(ppm)	N/D(2)	N/D(2)	N/D(2)	N/D(2)	N/D(2)	N/D(2)	N/D(2)	N/D(2)	29(2)	N/D(2)	N/D(2)	N/D(2)	N/D(2)	N/D(2)	N/D(2)
Cl (%)	N/D(1)	N/D(1)	N/D(1)	N/D(1)	N/D(1)	N/D(1)	N/D(1)	N/D(1)	N/D(1)	N/D(1)	N/D(1)	N/D(1)	N/D(1)	N/D(1)	N/D(1)

Oxides	2g			4g			6g			8g			10g		
	Fast	Full	Best	Fast	Full	Best	Fast	Full	Best	Fast	Full	Best	Fast	Full	Best
	N/D[2]	N/D[2]	0.02[2]	0.03[2]	0.04[2]	N/D[2]	N/D[2]	N/D[2]	0.02[2]	N/D[2]	N/D[2]	0.01[2]	N/D[2]	0.02[2]	N/D[2]
Nb_2O_5 (ppm)	N/D[1] N/D[2]	N/D[1] N/D[2]	N/D[1] N/D[2]	N/D[1] N/D[2]	N/D[1] N/D[2]	24[1] N/D[2]	N/D[1] N/D[2]	N/D[1] N/D[2]	N/D[1] 25[2]	N/D[1] N/D[2]	35[1] N/D[2]	N/D[1] N/D[2]	N/D[1] N/D[2]	N/D[1] N/D[2]	N/D[1] N/D[2]
V_2O_5 (%)	N/D[1] N/D[2]	N/D[1] N/D[2]	N/D[1] N/D[2]	N/D[1] N/D[2]	N/D[1] N/D[2]	N/D[1] N/D[2]	N/D[1] N/D[2]	N/D[1] N/D[2]	N/D[1] N/D[2]	N/D[1] N/D[2]	0.05[1] N/D[2]	N/D[1] N/D[2]	N/D[1] N/D[2]	0.04[1] N/D[2]	N/D[1] N/D[2]
Sc_2O_3 (%)	N/D[1] N/D[2]	N/D[1] N/D[2]	N/D[1] N/D[2]	N/D[1] N/D[2]	N/D[1] N/D[2]	N/D[1] N/D[2]	N/D[1] N/D[2]	N/D[1] N/D[2]	N/D[1] N/D[2]	N/D[1] 0,04[2]	N/D[1] N/D[2]	N/D[1] N/D[2]	N/D[1] N/D[2]	N/D[1] N/D[2]	N/D[1] N/D[2]
SO_3 (%)	0.19[1] 0.16[2]	0.14[1] 0.16[2]	0.15[1] 0.15[2]	0.15[1] N/D[2]	0.17[1] 0.16[2]	0.15[1] 0.16[2]	0.15[1] 0.20[2]	0.15[1] 0.15[2]	0.14[1] 0.16[2]	N/D[1] 0.19[2]	0.14[1] 0.14[2]	0.15[1] 0.16[2]	N/D[1] 0.19[2]	0.13[1] 0.15[2]	0.14[1] 0.14[2]

[1] Bat = 3.5g; [2] Bat1 = 5g.

CONCLUSION

The experiments described in this chapter, considering different laboratorial conditions applied to the Batateira layer sample, have indicated that the *Best* analysis mode (counting time = 15 minutes) is the better choice to found a larger suite of oxides than the other reading modes (*Full*, counting time = 8 minutes; *Fast*, counting time = 5 minutes). It was possible to identify sixteen oxides in the *Best* method that weren't identified in the other two analysis method. It is possible to say that the extra 1.5g of the boric acid in the sample does not provide a significant interference in the results. Therefore, it is preferable to use 3.5g instead of 5g for saving chemicals. In terms of the aliquot weight for preparing the powder pressed pellet, the most reliable results were found for 2g and 4g. Thus, these findings point out relevant information for realizing geochemical studies by XRF analysis in sedimentary basins.

ACKNOWLEDGMENTS

CNPq (National Council for Scientific and Technologic Development), Brazil, and UNESPetro - Geosciences Center Applied to Petroleum, IGCE-UNESP-Rio Claro (SP), Brazil, are greatly thanked for financial and infra-structure support aiming the development of the studies described in this chapter.

REFERENCES

[1] B. Beckhoff, B. Kanngießer, N. Langhoff, R. Wedell, H. Wolff, *Handbook of Practical X-Ray Fluorescence Analysis,* Springer, New York (2005).

[2] HORIBA Scientifics, *X-Ray Fluorescence – The Basic Process,* available online at <http://www. horiba.com/scientific/products/x-

ray-fluorescence-analysis/tutorial/x-ray-fluorescence-the-basic-process/>

[3] M. L. L Formoso, J. J. Trescases, C. V. Dutra, C. B. Gomes, *Técnicas analitícas instrumentais aplicadas à Geologia*, Edgard Blücher, São Paulo (1984). [*Instrumental analytical techniques applied to Geology*]

[4] F. C. Ponte, F.C. Ponte Filho, *Estrutura geológica e evolução tectônica da Bacia do Araripe*, DNPM, Recife (1996). [*Geological structure and tectonic evolution of the Araripe Basin*]

[5] M. L. Assine, *Sedimentação e Tectônica da Bacia do Araripe, Nordeste do Brasil*, Dissertação(Mestrado) - IGCE. Universidade Estadual Paulista Rio Claro (1990). [*Sedimentation and Tectonics of the Araripe Basin*]

[6] F.C. Ponte, C. J. Appi, *Proposta de revisão da coluna litoestratigráfica da Bacia do Araripe*, Congresso Brasileiro de Geologia (1990). [*Proposed revision of the lithostratigraphic column of the Araripe Basin*]

[7] F. C. Ponte, F. C. Ponte-Filho, *Estrutura geológica e evolução tectônica da Bacia do Araripe*, DNPM/DMME, Pernambuco/Ceará (1996a). [*Geological structure and tectonic evolution of the Araripe Basin*]

[8] F. C. Ponte, F. C. Ponte-Filho, *Evolução tectônica e classificação da Bacia do Araripe*, Simpósio sobre o Cretácio do Brasil, Águasde São Pedro (1996b). [*Tectonic evolution and classification of the Araripe Basin*]

[9] G. L. Fambrini, D. R. de Lemos, S. Tesser Jr., J. T. de Araujo, W. F. da Silva-Filho, B. Y. C. de Souza, V. H. M. L. Neumann, *Geol. USP, Sér. cient.* 11 (2), 55 (2011).

[10] A. T. Hashimoto, C. J. Appi, A. L Soldan, J. R. Cerqueira, *Revista Brasileira de Geociências* 17 (2), 118 (1987). [*Brazilian Journal of Geosciences*]

[11] P. W. Thrush, U.S. Staff, *A Dictionary of Mining, Mineral and Related Terms*, U.S. Dept. of Interior, Bureau of Mines (1968).

INDEX

A

acid, xi, 72, 76, 82, 90
age, ix, 2, 4, 7, 10, 11, 12, 13, 26, 31, 36, 46, 52, 58
Araripe Basin, 76, 77, 78, 99

B

base, 6, 15, 20, 21, 24, 51
Batateira layers, viii, xi, 76
bedding, 77
beryllium, 79
boric acid, xi, 76, 81, 82, 90, 92, 93, 94, 98
Brazil, v, viii, xi, 75, 78, 79, 98
building blocks, 12
buried volcanic structures, 3, 32

C

case studies, vii, ix, 34, 44, 70
Ceará State, v, viii, xi, 75, 76, 78
Cenozoic era, 48
chemical, 15, 69, 76, 98
coal, 45, 47, 49, 51, 67, 68, 69
compaction, 14
composition, 15, 61, 69
convergence, x, 44
cooling, xi, 45, 46, 59
correlation, xi, 16, 28, 76
  coefficient, xi, 76
cracks, 47, 59
Cretaceous volcanism, 45, 47, 52, 61, 68

D

data set, 50, 60
database, 15, 82, 90
Delta, 33, 39
delta progradation, 34
deposition, x, 22, 33, 37, 44, 49, 51, 61, 77
deposits, viii, 2, 4, 6, 7, 9, 10, 12, 14, 17, 18, 20, 24, 25, 26, 27, 28, 29, 30
depth, 8, 12, 13, 14, 16, 54, 64, 65, 69, 77
depth perception, 65, 69
ddisposition, 48, 51, 58, 62, 64, 66
distillation, xi, 45, 67
distribution, 6, 12, 53
dyke swarms, 45, 46, 51, 59, 61, 62, 63, 69, 72

dykes, vii, ix, 44, 46, 47, 55, 59, 61, 62, 63, 68, 69

E

earthquakes, 51
effusion, 49, 55, 59
elements concentration, xi, 75, 76
elongation, 63
energy, xi, 4, 49, 75
environment, 4, 5, 6, 13, 27
equipment, xi, 76, 79
erosion, 26
evolution, vii, viii, 1, 4, 5, 6, 13, 14, 28, 32, 33, 34, 36, 37, 40, 41
excitation, xi, 75
experimental condition, xi, 76, 90

F

facies, 4, 19, 26, 49, 52
financial, xi, 75, 79, 98
financial support, xi, 75, 79
fluctuations, 5, 35, 38
fluorescence, 76, 99
formation, vii, ix, xi, 14, 44, 55, 67, 76, 77
fossils, 13, 58
fractures, 58, 68, 69
fragments, 15, 78

G

geological history, 46, 48, 49
geological models, 3
geology, 47
geometry, 3, 4, 11, 18
glasses, 15
grain size, 77
gravity, 50, 67
growth, x, 39, 44
GSA, 37

H

Hawaii, 11
history, 33, 34, 52, 59, 68, 70, 71
Holocene, 20, 34, 35, 40
host, 47, 49
hot spots, 60
hot springs, 50, 68
hydrocarbon exploration, 11, 34, 45, 53, 57, 62, 68
hydrocarbons, x, 44, 46, 47, 49, 53, 55, 58, 63, 65, 67
hypothesis, 82

I

identification, vii, viii, 1, 30, 46, 82
imagery, 45, 46, 47, 57, 69
India, v, vii, ix, 43, 44, 45, 46, 47, 48, 50, 51, 52, 53, 60, 61, 62, 63, 67, 68, 70, 71, 72, 73
individuation, 5
initiation, 40
integration, 5
interference, 98
Italy, v, 1, 3, 15, 31, 32, 33, 34, 35, 36, 38, 39, 40

K

K-T boundary, x, 44, 45

L

Late Pleistocene, ix, 2, 10, 14, 24, 26, 28, 30
light, 33, 89, 91, 92, 93
limestone, x, 44
lithology, 15

M

magnesium, 79
mantle, 69
mapping, 45, 46, 50, 57, 61, 66
Mediterranean, viii, 2, 30, 33, 34, 38, 39, 40
melting, x, xi, 44, 49, 51, 55, 58, 59, 69
migration, 5, 38
minerals, xi, 75, 76
Miocene, viii, 2, 4, 6, 7, 9, 12, 19, 27, 30
models, 3, 11, 45
morphology, 6
mountain ranges, 54
multichannel seismic profiles, 3, 10, 19
Multichannel seismic profiles, 3

N

National Research Council, 1
natural gas, 58, 66
Northern Campania Tyrrhenian margin, v, 1
nucleation, 51

O

oceanic areas, 54
oil, xi, 15, 16, 45, 51, 58, 63, 64, 67
organic matter, x, 44
oxygen, 79

P

parallel, ix, 2, 6, 10, 14, 18, 19, 20, 21, 31, 34, 36, 48, 51, 55, 61, 62, 67, 69
parallelism, 47, 61, 67
pathways, 35
permeability, 58
permission, iv
Petroleum, xi, 37, 43, 70, 71, 72, 75, 79, 98
PGD, 73
photographs, 46
photons, xi, 75
platform, viii, ix, 2, 25, 30, 31
Pliocene, 4, 6, 10, 40
pollen, 78
pools, 49, 63, 64, 67
porosity, 58
potassium, 79
preparation, iv, xi, 70, 76
producers, 47, 58, 66
project, 15, 39
propagation, 51, 60
pull-apart basins, v, vii, ix, xi, 43, 45, 47

Q

quantification, 79
quartz, 45, 61, 69
Quaternary geologic evolution, vii, viii, 1, 28

R

reading, 82, 86, 89, 90, 95, 96, 98
recognition, 57, 60
recommendations, iv
reconstruction, 32
resistance, 49
resolution, vii, ix, 32, 39, 44, 54
resources, 49
rift and grabens, 45, 46, 48, 49, 50, 51, 53, 58, 59, 61, 62, 63, 67, 69
rocks, ix, x, xi, 2, 10, 31, 34, 37, 44, 45, 46, 48, 50, 51, 54, 55, 62, 68, 72, 75, 76

S

sea level, 5, 14, 26, 33, 38, 40
sea-level rise, 40
sediment, 33, 35, 38

sedimentary basins, v, vii, viii, xi, 1, 3, 5, 28, 32, 49, 50, 52, 60, 62, 67, 68, 70, 72, 75, 76, 98
sedimentary records, 77
sedimentation, viii, ix, x, 12, 14, 44, 49, 67
sediments, ix, x, xi, 2, 11, 14, 31, 44, 45, 46, 47, 49, 51, 52, 54, 55, 57, 58, 65, 66, 67, 68, 69, 72, 73, 75, 76, 77
seismic data, vii, viii, ix, 1, 3, 6, 11, 12, 16, 30, 39, 44, 46, 52, 65, 69
showing, 19, 25, 48, 50, 53, 62, 64, 65
silica, 13
silicon, 79
SiO2, 86, 88, 94
sodium, 79
software, xi, 75, 79, 81
soils, xi, 75, 76
Southern Italy, v, 1, 3, 31, 33, 34, 36, 39
stratification, 77
structure, ix, x, 2, 7, 12, 13, 19, 31, 32, 33, 36, 44, 49, 55, 61, 63, 69, 98
succession, x, 29, 44, 46, 47, 49, 51, 52, 53, 54, 55, 58, 60, 61, 66, 69, 73, 77
susceptibility, 68

T

techniques, vii, ix, 28, 44, 46, 65, 66, 69, 70
temperature, 68
transgression, 33
transportation, 69

U

uniform, 54
updating, 16
uranium, 79
USA, 31

V

variations, 33, 94
velocity, 18
visualization, 40
volcano-sedimentary sequence, v, vii, ix, x, 43, 44, 45, 49, 52, 58

W

Washington, 45, 73
water, 6, 14, 33, 52, 79
wells, 3, 7, 8, 9, 12, 17
workers, 45, 55, 57

X

X-Rays Fluorescence (XRF) Technique, xi, 75

Z

zeolites, 68
ZnO, 96